Design, Synthesis and Characterization of Novel (Multiblock) Copoly(esterimide)s and their Shape-memory Properties

Guan, Qingbao

Important note
To cite this publication, please use the final published version (if applicable).
Please check the document version above.

Design, Synthesis and Characterization of Novel (Multiblock) Copoly(esterimide)s and Their Shape-memory Properties

Door

Qingbao GUAN

Master of Science in Materials Science
Soochow University, Suzhou, China
geboren te Qingdao, China

Contents

CHAPTER 1

Introduction

1.1   High-performance polymers

The development of high-performance polymers began in the late 1950s primarily to satisfy the needs of the aerospace and electronics industry. During the next 60 years, many researchers spent a lot of effort to improve the properties of polymers including chemical resistance, thermal and mechanical properties. The term "high-performance" refers to exceptional stability upon exposure to some type of harsh environment and to properties that surpass those of commodity and engineering polymers. High-performance polymers typically exhibit high glass transition temperatures (T_g > 200 °C), high decomposition temperatures (> 450 °C), and excellent mechanical properties.[1-2] For example, aromatic polyesters, polyamides, polyaryletherketones, and polyimides have decomposition temperatures around 480–500 °C, whereas polybenzimid-azoles, polypyrroles and poly(*p*-phenylene)s decompose around 650 °C. Several well-known examples of high-performance polymers are listed in Table 1.1.[3-8]

Looking at the chemical composition, high-performance polymers often make extensive use of aromatic (heterocyclic) monomers, that is, all carbon (hetero)atoms have a high sp^2-bonding character and preferentially lack sp^3-type bonding. The primary reason is that the C=C bond dissociation energy of 614 kJ·mol^{-1} is substantially higher than the 348 kJ·mol^{-1} bond dissociation energy for the C–C bond. Incorporating aromatic units and avoiding aliphatic units was the first step towards the design of high-performance polymers such as Kapton® and Upilex®, both poly(etherimide)s, and main-chain all-aromatic liquid crystal polymers (LCPs) (*i.e.* Twaron® and Kevlar®). Although these polymers display excellent thermomechanical properties, they are inherently difficult to process. Many of them do not melt and need to be processed from a soluble precursor state, for example, the polyamic acid state, or the final polymer must be processed from aggressive solvents such as sulfuric acid or polyphosphoric acid.[9]

Table 1.1. Examples of well-known high-performance polymers.

Entry	Chemical structure	Category	T_g (°C)	T_m (°C)	Polymerization method	Morphology
1		Polyetherimide (PEI)[3]	400	dec*	Solution	Amorphous
2		Polyamide (PPTA)[4-5]	-	dec*	Solution	Lyotropic in sulfuric acid
3		Polyetherether-ketone (PEEK)[6]	143	334	Solution	Semi-crystalline
4		Polyethersulfone (PES)[7]	220	-	Solution	Amorphous
5		Polyester[8]	110	280	Melt	Thermotropic
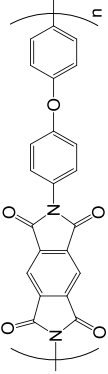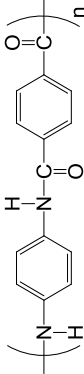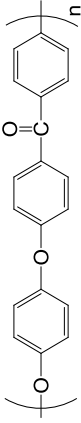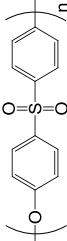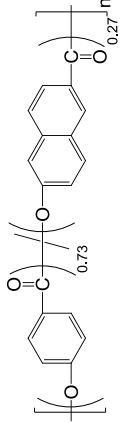
*T_m is above the decomposition (dec) temperature.

High-performance polymers can either be amorphous or semi-crystalline. Poly(etherimide)s (e.g. entry 1) and polyethersulfones (e.g. entry 4), for example are often amorphous; polyetheretherketone (entry 3) and polyetherketoneketone (PEKK), however tend to be semi-crystalline. Semi-crystalline polymers, especially when reinforced with fillers, can be used for a limited amount of time above their T_g. Another advantage of using semi-crystalline polymers is their high resistance against chemical substances. PEEK, for example, is relatively stable in the presence of aqueous acids, alkalies and organic solvents.[10] In comparison to semi-crystalline polymers, the advantage of amorphous ones is that they can be processed at temperatures above their T_g.[11]

LCPs are a unique class of aromatic polymers and are capable of forming highly ordered structures while in solution (lyotropic, e.g. PPTA entry 2) or molten phase (thermotropic, entry 5). Processing LCPs from the liquid crystal phase gives rise to fibers and injected polymers where the polymer chains exhibit a high degree of alignment. LC fibers and articles show typical anisotropic properties such as excellent tensile strength in the processing direction and poor strength in the transverse direction.[12-14] One of the most extensive studied thermotropic LCP is Vectra A® (Ticona GmbH, entry 5), a random copolyester based on 4-hydroxybenzoic acid (HBA) and 6-hydroxy-2-naphthoic acid (HNA). Injection molded articles show a tensile strength of ~180 MPa, a tensile modulus of ~10 GPa and an elongation at break of ~3.4%.[15]

1.2   Polycondensation chemistry

Polycondensation is the preferred method towards synthesizing high-performance polymers such as polyesters (LCPs), polyamides (PPTA), poly(aryletherketone)s (PEEK and PEKK) *etc*. In polycondensation, polymer formation occurs by reacting two molecules containing reactive

functional end-groups, *e.g.* a diamine reacts with a diacid chloride to form high molecular weight PPTA. The primary characteristics of this polymerization is that any two species containing functional end-groups in a reaction mixture can react with each other, and that the polymer molecular weight increases gradually with functional group conversion.[16-18] High molecular weight is obtained in the final stage of the polymerization and can only be achieved at high functional group conversion (> 99.9%).

Carothers[19] and Flory,[20] showed that the number average degree of polymerization ($\bar{x}_n$), characteristic for the molecular weight of polymers synthesized *via* a polycondensation reaction, can be calculated for linear polymers using the extent of reaction p and the stoichiometric monomer ratio r. The general form of the Carothers equation is given by eqn. 1.1.

$$\bar{x}_n = \frac{1+r}{1+r-2rp} \qquad (1.1)$$

The number average molar mass $\bar{M}_n$ can be calculated from $\bar{x}_n$ and $\bar{M}_n$ *via* eqn. 1.2.

$$\bar{M}_n = \bar{M}_0 \cdot \bar{x}_n \qquad (1.2)$$

where $\bar{M}_0$ is the mean molar mass of the monomers in the polymer repeat unit. As is clear from eqns. 1.1 and 1.2, in order to achieve high molecular weight polymer the conversion has to reach 100% ($p \rightarrow 1$) and perfect stoichiometry is needed.

When the final molecular weight ($\bar{M}_n$) needs to be controlled, *i.e.* a oligomeric species is desired, an offset in the monomer feed ratio should be used. For the polymerization of AA and BB (e.g. diol and diacid) where BB is present in excess, the stoichiometric ratio r can be expressed as

$$r = \frac{N_A}{N_B} \qquad (1.3)$$

where N_A is the concentration of monomers with functionality A, N_B is the concentration of monomers with functionality B. When the extent of reaction p is known (typically assumed to be 1), the value of $\bar{x}_n$ and $\bar{M}_n$ can be calculated using eqns. 1.1 and 1.3.

Carothers' equation can also be adapted towards the use of mono-functional end-capping groups. In this case r must be redefined as

$$r = \frac{N_A}{N_B + 2N_{B'}} \qquad (1.4)$$

where $N_{B'}$ is the concentration of (mono-functional B) molecules present and $N_A = N_B$. The coefficient 2 in front of $N_{B'}$ is required since one B molecule has the same quantitative effect as one BB molecule in excess, limiting the growth of the polymer chain. For example, to prepare an oligomer with a certain $\bar{M}_n$, $\bar{x}_n$ is calculated using eqn. 1.2. Assuming complete polymerization, p will approach 1 and the concentration of a mono-functional end-capping compound can be calculated using eqns. 1.1 and 1.4.

Polycondensation can be carried out by various polymerization techniques including *melt polymerization*, *solution polymerization*, *solid-state polymerization*, interfacial polymerization and emulsion polymerization. The first three methods are more widely and frequently used to prepare high-performance polymers, which will be summarized briefly in the following paragraphs. Detailed reviews for the other polycondensation techniques can be found in refs. [21-28].

Solution polycondensation is used in industry to produce poly(etherimide)s (PEIs), polyethersulfones (PES), polyaryletherketones (PAEKs), certain types of polyamides (PPTA) and polyesters. Polycondensation in solution is most frequently used when melt polymerization is impossible or too difficult because the target polymers do not melt. Solution polycondensation typically takes place at lower temperature than melt polymerization. However, solution polycondensation requires polymer separation from solution, recovery of solvent, and additional polymer washing and drying steps.[27]

In melt polymerization, the condensation reaction takes place in a homogeneous molten phase at a temperature above the polymer's T_m and at low pressure. The final polymer product obtained by this process is typically used directly without additional product purification steps. Since the viscosity of the polymer melt increases dramatically as the conversion increases, the removal of low molar mass by-products is often the rate-limiting process. Care has to be taken to control the temperature of the polymer melt as the high temperatures employed for melt polymerizations can cause unwanted side reactions.[29]

Solid-state polymerization, often referred to as solid-state post condensation, is often used in the final stages of high-performance polymer production processes and the aim is to boost the molecular weight of the final polymer. As already discussed in the previous section, preparing high molecular weight polymer in the melt reactor is impractical as the final melt viscosity is often too high and the polymer can not be recovered from the reactor by melt extrusion. In the solid-state reactor, the low molecular weight polymer intermediate is held at a temperature above the T_g but below the T_m of the polymer so that functional end-groups are sufficiently mobile to react. The polycondensation by-product is removed by applying high vacuum or by conducting the polymerization in an inert gas stream (N_2 or dry air). The

relatively low temperature employed in solid-state polymerization makes it advantageous for production of polymers that are prone to undesirable thermal degradation reactions. Since the polymerization rate is very low, the residence time in solid-state polymerization reactors are long (20 hours or longer).[30-32] A solid-state post condensation is a technique that is often used to increase the molecular weight of aliphatic, semi-aromatic and aromatic polyesters.

1.3   Polyesters

All-aromatic liquid crystal polyesters are an interesting class of high-performance polymers, because of the availability of monomers and the overall combination of properties and cost. All-aromatic polyesters consist of aromatic moieties linked by an ester functionality. They exhibit excellent mechanical and thermal properties that are attributed to their high aspect ratio (L/D) rigid-rod all-aromatic backbone.[33-34]

1.3.1   Polyester synthesis

Polycondensation reactions used to prepare polyesters can be divided into non-reversible and reversible reactions. Scheme 1.1 shows an overview of the condensation and exchange reactions commonly used for the preparation of aliphatic, semi-aromatic and all-aromatic polyesters.

A straightforward reaction to use for the preparation of polyesters in a solvent is the irreversible polycondensation reaction (Scheme 1.1A). In general, for this reaction, the polymerization proceeds as long as the polymer is soluble and the end-groups of the monomers do not undergo side reactions. The final polymer can be isolated *via* precipitation in a non-solvent after (near) full conversion is achieved. There are several

fluorinated polyesters synthesized *via* this route, using solvents such as *o*-chlorobenzene, diphenyl ether or 1,1,2,2-tetrachloroethane.[35]
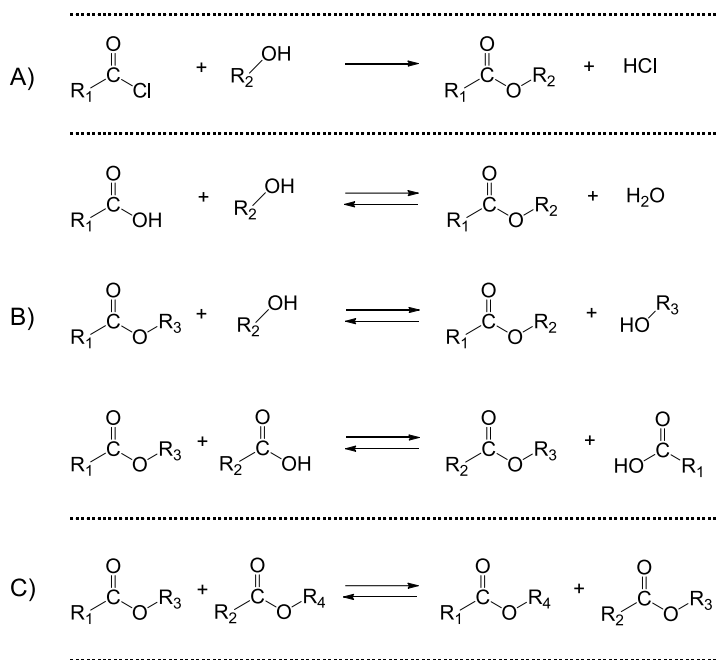
Scheme 1.1. Examples of different condensation reactions used to prepare polyester. **A-** The irreversible condensation reaction between an acyl chloride group and an alcohol. **B-** Reversible esterification, alcoholysis, and acidolysis condensation reactions (typically catalyzed by acids). **C-** Transesterification or ester exchange reaction occurring between two ester groups.

The solubility of all-aromatic polyesters is poor and molecular weight build-up is limited by the precipitation of the polymers during polymerization. Therefore, alcoholysis- and acidolysis- melt

polycondensations are more frequently used for the preparation of all-aromatic (liquid crystal) polyesters (Schemes 1.1B). Although these reactions are reversible, high molecular weight (M_n > 10,000 g·mol^{-1}) polymers can be synthesized *via* this method by the removal of condensation by-products. If required, the molecular weight of the final polymer obtained after the melt polycondensation reaction can be increased further by performing a solid-state post-condensation (discussed in the previous section), easily reaching M_w values in the range between 50,000 to 100,000 g·mol^{-1}.[36]

A reaction that occurs in a polyester melt is transesterification or ester exchange (Scheme 1.1C). This ester exchange reaction can influence the monomer distribution in the final polymer. For example, when a copolymerization is performed and the ester bonds in the copolymer are not equally reactive towards transesterification, monomers can form distinct blocks resulting in a non-random distribution along the polymer chain.[37-38] In contrast, a random copolymer is obtained when all ester bonds are equally susceptible towards transesterification. The distribution of the monomers along the polymer backbone can greatly affect the thermal properties, processability, and mechanical performance of the synthesized polymers.[39-40]

Since the focus in this thesis lies on the preparation of polymers using melt polycondensation, the development of all-aromatic liquid crystal polyesters using this polymerization method is discussed in more detail in the following section.

1.3.2   *Structural backbone modifications*

Poly(4-oxybenzoate), poly(6-oxy-2-naphthoate), poly(4,4'-biphenylene terephthalate) and poly(4'-oxybiphenyl-4-carboxylate) have, in principle, ideal structures for forming thermally stable polyesters, as listed in Table 1.2. Yet, the high linearity, a regular array of dipole

moments and van der Waals' forces result in an unusually high degree of crystallinity and a very stable (high melting) crystal lattice. Consequently, these polymers are characterized by a high T_m and they decompose far before melting.[41-44] Also, they are insoluble in most, if not all, solvents.

Table 1.2. Examples of all-aromatic polyesters that undergo thermal degradation ($T_m \gg T_{dec}$) before melting.

Entry	Chemical structure	Name	T_m (°C)
6		Poly(4-oxybenzoate)	> 600
7		Poly(6-oxy-2-naphthoate)	> 600
8		Poly(4,4'-biphenylene terephthalate)	> 600
9		Poly(4'-oxybiphenyl-4-carboxylate)	> 600
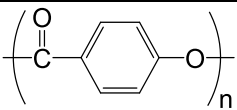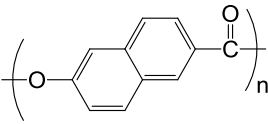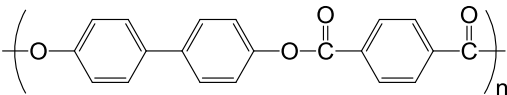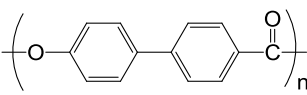
Since T_m is a first-order transition, it can be represented by eqn. 1.5:

$$T_m = \Delta H_m / \Delta S_m \qquad (1.5)$$

where ΔH_m is the enthalpy change of melting and ΔS_m is the entropy change of melting. Generally, a homopolyester has high ΔH_m and low ΔS_m. Therefore, several types of structural modifications are required to decrease the T_m values of this class of polymers to a convenient level so

melt processing becomes possible while limiting thermal degradation. These structural modifications are aimed at decreasing ΔH_m and increasing ΔS_m, which should result in obtaining aromatic polyesters with a low T_m. However, the enthalpy is mainly dominated by inter-chain separation and atomic registry between adjacent polymer chains.[45-46] The structural modifications that are most commonly employed to control the T_m values of polyesters include the following:[47-52]

1. Copolymerization of different monomers to lower the symmetry of the polyester backbone structure is the most simple and straight forward method. Readily available monomers are terephthalic acid (TA), 4,4'-biphenol (BP), hydroquinone (HQ), 4-hydroxybenzoic acid (HBA) and 6-hydroxy-2-naphthoic acid (HNA). For example, 4,4'-biphenylene terephthalate copolymerized with HBA results in a T_{K-N} of about 400 °C (entry 10, Table 1.3).[53] Vectra A®, a LC polyester comprised of 27 mol% HNA and 73 mol% HBA, has a convenient T_{K-N} range of 250–310 °C.[15] The addition of an aminophenol-based monomer allows to lower the T_{K-N} and improve the adhesive property of polyesters. A liquid crystal copolyesteramide composed of 60 mol% HNA, 20 mol% TA and 20 mol% 4-acetamidophenol (AAP), shown in Figure 1.1, is well-known for its outstanding mechanical, thermal and adhesive properties.[54-56] The decrease in T_{K-N} for this series of copolyesters is the result of a mismatch in the packing of the ester linkages of neighboring polyester chains.
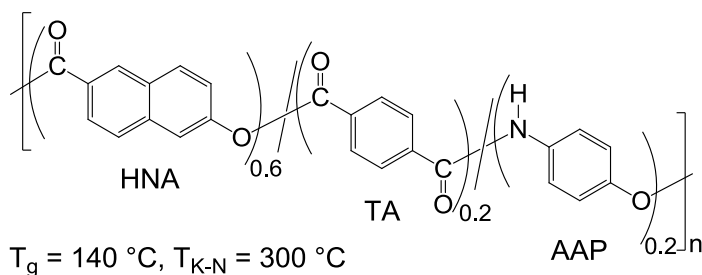
Figure 1.1. Molecular structure of copolyesteramide HNA/TA/AAP.

Table 1.3. Examples of all-aromatic LC polyesters that have been modified with side-groups or using comonomers.

Entry	Chemical structure	Modification	$T_{K\text{-}N}$ (°C)*
10		Copolymerization of different monomers	400
11		Substituent on one of the aromatic moieties	270
12		Bulky substituent on one of the aromatic moieties	255
13		Copolymerization of nonlinear aromatic monomers	255
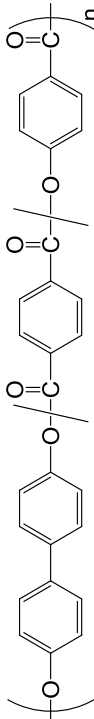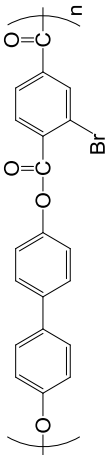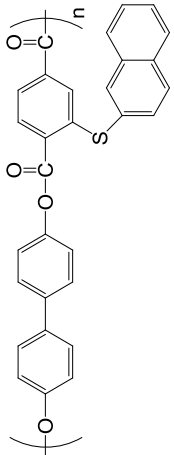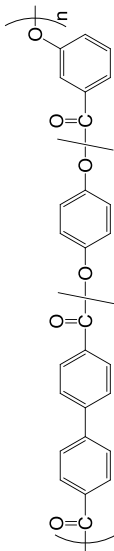
*$T_{K\text{-}N}$ refers to the crystal-to-nematic melt transition.

13

2. The introduction of substituents of various sizes on either the aromatic dicarboxylic acid, the aromatic diol or on both moieties to disrupt lateral packing. The presence of a substituent can decrease the crystallinity and hence reduce the T_{K-N} of the polymer. Heitz *et. al.*[57] prepared polyester 11 (Table 1.3) based on 4,4'-biphenol (BP) and brominated terephthalic acid (TA), which melts at 270 °C. Its T_{K-N} is much lower than that of the parent homopolymer, poly(4,4'-biphenylene terephthalate) (T_{K-N} > 600 °C, Table 1.2, entry 8). As anticipated, a bulky substituent, such as 2-naphthalenethiol of polyester 12 (Table 1.3), produces an even larger decrease in T_{K-N}.[58] The substituent disturbs the packing of the polyester chains by inter-chain separation and by its random arrangement. These arise because of the head-to-head and head-to-tail addition along the polyester chain *via* the so-called internal copolymerization effect.

3. The introduction of kinked or bent (non-linear) monomers to disrupt the lateral interactions between adjacent polymer chains. Generally, this type of monomer decreases the rigidity of the polymer chain and makes extended close packing and crystallization difficult. Consequently, the T_{K-N} of a polyester decreases. When the concentration of a non-linear monomer is increased beyond a certain critical value, the (liquid) crystallinity of a polyester may be lost all together. This modification also leads to a large number of melt processable liquid crystalline polyesters. Irwin *et. al.*[59] incorporated a kinked monomer 3-hydroxybenzoic acid into a polyester based on hydroquinone and 4,4'-biphenyldicarboxylic acid, lowering the T_{K-N} to 255 °C (entry 13, Table 1.3).

Additionally, many other kinked monomers, such as ether-, amide- or imide-based, were also employed. In order to decrease the T_{K-N} of poly(4-oxybenzoate), the kinked aromatic imide-based moiety, *N*-(3'-hydroxyphenyl)trimellitimide (IM), was incorporated (Figure 1.2).[60-63] A

series of poly(esterimide)s with melting endotherms in the range of 330–380 °C was obtained. The reported polymers have T_gs in the range of 200–235 °C. Unfortunately, the processability and bulk properties, such as tensile strength and modulus, were not published.
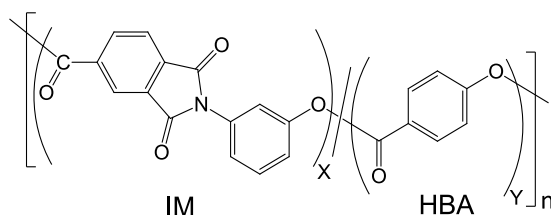
Figure 1.2. Chemical structure of the non-linear IM/HBA poly(esterimide)s based on *N*-(3'-hydroxyphenyl)trimellitimide (IM) and 4-hydroxybenzoic acid (HBA).

4. The final and last approach is the introduction of reactive functionalities such as the phenylethynyl end-group (Table 1.4) to reduce the molecular weight of the polymer backbone (typically M_n = 1,000–10,000 g·mol^{-1}). This lowers the T_{K-N} and melt viscosity and makes it possible to process all-aromatic reactive oligomers, which are allowed to chain extend or cross-link in a successive high-temperature post-treatment step. This route yields nematic polyester thermosets with excellent thermomechanical properties that are otherwise not accessible.[64-66]

Table 1.4 Reactive end-groups suitable for preparing high-performance polymers *via* melt polycondensation.

Chemical structure	Name	Cure temperature (°C)
	Phenylethynyl	350
	Nadimide	350
	Biphenylene	350
—CN	Cyano	350
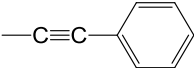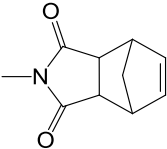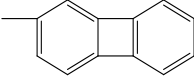
Dingemans and co-workers[67] have synthesized a series of all-aromatic liquid crystalline polyester thermosets based on TA and HQ end-capped with phenylethynyl groups (Figure 1.3). The overall mesogenic shape of *meta* substituted oligomers becomes significantly compromised, and this results in a reduction of the crystalline melting point (T_{K-N}) to 128 °C. All reactive oligomers display nematic mesophases and in most cases, the nematic order is maintained after cure. The nematic thermosets exhibit T_gs in the range of 275-309 °C and high storage moduli (> 1.0 GPa at 200 °C). The advantage of this approach is that one could combine the processability of a thermoplastic with the thermomechanical properties of a thermoset.
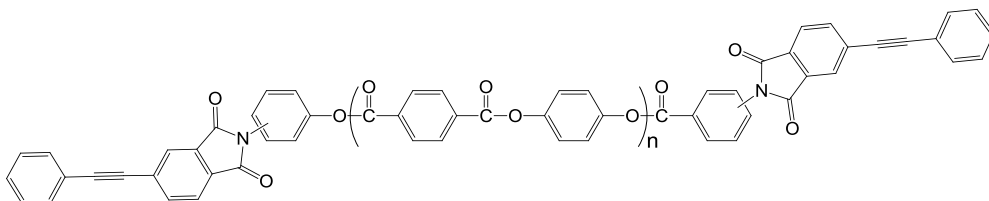
Figure 1.3. Molecular structure of an all-aromatic liquid crystalline polyester based on terephthalic acid and hydroquinone end-capped with *para-* or *meta-* substituted phenylethynyl groups.

1.4 Scope and outline of the thesis

The research described in this thesis is focused on understanding the structure-properties relationship of all-aromatic poly(esterimide)s and crosslinkable oligomers thereof. We specifically target this family because introducing imide moieties in a polyester host polymer allows us to modify the backbone with a polar monomeric unit that has the ability to increase the T_g (> 200 °C) and lower T_m of the final polymer and at the same time introduce strong chain-chain interactions *via* imide-imide π-π stacking interactions. Our main interest is in understanding how N-(3'-hydroxyphenyl)trimellitimide, an AB-type imide monomer, will affect the overall polymer morphology (amorphous vs. semi-crystalline), the melt behavior (isotropic vs. anisotropic), processing characteristics and the final thermomechanical properties of thin films.

In **Chapter 2** the synthesis of an all-aromatic semi-crystalline polyesterimide based on 30 mol% N-(3'-hydroxyphenyl)trimellitimide (IM) and 70 mol% 4-hydroxybenzoic acid (HBA) and an analogous series of reactive oligomers end-capped with phenylethynyl groups will be discussed. In this series we will explore the ability of IM to lower

transition temperatures of a rigid highly crystalline pHBA host. This approach resulted in a complex multi-phase polymer composite. The phase behavior, the thermal- and mechanical properties of the reference polymer and cured thermosets will be discussed.

The syntheses of analogous poly(esterimide)s with larger concentrations of IM (40, 50 and 70 mol%) will be presented in **Chapter 3**. The aim is to explore more processable IM/HBA formulations. All poly(esterimide)s powders show semi-crystalline features whereas all melt pressed films are amorphous. The effect of IM concentration and reactive end-group concentration on the properties of the final polymers will be discussed.

In **Chapter 4** we will discuss liquid crystal formulations prepared by adding 6-hydroxy-2-naphthoic acid (HNA) to the IM/HBA base polymer. Doing so did not result in a random block co-polymer but in a ABA-type block-copolymer with two distinct T_gs. This is the first example, to the best of our knowledge, of a main-chain LC block co-polymer prepared *via* a one-pot melt polymerization method. The processability, morphology, thermal and mechanical properties of the novel liquid crystal poly(esterimide)s and thermosets will be discussed in detail.

Finally, motivated by the unique thermomechanical properties of the LC polymers discussed in Chapter 4, we explored the possibility of using the nematic thermosets as high temperature single component shape-memory materials. Aligned thin films were tested using a viscometer in torsion mode. The strain fixity (R_f) and strain recovery (R_r) of the LC block-copolymers and thermosets thereof was investigated at elevated temperatures (T ~210 °C) and contrasted with a LCP thermoplastic HBA/HNA-based reference polymer.

1.5   References

[1]   P. M. Hergenrother, *High Perform. Polym.* **2003**, *15*, 3.

[2]   M. Friedman, G. Walsh, *Polym. Eng. Sci.* **2002**, *42*, 1756.

[3]   G. Rabilloud, *High performance polymers 3: polyimides in electronics; chemistry and applications*, Editions Technip, Paris, **2000**.

[4]   P. E. Cassidy, *Thermally stable polymers*, Marcel Dekker Inc., New York, **1980**.

[5]   S. C. Lin, E. M. Pearce, *High-performance Thermosets*, Hanser, New York, **1993**.

[6]   P. M. Hergenrother, *High Performance Polymers, Advances in Polymer Science,* Springer-Verlag, Heidelberg, **1994**.

[7]   R. J. Cotter, *Engineering plastics: a handbook of polyarylene ethers*, Gordon and Breach Science Publishers SA, Amstradam, **1995**.

[8]   K. F. Johannes, *High performance polymer*, William Andrew Publishers, Norwich NY, **2008**.

[9]   T. J. Dingemans, *High-Temperature Thermosets*, *Polymer Science: A Comprehensive Reference*, Elsevier BV, Amsterdam, **2012**.

[10]   P. David; J. Bussink, H. T. van de Grampel, G. W. Wheatley, E. Dorf, E. Ostlinning, K. Reinking, F. Schubert, O. Jünger, *Polymers, High-Temperature*, Ullmann's Encyclopedia of Industrial Chemistry, Wiley-VCH Verlag, **2012**.

[11]   D. E. Turek, G. P. Simon, Polym. Int. **1992**, *27*, 165.

[12]   E. B. Priestley, P. J. Wojtowicz, P. Sheng, *Introduction to Liquid Crystals*, Plenum Press, New York, **1974**.

[13]   S. Chandrasekhar, *Liquid Crystals*, Cambridge University Press, Cambridge, **1992**.

[14]   T. J. Sluckin, D. A. Dunmur, H. Stegemeyer, *Crystals That Flow – classic papers from the history of liquid crystals*, Taylor & Francis, London, **2004**.

[15]   "Ticona Vectra Liquid Crystal Polymer (LCP) Product Information," Ticona, Summit, NJ, 07901, **2000**.

[16]   P. J. Flory, *Principles of Polymer Chemistry*, Cornell University Press, Ithaca, NY, **1953**.

[17]   H. F. Mark, N. M. Bikales, C. G. Overberger, G. Menges, *Encyclopedia of Polymer Science and Engineering*, Wiley-Interscience, New York, **1988**.

[18]   M. P. Stevens, *Polymer Chemistry An Introduction*, Oxford University Press, New York, **1990**.

[19]   W. H. Carothers, *Chem. Rev.* **1931**, *8*, 353.

[20]   P. J. Flory, *Chem. Rev.* **1946**, *39*, 137.

[21]   G. Odian, *Principles of polymerization*, John Wiley& Sons, INC, New York, **1991**.

[22]   H. R. Kricheldorf, *Polycondensation: History and New Results*, Springer-Verlag, Berlin, **2014**.

[23]   F. W. Billmeyer, Jr., *Textbook of Polymer Science*, Wiley, New York, **1984**.

[24]   H. G. Elias, *Macromolecules*, Plenum, New York, **1977**.

[25]   W. H. Ray, *J. Macromol. Sci. –Revs. Macromol. Chem.* **1972**, *C8*, 1.

[26]   P. W. Morgan, *Condensation Polymers: By Interfacial and Solution Methods*, Interscience, New York, **1965**.

[27]   L. B. Sokolov, *Synthesis of Polymers by Polycondensation*, Israel Program for Scientific Translation, Jerusalem, **1968**.

[28]   D. H. Solomon, *Step-Growth Polymerization*, Marcel Dekker, New York, **1972**.

[29]   M. A. Schaffer, E. K. Marchildon, K. B. McAuley, M. F. Cunningham, *J. Macromol. Sci.–Revs. Macromol. Chem. Phys.* **2000**, *C40*, 233.

[30]   M. A. G. Jansen, J. G. P. Goossens, G. de Wit, C. Bailly, C. Schick, C. E. Koning, *Macromolecules*, **2005**, *38*, 10658.

[31]   M. A. G. Jansen, L. H. Wu, J. G. P. Goossens, G. de Wit, C. Bailly, C. E. Koning *J. Polym. Sci., Part A: Polym. Chem.* **2007**, *45*, 882.

[32]   E. Gubbels, C. Lavilla, A. M. de Ilarduya, B. A. J. Noordover, C. E. Koning, S. Muñoz-Guerra*, J. Polym. Sci., Part A: Polym. Chem.* **2014**, *52*, 164.

[33]   G. W. Calundann, *US Patent* 4161470, **1979**.

[34]   T. Chung, X. Jin, *Polym. Eng. Sci.* **2000**, *40*, 841.

[35]   C. Carfagna, *Liquid Crystalline Polymers*, Pergamon Press, Oxford, UK, **1994**.

[36]   S. N. Vouyiouka, E. K. Karakatsani, C. D. Papaspyrides, *Prog. Polym. Sci.* **2005**, *30*, 10.

[37]   V. A. Nicely, J. T. Dougherty, L. W. Renfro, *Macromolecules* **1987**, *20*, 573.

[38]   L. Quach, E. Hornogen, W. Volksen, J. Economy, *J. Polym. Sci. Part A: Polym. Chem.* **1989**, *27*, 775.

[39]   D. K. Yang, W. R. Krigbaum, *J. Polym. Sci. Part B: Polym. Phys.* **1989**, *27*, 819.

[40]   H. Muramatsu, W. R. Krigbaum, *J. Polym. Sci. Part B: Polym. Phys.* **1987**, *25*, 2303.

[41]   J. Economy, R. S. Storm, M. I. Matkovick, S.G. Cottis, B. E. Novak, *J. Polym. Sci. Polym. Chem. Ed.* **1976**, *14*, 2207.

[42]   H. R. Kricheldorf, G. Schwarz, *Makromol. Chem.* **1983**, *184*, 475.

[43]   G. Schwarz, H. R. Kricheldorf, *Makromol. Chem., Rapid Commun.* **1988**, *9*, 717.

[44]   H. R. Kricheldorf, A. Conradi, R. Pakull, G. Schwarz, *Makromol. Chem. Makromol. Symp.* **1989**, *26*, 25.

[45]   A. M. Donald, A. H. Windle, *Liquid Crystalline Polymers*, Cambridge University Press, Cambridge, **1992**.

[46]   H. N. Yoon, L. F. Charbonneau, G. W. Calundann, *Adv. Mater.* **1992**, *4*, 206.

[47]   W. R. Krigbaum, H. Hakemi, R. Kotek, *Macromolecules* **1985**, *18*, 965.

[48]   R. S. Irwin, W. Sweeny, K. H. Gardner, C. R. Gochanour, M. Weinberg, *Macromolecules* **1989**, *22*, 1065.

[49]   W. Hatke, H.-T. Land, H.-W. Schmidt, W. Heitz, *Mukromol. Chem., Rapid Commun.* **1991**, *12*, 235.

[50]   P. K. Bhowmik, E. D. T. Atkins, R. W. Lenz, *Macromolecules* **1993**, *26*, 440.

[51]   B. P. Griffin, M. K. Cox, *Br. Polym. J.* **1980**, *12*, 147.

[52]   G. W. Calundann, L. F. Charbonneau, B. K. Benicewicz, US Patent 4473682, **1985**.

[53]   S. J. Cottis, J. Economy, L. C. Wohrer, US Patent 3975487, **1976**.

[54]   P. K. Mandal, S. K. Siddhanta, D. Chakraborty, *J. Appl. Polym. Sci.* **2011**, *119*, 1034.

[55]   J. Alfageme, J. J. Iruin, C. Uriarte, *Int. J. Polym. Anal. Charact.* **1995**, *1*, 349.

[56]   T. S. Chung, M. Cheng, P. K. Pallathadka, *Polym. Eng. Sci.* **1999**, *39*, 953.

[57]   T. Heitz, P. Rohrback, H. Höcker, *Makromol. Chem.* **1989**, *190*, 3295.

[58]   H. R. Kricheldorf, V. Döring, I. Beuermann, V. Eckhardt, *Makromol. Chem.* **1988**, *189*, 1437.

[59]   R. S. Irwin, US Patent 4245082, **1981**.

[60]   H. R. Dicke, J. Genz, V. Eckhardt, L. Bottenbruch. C. A. (Bayer AG), DE 37 37 067, **1987**.

[61]   H. Land, M. Gedan, M. Rätzsch, F. Böhme (Hoechst Aktiengesellschaft), EP0582220 A2, **1994**.

[62]   H. R. Kricheldorf, V. Linzer, C. Bruhn, *Eur. Polym. J.* **1994**, *30*, 549.

[63]   M. Gedan-Smolka, D. Jehnichen, Hartmut Komber, D. Voigt, F. Böhme, M. Rätzsch, *Angew. Makromol. Chem.* **1995**, *229*, 159.

[64]   J. W. Connell, J. G. Smith, P. M. Hergenrother, *J. Macromol. Sci., Rev. Macromol. Chem. Phys* **2000**, *40*, 207.

[65]   A. Knijnenberg, E. S. Weiser, T. L. StClair, E. Mendes, T. J. Dingemans, *Macromolecules* **2006**, *39*, 6936.

[66]   M. Iqbal, T. J. Dingemans, *Eur. Polym. J.* **2010**, *46*, 2174.

[67]   M. Iqbal, B. Norder, E. Mendes, T. J. Dingemans, *J. Polym. Sci., Part A: Polym. Chem.* **2009**, *47*, 1368.

CHAPTER 2

A Semi-crystalline Polyesterimide and Reactive Esterimide Oligomers Thereof

Abstract

In order to understand the structure-property relationships of all-aromatic poly(esterimide)s, a high molecular weight reference polymer was synthesized based on N-(3'-hydroxyphenyl)trimellitimide (IM) and 4-hydroxybenzoic acid (HBA) with a molar ratio of 0.3/0.7. The resulting polyesterimide is brittle and difficult to process due to the existence of multiple fusible and infusible phases. By introducing reactive phenylethynyl end-groups an analogous series of reactive esterimide oligomers (3-IM/7-HBA–2K, 5K, and 9K) were obtained with excellent processability. Thermal post-treatment of all polymers, either by stretching the polymer films in the DMTA or by static post treatment, resulted in an unanticipated large increase in T_g. The T_g of 3-IM/7-HBA–Ref increased from 205 °C to 248 °C, whereas the T_g of 3-IM/7-HBA–5K increased from 207 °C to 284 °C. The thermally stretched 3-IM/7-HBA reference film and the cured 5K thermoset films exhibit similar tensile properties. Tensile strengths are in the range of ~110 MPa, elastic moduli ~4.0 GPa, and films exhibit an elongation at break of ~3.0%. The as-pressed films are typically brittle whereas the thermally stretched films are flexible, which makes them easy to handle.

2.1 Introduction

Over the last decades, extensive research has been performed to develop all-aromatic thermoplastic polymers.[1-2] All-aromatic polyesters are a sub-class of high-performance thermoplastic polymers, consisting of aromatic moieties linked by ester functionalities. They exhibit excellent mechanical and thermal properties that are attributed to their rigid-rod all-aromatic backbone.[3-4] A major drawback of all-aromatic main-chain polyesters is that they tend to have high melting temperatures (T_m),[5-7] which are typically close to their decomposition temperature, and low solubility in all but aggressive solvents. These factors make them difficult to process and have significantly limited their applicability. Economy *et. al.* explored poly(oxybenzoate) (pHBA) (Figure 2.1), a polyester with a T_m of approximately 500 °C and a glass transition temperature (T_g) of 315 °C.[8]

T_g = 315 °C, T_m > 500 °C
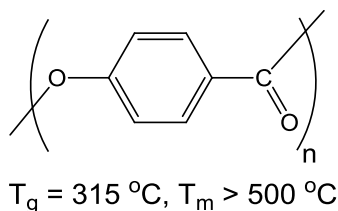
Figure 2.1. Chemical structure of the poly(oxybenzoate) (pHBA).

Several different types of backbone modifications have been implemented over the years, which were aimed to increase T_g, reduce T_m and improve the melt processability. For example, introducing non-aromatic bulky side-chain substitutions will increase T_g, but at the same time the thermal stability is reduced. Introducing nonlinear or kinked monomers that lower the backbone symmetry and disrupt crystallization, lowers the T_m effectively and retains the

thermomechanical properties.[9–10] Introducing reactive functionalities such as phenylethynyl or maleimide end-groups will reduce the molecular weight of the polymer backbone (typically Mn= 1,000–9,000 g·mol^{-1}). This lowers the T_m and melt viscosity and makes it possible to process all-aromatic reactive oligomers, which are allowed to chain extend or cross-link in a successive high-temperature post-treatment step. This route yields polymers with excellent thermomechanical properties that are otherwise not accessible.[11-13]

The copolymerization of kinked aromatic imide-based moieties, such as *N*-(3'-hydroxyphenyl)trimellitimide (IM), together with HBA was investigated in order to decrease the melting temperature of the pHBA backbone (Figure 2.2).[14]
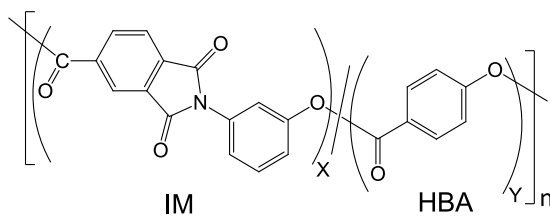
Figure 2.2. Chemical structure of the non-linear IM/HBA polyesterimide based on *N*-(3'-hydroxyphenyl)trimellitimide (IM) and 4-hydroxybenzoic acid (HBA) as disclosed in ref. [14].

Land *et al*. reported that the melt viscosity of IM/HBA with a molar ratio of 0.6/0.4 (6-IM/4-HBA) is 750 Pa·s (shear rate 1,000 rad/s; 350 °C). 6-IM/4-HBA tensile specimens were injection-molded at 350 °C, exhibiting tensile properties in terms of ultimate tensile strength (81 MPa), tensile modulus (2.3 GPa) and elongation at break (35%).[15] The syntheses and characterization of IM/HBA compositions with different molar ratios was reported by Kricheldorf and Gedan-Smolka.[16-17] Both

concluded that the T_gs (~200 °C) are high regardless of the backbone composition, but the phase behavior of the resulting poly(esterimide)s differs largely. Due to the high melting temperatures (> 330 °C) of most compositions, processing was only possible for IM/HBA compositions in the range of 0.4/0.6–0.6/0.4. As a consequence the thermal and mechanical properties of poly(esterimide)s with high molar ratios (> 60 mol% IM or HBA) could not be explored.

With the aim to explore more extreme molar ratio's with higher T_gs and hence access liquid crystal (nematic) poly(esterimide)s with higher end-use temperatures, we have selected a IM/HBA molar ratio of 0.3/0.7 (labelled 3-IM/7-HBA). In order to lower the T_m and improve the processability and thermomechanical properties, we end-capped the 3-IM/7-HBA chain-ends with reactive phenylethynyl end-groups. In this chapter we will report the synthesis, phase behavior and thermo-mechanical properties of processable all-aromatic poly(esterimide)s with cross-linkable end-groups having molecular weights in the range of 2,000–9,000 g·mol^{-1}.

2.2 Experimental

2.2.1 Materials

4-Hydroxybenzoic acid (4-HBA), trimellitic anhydride (TMA), 3-aminophenol (3-AP), glacial acetic acid, acetic anhydride and sulfuric acid (100%) were purchased from Aldrich (Zwijndrecht, The Netherlands). Potassium acetate was purchased from Acros Organics (Geel, Belgium). Poly(oxybenzoate) (pHBA) reference polymer was purchased from Polysciences Europe GmbH (Eppelheim, Germany). 4-Phenylethynylphthalic anhydride (PEPA) was obtained from Hangzhou Chempro Tech Co., Ltd. The synthesis of the reactive end-groups, *i.e.* N-

(4-carboxyphenyl)-4-phenylethynylphthalimide (PE-COOH) and N-(4-acetoxyphenyl)-4-phenylethynylphthalimide (PE-OAc) was reported elsewhere.[12]

2.2.2 Monomer and Reactive Oligomer Synthesis

N-(3'-hydroxyphenyl)trimellitimide (IM) A 500 mL flask equipped with a mechanical stirrer and reflux condenser was charged with 250 mL glacial acetic acid and trimellitic anhydride (0.1 mol, 21.01 g). The mixture was heated to ~120 °C and when all solids were dissolved, 3-aminophenol (0.1 mol, 10.91 g) was added. A thick suspension formed almost immediately and this reaction mixture was refluxed for 4 h. at 120 °C. After cooling the reaction mixture, the precipitated product was isolated by filtration and washed with acetic acid (2 X) and ethanol (2 X). The off-white N-(3'-hydroxyphenyl)trimellitimide (IM) as shown in Figure 2.3 was dried under vacuum at 140 °C for 24 h. Yield: 24.06 g. (0.085 mol, 85%); m.p. 304 °C (DSC) (301-306 °C in ref. [18]). FTIR: the characteristic absorption peaks of imide groups were observed at 1777, 1715, 1383 and 725 cm^{-1}; the broad band around 3500 cm^{-1} can be assigned to the phenolic hydroxyl group and carboxyl group. ^{1}H NMR (DMSO-d_6, 400 MHz): δ 6.82-6.90 (m; H^4, H^5, H^7); 7.30 (t; H^6), $J_{6,7}$= 8.27 Hz, $J_{6,5}$= 8.17 Hz; 8.06 (d; H^1), $J_{1,2}$= 7.74 Hz; 8.29 (s; H^3); 8.40 (dd; H^2), $J_{2,1}$= 7.75 Hz, $J_{2,3}$= 1.08 Hz; 9.77 (s; OH); 13.60 (s; COOH). ^{13}C NMR (DMSO-d_6, 100 MHz): δ 114.30, 115.20, 117.73, 123.32, 123.66, 129.45, 131.93, 132.55, 134.80, 135.34, 136.32, 157.59, 165.74, 166.13, 166.15. MS *m/z* (relative intensity): 283.05 (100%) (M$^+$), 239 (20.7), 120 (30.6), 103.05 (27.8), 92 (46.1), 75 (32.1).
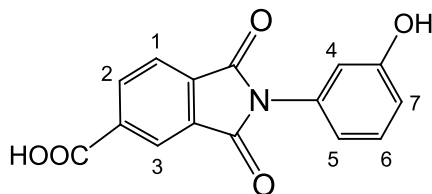
Figure 2.3. Chemical structure of N-(3'-hydroxyphenyl)trimellitimide (IM).

A series of reactive polyesterimide oligomers and a reference polymer based on N-(3'-hydroxyphenyl)trimellitimide (IM) and 4-hydroxybenzoic acid (HBA) with a molar ratio of 0.3/0.7 (3-IM/7-HBA) was synthesized using standard melt condensation techniques as shown in Scheme 2.1. Three reactive oligomers with a target number average molecular weight M_n of 2,000, 5,000, and 9,000 g·mol^{-1} were prepared by controlling the concentration of the reactive end-groups using the Carothers equation.[19] The samples were labeled, 3-IM/7-HBA–2K, 3-IM/7-HBA–5K and 3-IM/7-HBA–9K, respectively, where 3-IM/7-HBA refers to the polymer backbone composition, *i.e.* 0.3 mol IM and 0.7 mol HBA. The integers refer to the polymer molecular weight, *i.e.* 2K = 2,000 g·mol^{-1}. The reference polymer was synthesized without reactive end-groups and was labeled 3-IM/7-HBA–Ref.
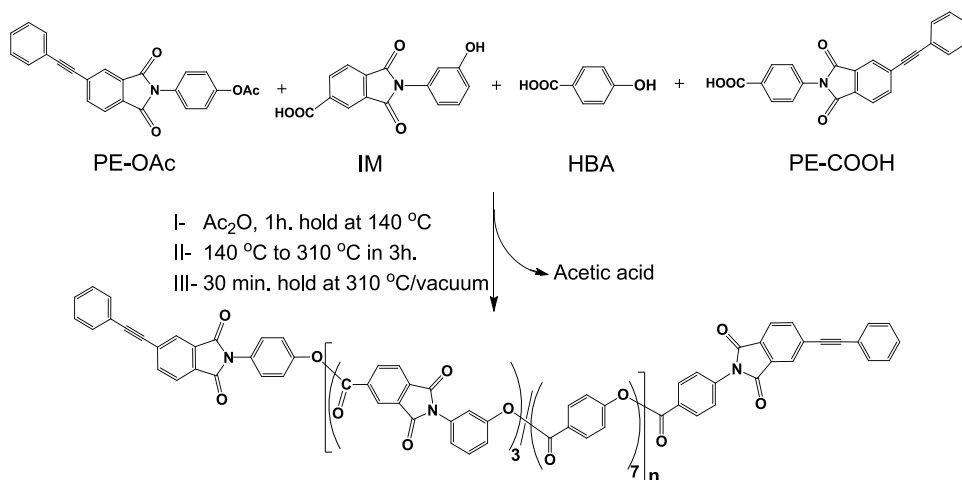
Scheme 2.1. Synthesis and backbone composition of the all-aromatic esterimide-based reactive 3-IM/7-HBA oligomers (Mn = 2K, 5K and 9K) with phenylethynyl end-groups and the reference polymer, 3-IM/7-HBA–Ref.

3-IM/7-HBA–9K reactive oligomer As a representative example, we describe the synthesis of a 9,000 g·mol^{-1} reactive oligomer with a IM/HBA molar ratio of 0.3/0.7, 3-IM/7-HBA–9K. To synthesize this oligomer, IM (0.3 mol, 84.915 g), HBA (0.7 mol, 96.621 g), PE-OAc (0.0185 mol, 7.06 g), PE-COOH (0.0185 mol, 6.80 g), and potassium acetate (0.1 mmol, 10 mg) were charged to a 250 mL three-neck round-bottom flask. The flask was equipped with a nitrogen gas inlet, an overhead mechanical stirrer, and a reflux condenser. The reactor was purged with nitrogen for 30 min. prior to the start of the reaction and a slow nitrogen flow was maintained throughout the duration of the synthetic procedure. Acetic anhydride (100 mL, 1.06 mol) was added for the *in-situ* acetylation of the monomers. The reaction mixture was slowly stirred under a nitrogen atmosphere and heated to 140 °C to allow acetylation to take place. After a 1 h. isothermal hold, the temperature of

29

the reaction mixture was slowly increased to 310 °C using a heating rate of 1 °C·min⁻¹. During this process acetic acid was collected as the polycondensation by-product. At 310 °C the nitrogen flow was stopped and a vacuum was applied to remove the residual acetic acid and other low molecular weight side products. The reaction flask was allowed to cool down overnight under a nitrogen flow and the final product was removed from the flask and processed into a powder. A solid-state post-condensation step was performed at 270 °C for 24 h. under vacuum in order to remove all volatiles and ensure full polymerization. Yields for these syntheses were generally above 95%. The reference polymers were prepared under identical conditions but without PE-OAc and PE-COOH end-groups.

2.2.3 Preparation of thin films

Melt pressed thin films were prepared using standard melt pressing techniques. The post-condensed polymer powder was placed between two Kapton™ films and consolidated in a preheated Joos hot press at 370 °C for 45 min. with 5 kN force. During the melt-pressing step no attempts were made to align the polymer melt.

Thermal stretching The films were thermally stretched in a Perkin Elmer Diamond dynamic mechanical thermal analyzer (DMTA) and were used for mechanical and thermomechanical testing. For thermomechanical testing, the same film was stretched four times. The stretch ratio (SR) was calculated using eqn. 2.1.

$$\text{Stretch ratio} = L/L_0 \qquad (2.1)$$

where L and L_0 represent the length of stretched and original samples. After the first stretch experiment (SR = 2), the film was removed from

the clamps and cut into L_0, and the new dimensions were measured and used for the next experiment. In four consecutive experiments, we were able to stretch the films up to SR = 16. These samples were labelled SR1 (SR = 1), SR2 (SR = 2), SR4 (SR = 4), SR8 (SR = 8), and SR16 (SR = 16). After stretching the films four times, the films became too thin and too difficult to handle, effectively ending the thermal stretching experiments.

Thermal treatment In order to understand the effect of thermal treatment on properties such as the glass transition temperature (T_g) and storage modulus (E'), the films were heated individually without stretching. The heating program is exactly the same as the thermal stretching procedure used in the DMTA, from 25 °C to the predetermined temperature at a heating rate of 2 °C·min^{-1}.

2.2.4 Characterization

^{1}H and ^{13}C nuclear magnetic resonance (NMR) spectra were recorded on a 400 MHz Bruker WM-400 at 25 °C. IR spectra were recorded using a Perkin Elmer Spectrum 100 FT-IR spectrometer. Mass spectra were recorded using a Shimadzu QP2010S with a direct injection port. Mass spectra were generated by electron impact and data was collected over the m/z range 45–900. The oven was heated from 50–300 °C at a rate of 10 °C·min^{-1} under a vacuum of 0.055 mbar. The sample was injected using an Atas GL Optic 3 inlet, which was heated from 50–300 °C in one minute.

A Perkin Elmer Pyris Diamond TG/DTA was used to study the dynamic thermal stability. The polymers were initially heated to 370 °C and isothermally held at 370 °C for 1 h. under nitrogen to ensure full polymerization. After cooling to 25 °C, the samples were analyzed using a heating rate of 10 °C·min^{-1} under a nitrogen atmosphere.

The melt behavior of the polymers was determined by differential scanning calorimetry (DSC) using a Perkin Elmer Sapphire DSC with a heating rate of 20 °C·min^{-1}. All measurements were conducted under a nitrogen atmosphere.

A Leica DMLM optical microscope equipped with a Linkham hot stage was used to investigate the melt behavior as a function of time and temperature. The samples were investigated between glass slides upon heating using a heating rate of 50 °C·min^{-1}.

The complex melt viscosity of the polymers was investigated using a Thermofisher Haake MARS Ш rheometer equipped with a force-rebalanced transducer in a parallel plate geometry. Parallel plates of 8 mm diameter were used and samples were prepared by compression molding (8 mm in diameter and 0.2 mm thick). The samples were investigated under a nitrogen atmosphere with temperature ramping (5 °C·min^{-1}) from 150 °C to 370 °C followed by an isothermal hold at 370 °C for 1 h. All experiments were performed at a frequency of 1.0 Hz and a strain amplitude of 0.1%, which is well within the linear viscoelastic range (frequency of 0.1–10 Hz and a strain amplitude of 0.001–1.0%).

X-ray diffraction (XRD) analysis was conducted on a Bruker AXS D8 Discovery diffractometer, using a Cu-Kα radiation source. Wide-angle X-ray diffraction (WAXD) was performed using a distance of 6 cm between the sample and the detector and the exposure time was set to 5 min. The samples were also investigated as a function of temperature using a heating rate of 10 °C·min^{-1} in the temperature range of 250–350 °C. The degree of crystallinity (%) was calculated using eqn. 2.2.

$$\text{Crystallinity } (\%) = \frac{\text{crystalline area}}{(\text{crystalline + amorphous}) \text{ area}} \qquad (2.2)$$

Dynamic mechanical thermal analyses (DMTA) were performed with a Perkin Elmer Diamond DMTA in tension mode, using thin films (20 ± 0.2) mm × (5 ± 0.2) mm × (0.25 ± 0.05) mm under a nitrogen atmosphere and at a heating rate of 2 °C·min^{-1}. All experiments were performed at a frequency of 1.0 Hz, static tension force of 2,000 mN, minimum tension force of 200 mN, tension gain of 1.5 and length amplitude of 5 μm. The minimum recordable storage modulus (E') was set to 1×10^4 Pa.

A Zwick 1445 tensile tester with a 1 kN force cell was used to investigate the stress-strain behavior of the polymer films. Tensile tests were performed by fixating the films with an adhesive onto a rectangular frame with the side arms cut. All experiments were performed at 25 °C at a strain rate of 1 mm·min^{-1}. The data were reported as an average of 5 samples. The elastic modulus was measured by calculating the slope of the stress-strain curve between 0.1% and 0.3% strain.

A high-resolution JEOL scanning electron microscope (HR-SEM) operating at 5 kV was employed to study the fracture surfaces of the films after stretching. After sputtering with gold, the samples were placed in the SEM vacuum chamber, and the electron beam was focused on the fracture surface along the stretching axis.

2.3 Results and discussion

2.3.1 Synthesis of 3-IM/7-HBA reference polymer and reactive oligomers

All oligomers with phenylethynyl end-groups could be synthesized using a simple environmentally benign one-pot melt condensation procedure. The polymerizations were straightforward and no premature cross-linking (gelation) of the phenylethynyl end-groups could be observed. Since the maximum polymerization temperature was 310 °C some of the reactive oligomers solidified towards the end of the polymerization. The solid-state post-condensation procedure appeared very useful in this context since it ensured complete polymerization of all reactive oligomers. The oligomers were ground into a fine powder and this powder was post condensed at 270 °C for 24 h. under vacuum prior to further use. All oligomers were easily synthesized in high yields and the synthetic procedure is very amenable to scale-up.

To quantify the molecular weight of the reference polymer and reactive oligomers, we attempted to find suitable solvents or solvent mixtures, *e.g.* dimethylacetamide, trifluoroacetic acid, pentafluoro-phenol/hexafluoroisopropanol (1:1 v/v). However, all oligomers and reference polymer appeared completely insoluble at 25 °C and elevated temperature, which precludes size exclusion chromatography (SEC) and inherent viscosity measurements. Although it is well known that all-aromatic polyesters and polyimides are not stable in 100% sulfuric acid, we used this solvent in a final attempt to prepare polymer solutions suitable for inherent viscosity measurements. The reference polymer and reactive oligomers could be dissolved in 100% sulfuric acid, however, the inherent viscosity dropped too fast, due to backbone degradation reactions (hydrolysis), making it impossible to calculate a representative inherent viscosity.

2.3.2 Thermal properties

TGA The thermal stability of the reference polymer and cured thermosets were evaluated using dynamic thermogravimetric analysis (TGA) at a heating rate of 10 °C·min^{-1}. High decomposition values ($T_d^{5\%}$ = 454–461 °C) and high char yields (57–64 wt%) were found, indicating that the dynamic thermal stability of these polymers is comparable to that of commercial high-performance polymers such as bismaleimide (BMI) and bisnadimide (PMR15).[20-21] The cured 3-IM/7-HBA–2K thermoset displays the best thermal stability among these polymers, which is most likely the result of the high density of cross-links. The thermal properties of the poly(esterimide)s are summarized in Table 2.1.

DSC The thermal behavior of the reference polymer and reactive oligomers was investigated using differential scanning calorimetry (DSC). Figure 2.4 depicts the first and second heating scans using a heating rate of 20 °C·min^{-1}. All oligomers and the reference polymer show a T_g and multiple endothermic peaks upon the first heat (Table 2.1). The DSC results show that all oligomers and reference polymer are essentially semi-crystalline poly(esterimide)s. The multiple endothermic peaks $T_{orth\text{-}orth'}$ and $T_{orth'\text{-}phex}$ upon the first heat might be attributed to the co-existence of different crystal types. Despite lowering the T_g by 24 °C, detectable upon the first heat only, the incorporation of phenylethynyl end-groups limits the molecular weight of the polymer and reduces the endothermic peak values when compared to the reference polymer. For example, 3-IM/7-HBA–2K shows multiple endothermic peaks $T_{orth\text{-}orth'}$ (280 °C) and $T_{orth'\text{-}phex}$ (325 °C), respectively, which are approximately 30 °C lower than that of 3-IM/7-HBA–Ref.

Table 2.1. Thermal properties of the reactive oligomers and their cured thermosets.

Sample	T_g (°C)[a]	$T_{orth-orth'}$ (°C)[a]	$T_{orth'-phex}$ (°C)[a]	$T_{K-K'}$ (°C)[a]	T_g (°C)[b]	E' (GPa) at 25 °C	$T_d^{5\%}$ (°C)[c]	Char yield (wt%)[d]
3-IM/7-HBA–2K	204	280	325	304	222	6	461	64
3-IM/7-HBA–5K	209	282	330	305	207	4	456	60
3-IM/7-HBA–9K	219	299	335	310	207	4	456	59
3-IM/7-HBA–Ref	238	310	342	327	205	4	454	57

[a] T_g, $T_{orth-orth'}$ and $T_{orth'-phex}$ data were obtained from the first heating scan of DSC experiments. $T_{K-K'}$ data were obtained from the second heating scan of DSC experiments. Heating rate 20 °C·min^{-1}/nitrogen atmosphere.
[b] T_g data were obtained from DMTA experiments using cross-linked films, defined by the maximum of the loss modulus (E″) peak. Heating rate 2 °C·min^{-1}/nitrogen atmosphere and a frequency of 1 Hz.
[c] Thermal stability was evaluated using dynamic TGA. The sample was cured by isothermal holding at 370 °C for 1 h. before the measurement. Heating rate 10 °C·min^{-1}/nitrogen atmosphere.
[d] Char yield at 600 °C.
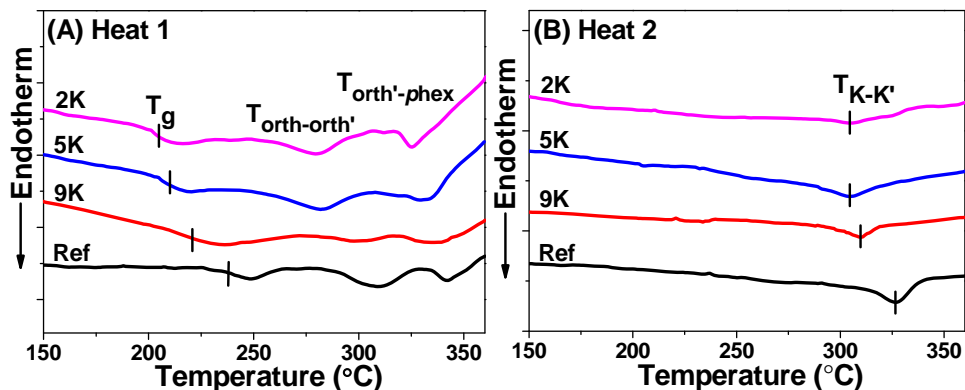
Figure 2.4. A- First and **B-** second DSC heating trace of the 3-IM/7-HBA reference polymer and reactive oligomers after post-condensation (24 h. at 270 °C). Heating rate 20 °C·min^{-1}/nitrogen atmosphere. $T_{orth\text{-}orth'}$ and $T_{orth'\text{-}phex}$ represent a transition temperature of orthorhombic to orthorhombic modification structure and a transition temperature of orthorhombic modification to pseudohexagonal structure, respectively. $T_{K\text{-}K'}$ represents a combined crystal structure transition temperature.

Erasing the thermal history by quenching the samples from 370 °C to 25 °C prevents the polymer chains from crystallizing properly. Therefore the second heat shows one broad endothermic peak $T_{K\text{-}K'}$ only, instead of multiple endothermic peaks. 3-IM/7-HBA–2K has a $T_{K\text{-}K'}$ of 304 °C whereas 3-IM/7-HBA–Ref exhibits a $T_{K\text{-}K'}$ of 327 °C. More details with respect to the polymer morphology will be discussed in section 2.3.4 (X-ray diffraction experiments).

Hot-stage optical microscopy In order to understand the phase behavior in more detail we investigated the reference polymer and reactive oligomers using hot-stage optical microscopy. The melt behavior of 3-IM/7-HBA is complex in that the polymer forms a biphasic melt. Polymer chains with a more random composition melt

but polymer chains with a high HBA concentration do not melt. The biphasic melt of 3-IM/7-HBA–Ref at 370 °C is shown in Figure 2.5A. Increasing the temperature to well above the decomposition temperature does not improve the melt flow. However, shearing the biphasic melt of 3-IM/7-HBA–Ref at 370 °C reveals a crystalline phase coexisting with a liquid crystalline phase (Figures 2.5B and 2.5C). Reducing the molecular weight and introducing reactive end-groups lowers the onset of the biphasic melt temperature. Shearing the reactive oligomers also reveals the presence of a liquid crystalline/crystalline phase (Figure 2.5D).
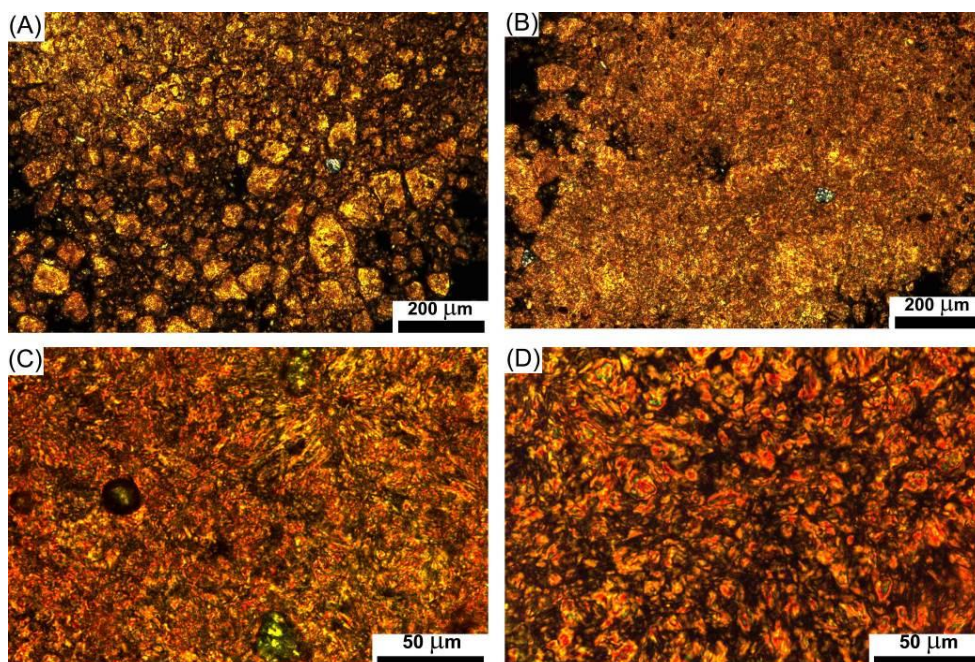
Figure 2.5. Microphotographs of the poly(esterimide)s powders at 370 °C (after post-condensation for 24 h. at 270 °C). **A-** 3-IM/7-HBA–Ref forms a viscous biphasic melt. **B-** Shearing 3-IM/7-HBA–Ref reveals the presence of a liquid crystalline phase co-existing with a crystal phase. **C-** Larger magnification of photograph **B**. **D-** Shearing 3-IM/7-HBA–5K also reveals a liquid crystalline phase co-existing with a crystal phase.

2.3.3 Rheology

Understanding the melt behavior of our polymers is critical in terms of defining the processing window. The complex melt viscosity ($|\eta^*|$) of the reference polymer and reactive oligomers as function of temperature and time was measured using a rheometer. Figure 2.6 shows that 3-IM/7-HBA–Ref has an acceptable processing window of approximately 30 min. at 370 °C. The melt viscosity drops rapidly at 330 °C and reaches a minimum value (4×10^5 Pa·s) at 370 °C.
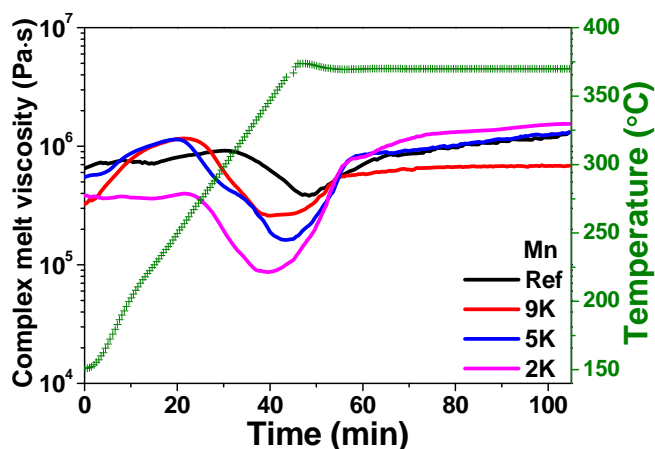
Figure 2.6. Complex melt viscosities ($|\eta^*|$) for the 3-IM/7-HBA reference polymer and reactive oligomers as a function of temperature and a 1 h. hold at 370 °C. Experiments were performed using a frequency of 1 Hz and heating rate of 5 °C·min^{-1}/nitrogen atmosphere. The test specimens were prepared after the polymers post-condensed at 270 °C for 24 h.

However, the reactive oligomers have an even broader processing window. For instance, the melt viscosity of 3-IM/7-HBA–2K starts to decrease at 280 °C and reaches a minimum value (7×10^4 Pa·s) at 350 °C.

After reaching the minimum value, the viscosity of 3-IM/7-HBA–Ref starts increasing and leveling off after a 30 min. hold at 370 °C, suggesting that transesterification and polymerization are taking place during the 1 h. hold (effectively, post condensing the polymer). In the case of 3-IM/7-HBA–2K, chain extension and cross-linking are taking place from 350 °C, which results in an increase in molecular weight and hence a rapid increase in |η*|. After a 30 min. hold at 370 °C, the chain extension and cross-linking chemistry is mostly complete and the viscosity levels off. Similar results were reported by Iqbal *et al.* in 2009.[22] From the rheology experiments it is clear that our reactive oligomers have a broader and more accessible processing window than that of the high molecular weight reference polymer. An isothermal hold at 370 °C for 1 h. can cure the reactive oligomers to form cross-linked thermosets.

2.3.4 X-ray diffraction (XRD) analysis

Wide-angle X-ray diffraction (WAXD) study was performed to investigate the morphology of the poly(esterimide)s powders and melt processed films. Figure 2.7A shows that the WAXD patterns of 3-IM/7-HBA–Ref and 3-IM/7-HBA–5K powders after post-condensation (24 h. at 270 °C) are to a large degree similar to that of the poly(oxybenzoate) (pHBA) reference polymer. From the XRD data it is clear that incorporation of 30 mol% co-monomer in pHBA reduces the degree of crystallinity from 82% to 20% and the perfection of crystallites but does not change the crystal lattice of the homopolymer. The incorporation of phenylethynyl reactive end-groups also disrupts crystallization, such that 3-IM/7-HBA–5K powder possesses a degree of crystallinity of 14%. This is an additional reason for the reduction of the endothermic peak values in DSC. Processing the powders into films using a hot press at

370 °C, results in stiff and brittle films. Figure 2.7B shows that the crystallinity in 3-IM/7-HBA–Ref is completely maintained (20%) but the 3-IM/7-HBA–5K film has only 7.4% crystallinity remaining. This indicates that the crystallinity of reactive oligomers, induced during the post-condensation step, is mostly lost to a large degree due to the chain extension and cross-linking during the high temperature film processing step.
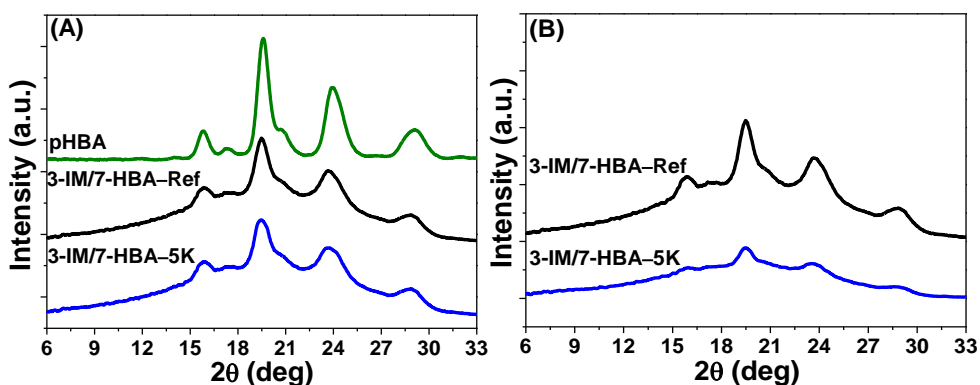
Figure 2.7. XRD analyses of the poly(esterimide)s at 25 °C. **A**- 3-IM/7-HBA–Ref and 3-IM/7-HBA–5K powders after post-condensation (24 h. at 270 °C). Also shown is the homopolymer of HBA (pHBA) for reference purposes. **B**- 3-IM/7-HBA–Ref and 3-IM/7-HBA–5K films were prepared using a hot press at 370 °C for 45 min.

Temperature dependence XRD experiments allow us to follow how the morphology of the poly(esterimide)s changes as a function of processing temperature. The temperature dependent WAXD patterns of 3-IM/7-HBA–Ref and 3-IM/7-HBA–5K are summarized in Figure 2.8. It exhibits a reversible first-order transition from orthorhombic modifications (I and II) to a pseudohexagonal modification (III) at 330 °C, which are well documented solid-state phase transitions of pHBA.[23-24] This indicates that the endothermic peaks ($T_{orth-orth'}$, $T_{orth'-phex}$

and $T_{K-K'}$) observed by DSC for 3-IM/7-HBA may be attributed to the presence of pHBA crystal polymorphs. This suggests that the 3-IM/7-HBA reference polymer and reactive oligomers thereof are rather complex polymers, probably composed of two fractions:

(i) A infusible pHBA fraction. pHBA crystals are formed by the homopolymerization of HBA. Kricheldorf *et al.* showed that the pseudohexagonal chain packing of pHBA is stable up to 500 °C.[25] Our XRD data confirms that the infusible pHBA fraction persists up to 350 °C.

(ii) A thermoplastic polyesterimide fraction with a random IM/HBA sequence distribution. Hot-stage optical microscopy observations indicate that the fusible polyesterimide fraction melts into a nematic liquid crystalline phase at 370 °C.

Most importantly, we believe this explains the presence of an immobile biphasic melt of 3-IM/7-HBA–Ref as observed by hot-stage optical microscopy at 370 °C (Figure 2.5A).
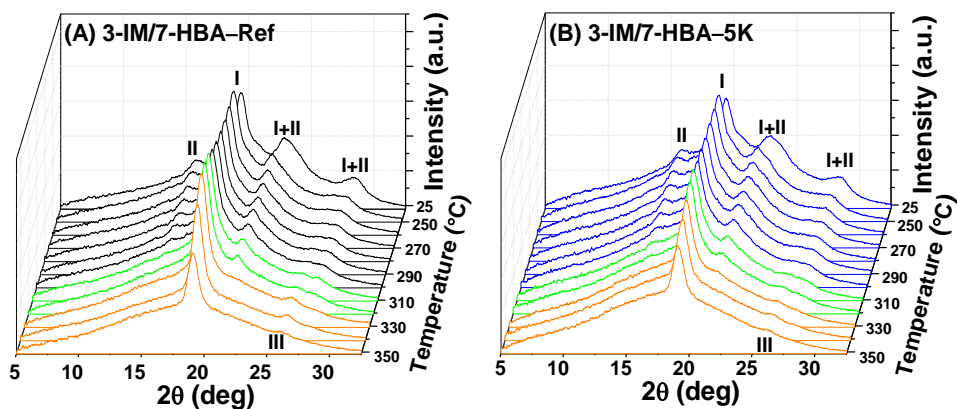
Figure 2.8. Temperature dependence WAXD patterns of **A-** 3-IM/7-HBA–Ref and **B-** 3-IM/7-HBA–5K powders after post-condensation (24 h. at 270 °C). The WAXD patterns were recorded at 25 °C and the temperature range of 250–350 °C with an interval of 10 °C.

42

The results so far strongly suggest that 3-IM/7-HBA and reactive oligomers thereof should be considered molecular composites. The pHBA crystals act as the stiff and rigid reinforcing phase and the polyesterimide fraction acts as the processable thermoplastic matrix. Figure 2.9 depicts the steps involved towards the production of a 3-IM/7-HBA molecular composite.
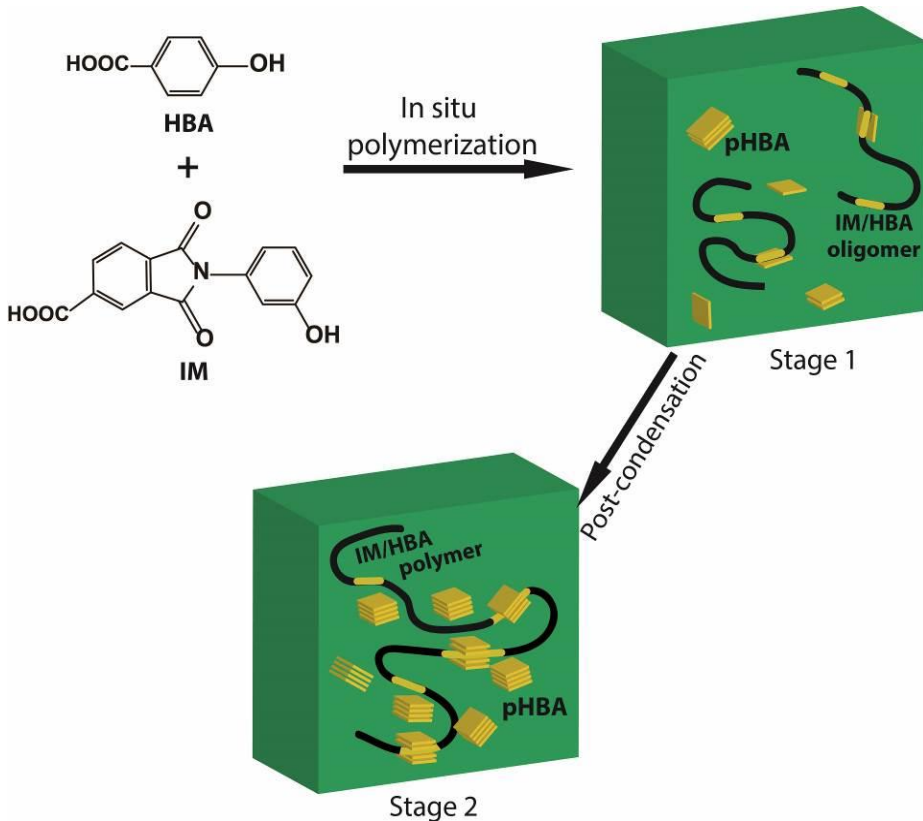
Figure 2.9. Schematic diagram depicting the formation of a 3-IM/7-HBA/pHBA-based molecular composite. **Stage 1-** The pHBA crystals and polyesterimide with a random IM/HBA sequence distribution were obtained in a one-step polymerization method. An *in-situ* synthesized molecular composite was formed. **Stage 2-** The molecular weight and crystallinity of the thermoplastic matrix were increased during the post-condensation step.

43

2.3.5 Dynamic mechanical thermal analysis (DMTA)

In order to explore the thermomechanical properties of our polymers, the storage modulus (E') and loss modulus (E") as function of temperature were studied using dynamic mechanical thermal analysis (DMTA). Thin films of the reference polymer and cured thermosets were used for these DMTA experiments and the results are summarized in Table 2.1 and Figure 2.10. The T_g was defined at maximum of E" instead of the Tan δ. Reporting the T_g at the maximum of E" is more appropriate, since this is the temperature where the polymer transits from a glassy to a rubbery state, whereas the Tan δ represents the E"/E' ratio.

Figure 2.10 shows that the incorporation of small concentrations of phenylethynyl reactive end-groups does not lead to a significant improvement in thermomechanical properties of the final after cure films. For instance, the storage modulus (4 GPa) and T_g (207 °C) of 3-IM/7-HBA–5K and 3-IM/7-HBA–9K are similar to that of 3-IM/7-HBA–Ref. However, 3-IM/7-HBA–2K, with the largest concentration of phenylethynyl end-groups, displays a storage modulus of 6 GPa at 25 °C and a T_g of 222 °C respectively. This is reasonable because the phenylethynyl end-groups cross-link during the curing process and form a partially cross-linked network, which typically increases the T_g and E' due to a reduction in chain mobility.
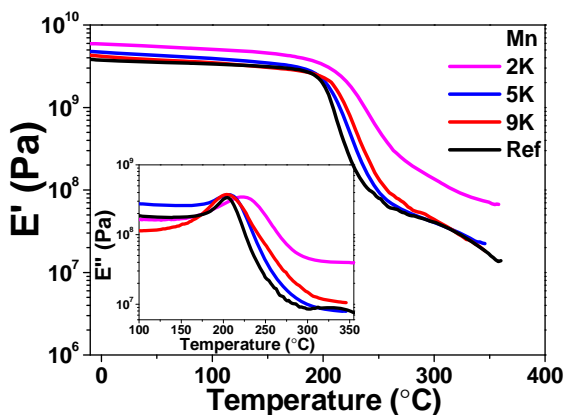
Figure 2.10. Storage modulus (E') as function of temperature for the 3-IM/7-HBA reference polymer and cured thermoset films. The inset shows the loss modulus (E") near the glass transition. Heating rate used is 2 °C·min^{-1}/ nitrogen atmosphere and a frequency of 1 Hz.

During the DMTA experiments we noticed that the reference polymer and the cured thermoset films showed an exceptional ability to stretch when heated above their T_g. In fact, they could be stretched at least four times, each time the film was elongated twofold (Figure 2.1S). The as-pressed films are brittle but upon stretching the films become flexible. In order to investigate the thermal stretching behavior and the effects on E' and T_g we performed several consecutive thermal stretching experiments using 3-IM/7-HBA–Ref and 3-IM/7-HBA–5K films.

From DMTA experiments it is clear that thermal stretching results in an increase in T_g of the 3-IM/7-HBA–Ref film, as shown in Figure 2.11A and Table 2.2. The as prepared 3-IM/7-HBA–Ref film (stretch ratio = 0) exhibits a T_g of 205 °C and the T_g increased to 248 °C after thermal stretching the film 3 times. For the cured thermosets, stretching 3-IM/7-HBA–5K film results in an even larger increase in T_g from 207 °C to

284 °C (Figure 2.11B). In addition, thermal stretching also improves the storage modulus of both 3-IM/7-HBA–Ref and 3-IM/7-HBA–5K films from 4 GPa to 6 GPa. It is important to note that the end temperature (T_{max} in Table 2.2) of the 3-IM/7-HBA–5K thermal stretching experiments keeps increasing, whereas T_{max} (~365 °C) of 3-IM/7-HBA–Ref is constant. This indicates that more cross-linked network is formed in 3-IM/7-HBA–5K during thermal stretching experiments.
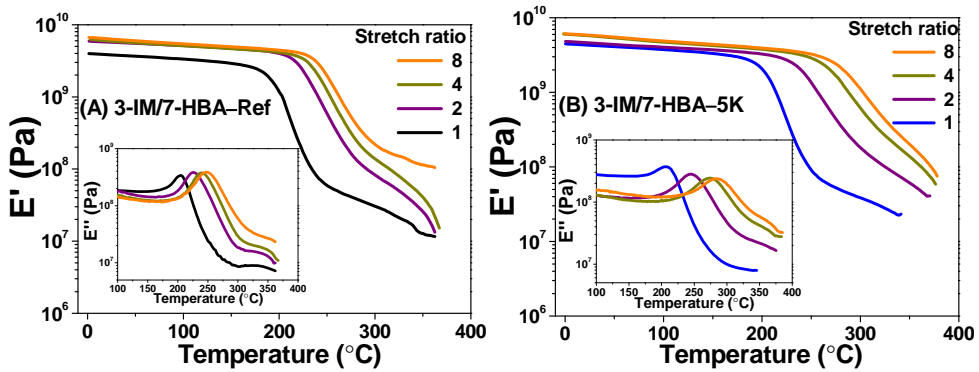
Figure 2.11. DMTA analysis of the reference polymer and cured thermoset films at different stretch ratios. **A-** Storage moduli (E') as function of temperature for the 3-IM/7-HBA–Ref film and **B-** Storage moduli (E') as function of temperature for the cured 3-IM/7-HBA–5K film. Heating rate 2 °C·min⁻¹/nitrogen atmosphere and a frequency of 1 Hz. The insets show the loss moduli (E") at the glass transition temperature (T_g).

Table 2.2. Summary of the DMTA results. All data collected under a nitrogen atmosphere and a heating rate of 2 °C·min^{-1} and 1 Hz. The as-pressed films are labeled SR1. Films stretch by 100%, 300% and 700% were labeled SR1, SR4 and SR8, respectively.

Sample	Modulus (GPa) at 25 °C	T_g (°C)[a]	T_{max} (°C)[b]
3-IM/7-HBA–Ref SR1	4	205	365
3-IM/7-HBA–Ref SR2	5	225	365
3-IM/7-HBA–Ref SR4	6	239	367
3-IM/7-HBA–Ref SR8	6	248	365
3-IM/7-HBA–5K SR1	4	207	345
3-IM/7-HBA–5K SR2	5	242	375
3-IM/7-HBA–5K SR4	6	274	385
3-IM/7-HBA–5K SR8	6	284	385

[a] T_g is reported at the maximum of E".

[b] T_{max} is the end temperature of each thermal stretching experiment.

In order to evaluate the increase in T_g of the films a thermal treatment procedure was performed without stretching using a heating program identical to what was used in our DMTA experiments (heating rate of 2 °C·min^{-1}). With an increase in thermal treatment temperature, the T_gs of 3-IM/7-HBA–Ref and 3-IM/7-HBA–5K show a dramatic increase (Figure 2.12). The higher the thermal treatment temperature, the larger the improvement in T_g. Both as-pressed films show an initial T_g of ~205 °C. When they were thermally treated from 25 °C to 400 °C, using a heating rate of 2 °C·min^{-1}, 3-IM/7-HBA–Ref film has a T_g of 243 °C, whereas 3-IM/7-HBA–5K film exhibits a T_g of 268 °C. 3-IM/7-HBA-5K seems to benefit most from the heat treatment in terms of increasing the T_g. The thermally treated films are brittle, and could not be used for stress-strain experiments.
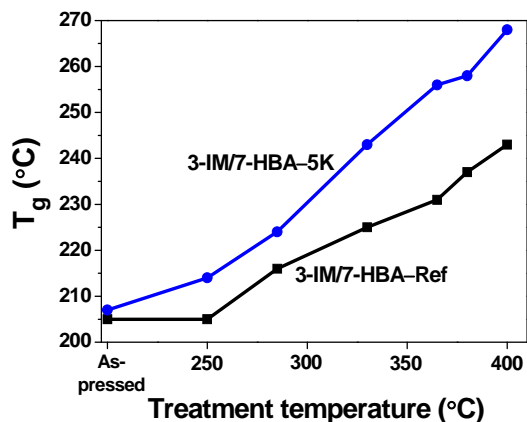
Figure 2.12. T_gs of 3-IM/7-HBA–Ref and 3-IM/7-HBA–5K plotted as function of thermal treatment temperature. All films were thermally treated from 25 °C to the predetermined temperature with a heating rate 2 °C·min^{-1}/nitrogen atmosphere and immediately cooled down to 25 °C (cooling rate ~3 °C·min^{-1}). T_gs were measured using DMTA (maximum of E") with a heating rate 2 °C·min^{-1}/nitrogen atmosphere and a frequency of 1 Hz.

2.3.6 Origin of the T_g increase

To understand why the T_g in both model systems shows such a large increase upon thermal treatment we performed some additional experiments. The most intuitive answer, perhaps, might be related to an increase in molecular alignment. However, in the case of 3-IM/7-HBA– Ref and 3-IM/7-HBA–5K, no trace of alignment could be detected by XRD. Not only in the as-pressed films, but also in the thermally stretched films (Figure 2.2S). The XRD patterns of thermal stretched films are shown in Figure 2.3S. By calculating the ratio of the area under the crystalline peaks to the total area of the XRD pattern, the degree of

crystallinity in the films was obtained. Figure 2.13 shows that the degree of crystallinity of the 3-IM/7-HBA–Ref and 3-IM/7-HBA–5K films increase by as little as 2.5% and 0.9%, respectively, after thermal stretching the films 4 times. Clearly, such a marginal increase in the degree of crystallinity would not be the main contributor to the dramatic increase in T_g.
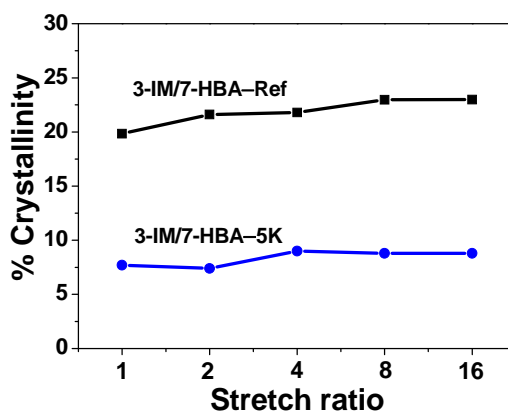
Figure 2.13. Degree of crystallinity as function of the film stretch ratio for 3-IM/7-HBA-Ref and 3-IM/7-HBA-5K.

Alternatively, the enhancement in T_g may be explained by an increase in polymer molecular weight and the removal of small molecule plasticizing species. Thermal treatment can induce further polymerization and trans-esterification, leading to an increase in molecular weight and even forming entanglements among polymer chains. The small molecules or polymerization by-products, which were entrapped in the as-pressed films could play the role as plasticizing agent and increase polymer chain mobility. This, in turn, would result in a reduction in polymer T_g. The weight loss of the 3-IM/7-HBA–Ref and 3-IM/7-HBA–5K films during each thermal treatment was measured by TGA and the results are summarized in Figure 2.14. From these data it

becomes clear that material is lost when the thermal treatment temperature is increased. This implies that small molecule plasticizing species are indeed effectively removed during the thermal treatment procedure, thereby decreasing the plasticization effect. The material lost by outgassing mainly consists of phenol and HBA monomer, which was confirmed by mass spectrometry. These changes result in restricted molecular motion, which could explain the increase in T_g for 3-IM/7-HBA–Ref and 3-IM/7-HBA–5K.
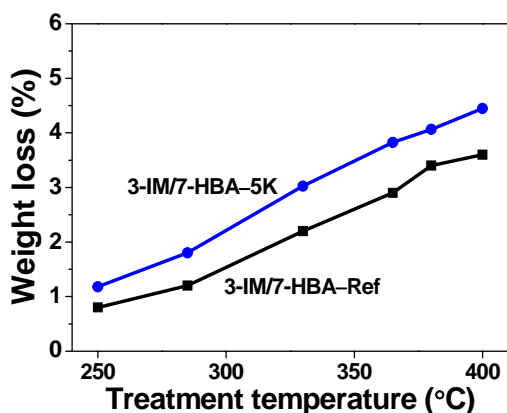
Figure 2.14. Weight loss of 3-IM/7-HBA–Ref and 3-IM/7-HBA–5K plotted as function of thermal treatment temperature as measured by TGA. The weight loss of the films was measured during thermal treatment from 25 °C to the predetermined temperatures with a heating rate 2 °C·min^{-1}/nitrogen atmosphere.

Due to the presence of phenylethynyl end-groups, 3-IM/7-HBA–5K must undergo more complex reactions during thermal treatment. Thermal treatment results in a more densely cross-linked network and additional chain extension. This explains why 3-IM/7-HBA–5K shows a larger increase in T_g than 3-IM/7-HBA–Ref when exposed to the same thermal treatment.

2.3.7 Tensile properties

The as-pressed and thermally stretched films were used to measure the tensile properties of 3-IM/7-HBA–Ref and 3-IM/7-HBA–5K. The tensile properties of the thin films are shown in Figure 2.15 and Figure 2.4S. The data are summarized in Table 2.1S. The as-pressed films, 3-IM/7-HBA–Ref SR1 and 3-IM/7-HBA–5K SR1 exhibited virtually the same tensile properties, *i.e.* a tensile strength of ~50 MPa, an elastic modulus of ~2.5 GPa, and elongation at break of ~2.3%, which are the typical values for an all-aromatic main-chain polymer. The scanning electron microscopy (SEM) analysis of the 3-IM/7-HBA–Ref SR1 (Figure 2.16B) and 3-IM/7-HBA–5K film (Figure 2.5SB) films revealed a porous, poorly consolidated fracture surface suggesting that brittle failure is likely to occur.

The thermally stretched films showed significant improvements in mechanical behavior. The tensile strength of 3-IM/7-HBA–Ref SR2 and SR4 increased by a factor of 1.5 and 2.3, respectively, compared to the as-pressed film. Their elastic modulus increased from 2.9 GPa to 3.5 and 3.9 GPa, respectively. 3-IM/7-HBA–5K SR2 and SR4 show a similar increasing trend. Typically, when polymer fibers or films are stretched, the tensile strength increases and the elongation at break decreases.[26] However, the elongation at break of our thermally stretched films showed a moderate increase from 2.3% to 3.0%. Overall, the excellent tensile properties of the thermally stretched 3-IM/7-HBA reference polymer and cured thermoset films are very similar. Their tensile properties are comparable to commercial high-performance polymers such as Vectra-A™.[27]
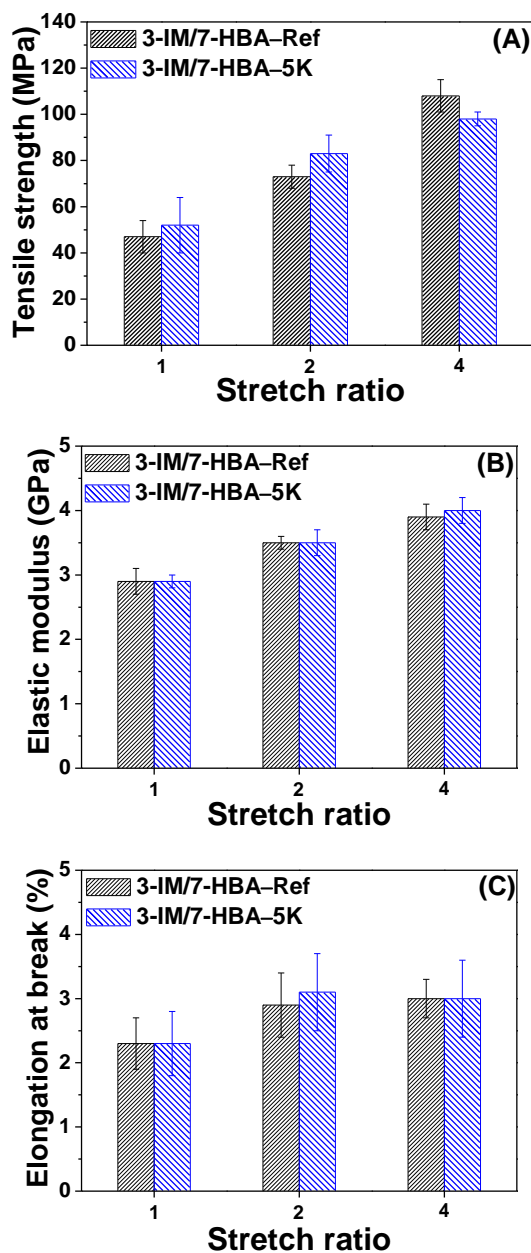
Figure 2.15. The tensile properties of the 3-IM/7-HBA reference polymer and cured thermoset films (5 samples) as function of stretch ratio. **A-** Tensile strength. **B-** Elastic modulus. **C-** Elongation at break.

The improvement in tensile properties illustrates that the stress transfer is better in the thermally stretched films than the as-pressed ones. This may be attributed to an increase in polymer molecular weight during the thermal stretching procedure and simultaneously the films become more consolidated. This was confirmed by the SEM analysis of the fracture surface along the stretching axis of the 3-IM/7-HBA–Ref film (Figure 2.16D). Under 20,000 X magnification, SEM images clearly showed a fibrous-like morphology of the 3-IM/7-HBA–Ref SR4 film, which was totally different from the granular morphology of the 3-IM/7-HBA–Ref SR1 film. A similar morphology variation was also observed in the 3-IM/7-HBA–5K film (Figure 2.5SD).
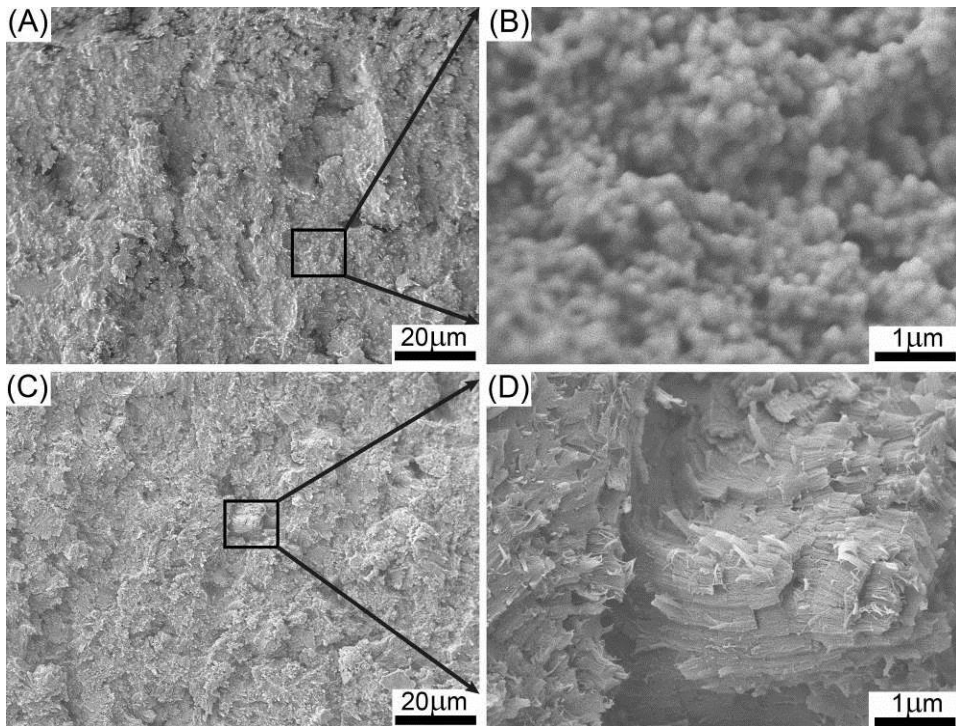
Figure 2.16. SEM images of 3-IM/7-HBA–Ref film fracture surface along the stretching axis. **A-** 3-IM/7-HBA–Ref SR1, 1,000 X, **B-** 3-IM/7-HBA–Ref SR1, 20,000 X, **C-** 3-IM/7-HBA–Ref SR4, 1,000 X, and **D-** 3-IM/7-HBA–Ref. SR4, 20,000 X.

2.4 Conclusions

We have prepared a series all-aromatic polyesterimide thermosets with excellent thermal and mechanical properties. Reactive oligomers based on N-(3'-hydroxyphenyl)trimellitimide (IM) and 4-hydroxybenzoic acid (HBA) (molar ratio of 0.3/0.7) were synthesized using a one-pot melt condensation method and could be melt processed. The as prepared oligomers are comprised of a distinct infusible crystal phase (pHBA) and a fusible random IM/HBA copolymer. Phenylethynyl end-groups were used to lower the molecular weight and hence improve the processability by lowering T_m and the melt viscosity. The as-pressed 3-IM/7-HBA reference film exhibits a T_g of 205 °C and the T_g increased to 248 °C after thermally stretching the films by a factor of 8. In contrast with 3-IM/7-HBA–5K film, where thermal stretching resulted in an even more dramatic increase in T_g from 207 °C to 284 °C. After thermally stretching, the obtained films are flexible and easy to handle. A static thermal post treatment results in a similar increase in T_g for all films but the films remain brittle and difficult to handle. The difference between the tensile properties of the thermally stretched 3-IM/7-HBA reference and the 3-IM/7-HBA–5K films, however, is negligible. The tensile strength increased from 50 MPa to 110 MPa after 2 thermal stretching experiments. Meanwhile the elastic modulus increased from 2.9 GPa to 4.0 GPa. No molecular alignment was detected by XRD in neither the as-pressed films nor the thermally stretched films.

Our results suggest that the increase in thermal and mechanical properties benefit from the repeated thermal (post)treatment. Thermal treatment most likely results in an increase in polymer molecular weight and the removal of low molecular weight plasticizers. For the thermoset films, thermal treatment results in a post-cure and hence an increase in the degree of cross-linking.

2.5 References

[1]   J. Mark, K. Ngai, W. Graessley, L. Mandelkern, E. Samulski, J. Koenig, G. Wignall, *Physical Properties of Polymers*, Cambridge University Press, Cambridge UK **2004**, p. 362.

[2]   C.E. Sroog, *Prog. Polym. Sci.,* **1991**, *16*, 561.

[3]   G. W. Calundann, *US Patent* 4161470, **1979**.

[4]   T. Chung, X. Jin, *Polym. Eng. Sci.* **2000**, *40*, 841.

[5]   K. D. Deak, R. W. Lenz, W. S. Kantor, *J. Polym. Sci., Part A: Polym. Chem.* **1997**, *35*, 197.

[6]   B. K. Chen, S. Y. Tsay, J. Y. Chen, *Polymer* **2005**, *46*, 8624.

[7]   H. R. Kricheldorf, R. Bürger, *Makromol. Chem.* **1993**, *194*, 2183.

[8]   J. Economy, B. E. Nowak, S. G. Cottis, *SAMPE J.* **1970**, *6*, 6.

[9]   S. Chang, C. D. Han, *Macromolecules* **1996**, *29*, 2103.

[10] P. K. Bhowmik, H. Han, *Macromolecules* **1993**, *26*, 5287.

[11] J. W. Connell, J. G. Smith, P. M. Hergenrother, *J. Macromol. Sci., Rev. Macromol. Chem. Phys* **2000**, *40*, 207.

[12] A. Knijnenberg, E. S. Weiser, T. L. StClair, E. Mendes, T. J. Dingemans, *Macromolecules* **2006**, *39*, 6936.

[13] M. Iqbal, T. J. Dingemans, *Eur. Polym. J.* **2010**, *46*, 2174.

[14] H. R. Dicke, J. Genz, V. Eckhardt, L. Bottenbruch. C. A. (Bayer AG), DE 37 37 067, **1987**.

[15] H. Land, M. Gedan, M. Rätzsch, F. Böhme (Hoechst Aktiengesellschaft), EP0582220 A2, **1994**.

[16] H. R. Kricheldorf, V. Linzer, C. Bruhn, *Eur. Polym. J.* **1994**, *30*, 549.

[17] M. Gedan-Smolka, D. Jehnichen, Hartmut Komber, D. Voigt, F. Böhme, M. Rätzsch, *Angew. Makromol. Chem.* **1995**, *229*, 159.

[18] M. Gedan-Smolka, D. Jehnichen, D. Fischer, L. Häußler, F. Böhme, M. Rätzsch, *Angew. Makromol. Chem.* **1995**, *228*, 41.

[19] H. R. Allcock, F.W. Lampe, J. E. Mark *Contemporary Polymer Chemistry*, Pearson Education, Inc., NJ USA **2003**.

[20] W. Xie, W.-P. Pan. K. C. Chuang, *J. Therm. Anal. Calorim.* **2001**, *64*,

477.

[21] R. Torrecillas, A. Baudry, J. Dufay, B. Mortaigne. *Polym. Degrad. Stab.* **1996**, *54*, 267.

[22] M. Iqbal, B. Norder, E. Mendes, T. J. Dingemans, *J. Polym. Sci., Part A: Polym. Chem.* **2009**, *47*, 1368.

[23] D. Y. Yoon, N. Masciocchi, L. E. Depero, C. Viney, W. Parrish, *Macromolecules* **1990**, *23*, 1793.

[24] J. Economy, W. Volksen, C. Viney, R. Geiss, R. Siemens, T. Karis, *Macromolecules* **1988**, *21*, 2777.

[25] H. R. Kricheldorf, G. Schwarz, *Polymer* **1990**, *31*, 481.

[26] N. S. Yoon, Y. J. Lim, M. Tahara, T. Takashi, Textile Res. J. **1996**, 66, 329.

[27] "Ticona Vectra Liquid Crystal Polymer (LCP) Product Information," Ticona, Summit, NJ, 07901, **2000**.

CHAPTER 3

Amorphous Poly(esterimide)s and Reactive Esterimide Oligomers Thereof

Abstract

A series of poly(esterimide)s with different molar ratios of N-(3'-hydroxyphenyl)trimellitimide (IM) and 4-hydroxybenzoic acid (HBA) (IM/HBA = 0.4/0.6, 0.5/0.5 and 0.7/0.3) were prepared with the aim to explore the morphology and thermomechanical properties of the poly(esterimide)s. All poly(esterimide)s, 4-IM/6-HBA, 5-IM/5-HBA and 7-IM/3-HBA, show semi-crystalline features whereas all melt pressed films are amorphous. By introducing reactive phenylethynyl end-groups an analogous series of reactive esterimide oligomers (7-IM/3-HBA–2K, 5K, and 9K) were obtained with excellent processability. We observe a flow point (T_f) for all 3 poly(esterimide)s films, which is associated with an increase in chain mobility and a decrease in segment–segment associations. The thermal and mechanical properties are independent on the molar composition and concentration of reactive end-groups. However, upon thermal post-treatment T_gs of 260 °C and 290 °C are obtained for 7-IM/3-HBA and 7-IM/3-HBA–2K, respectively. The as-pressed films show poor stress-strain behavior, *i.e.* tensile strengths of 35–49 MPa with an elongation at break of 1.5–2.2% were obtained. However, upon thermal stretching above the T_g the stress-strain results improve considerably. For instance, thermally stretched 7-IM/3-HBA shows a high tensile strength of 169 MPa and elongation at break of 3.3%.

3.1 Introduction

In the previous chapter we described the synthesis and properties of a biphasic semi-crystalline polyesterimide based on 30 mol% (3'-hydroxyphenyl)trimellitimide (IM) and 70 mol% 4-hydroxybenzoic acid (HBA) (Figure 3.1). Despite a glass transition temperature (T_g) of 205 °C, the as prepared films showed poor mechanical properties. Upon thermal stretching above the T_g the films show a dramatic increase in thermomechanical properties.

IM   HBA
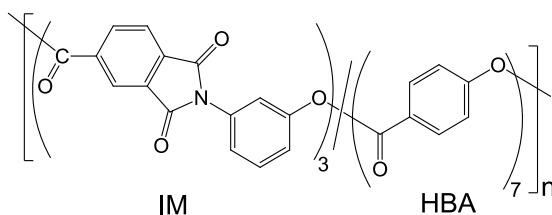
Figure 3.1. Chemical structure of the semi-crystalline polyesterimide 3-IM/7-HBA based on N-(3'-hydroxyphenyl)trimellitimide (IM) and 4-hydroxybenzoic acid (HBA) as discussed in *Chapter 2*.

In order to lower the melting temperature (T_m) and improve the processability and thermomechanical properties, we end-capped 3-IM/7-HBA with reactive phenylethynyl end-groups. In fact, introducing nonlinear or kinked monomers is another option to lower the backbone symmetry and disrupt crystallization. This lowers the T_m effectively while retaining the thermomechanical properties.[1–2] For instance, 3-IM/7-HBA has much better processability than poly(oxybenzoate) (pHBA) as presented in *Chapter* 2. Incorporating 30 mol% IM into pHBA effectively reduced the degree of crystallinity from 82% to 20%. This brings up the question whether a larger IM concentration can further improve the processability and thermomechanical properties of the polymer.

To further explore the effect of IM concentration on the processability, morphology, and thermomechanical properties, a series of poly(esterimide)s with different IM/HBA molar ratios (0.4/0.6, 0.5/0.5 and 0.7/0.3) was prepared and the results will be discussed in this chapter. Although poly(esterimide)s with the same composition have been synthesized by Gedan-Smolka[3] and Kricheldorf[4] under different polymerization conditions, the structure-property relationship of the resulting polymers are not yet fully understood. For example, Gedan-Smolka reported that poly(esterimide)s with IM/HBA molar ratio's of 0.5/0.5 and 0.7/0.3 are soluble in pentafluorophenol /chloroform-mixtures (1:1 v/v) at 25 °C. Kricheldorf, however, reported that the whole series poly(esterimide)s prepared in their laboratories are not soluble in any solvent. Furthermore, the processability and bulk properties, such as tensile strength and modulus, were not published. Therefore, a more detailed study on this series of poly(esterimide)s is needed. In addition, the effects of introducing phenylethynyl end-groups and applying a thermal post-treatment step will be discussed.

3.2 Experimental

3.2.1 Materials

4-Hydroxybenzoic acid (4-HBA) and acetic anhydride were purchased from Aldrich (Zwijndrecht, The Netherlands). Potassium acetate was purchased from Acros Organics (Geel, Belgium). 4-Phenylethynylphthalic anhydride (PEPA) was obtained from Hangzhou Chempro Tech Co., Ltd. The synthesis of the reactive end-groups, *i.e.* N-(4-carboxyphenyl)-4-phenylethynylphthalimide (PE-COOH) and N-(4-acetoxyphenyl)-4-phenylethynylphthalimide (PE-OAc) were reported elsewhere.[5] The detailed synthetic procedure of N-(3'-hydroxyphenyl)trimellitimide (IM)

has been described in *Chapter* 2. Poly(oxybenzoate) (pHBA) was purchased from Polysciences Europe GmbH (Eppelheim, Germany).

3.2.2 Synthesis of poly(esterimide)s and reactive oligomers

A series of poly(esterimide)s based on N-(3'-hydroxyphenyl)-trimellitimide (IM) and 4-hydroxybenzoic acid (HBA) with a molar ratio of 0.4/0.6, 0.5/0.5 and 0.7/0.3 were synthesized using standard melt condensation techniques as shown in Scheme 3.1. The polymers were labeled, 4-IM/6-HBA, 5-IM/5-HBA and 7-IM/3-HBA, respectively. The homopolymer of IM (pIM) was synthesized according to an identical procedure.

In order to study the effect of reactive end-groups on the processability and thermomechanical properties of IM rich poly(esterimide)s, we selected the 7-IM/3-HBA formulation as a representative backbone for our thermoset series. Three reactive oligomers based on 7-IM/3-HBA with a target number average molecular weight M_n of 2,000, 5,000, and 9,000 g·mol⁻¹ were prepared by controlling the concentration of the reactive end-groups using the Carothers equation.[6] The samples were labeled, 7-IM/3-HBA–2K, 7-IM/3-HBA–5K and 7-IM/3-HBA–9K, respectively. The integers refer to the polymer molecular weight, *i.e.* 2K = 2,000 g·mol⁻¹.
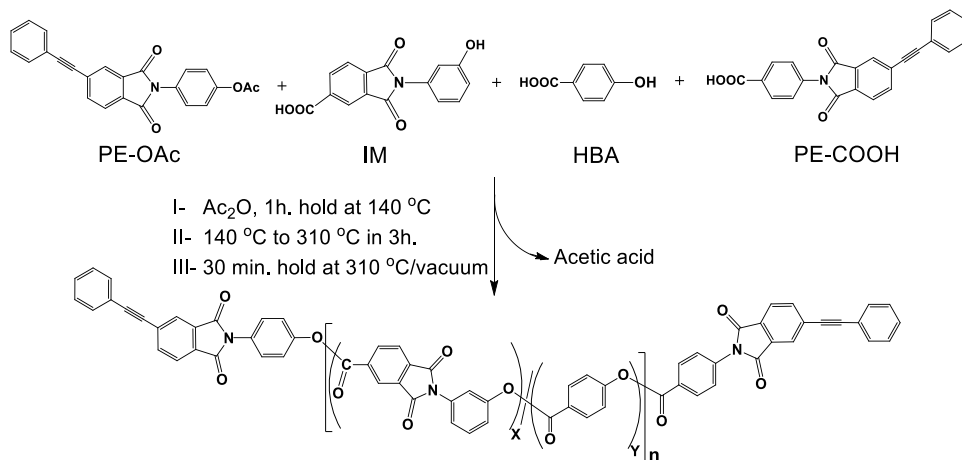
Scheme 3.1. Synthesis and backbone composition of the all-aromatic esterimide-based polymers and reactive oligomers with phenylethynyl end-groups.

The poly(esterimide)s and reactive oligomers thereof were prepared using the method described in *Chapter* 2 (section 2.2.2). The polymer backbone compositions are summarized in Table 3.1.

Table 3.1. Backbone composition of the poly(esterimide)s and reactive oligomers.

Sample	Molar ratio IM/HBA	End-group PE-OAc (mol/kg)	End-group PE-COOH (mol/kg)
4-IM/6-HBA	0.4/0.6	-	-
5-IM/5-HBA	0.5/0.5	-	-
7-IM/3-HBA	0.7/0.3	-	-
7-IM/3-HBA–9K	0.7/0.3	0.098	0.098
7-IM/3-HBA–5K	0.7/0.3	0.169	0.169
7-IM/3-HBA–2K	0.7/0.3	0.374	0.374

3.2.3 Preparation of thin films

The poly(esterimide)s and cured thermoset poly(esterimide)s films were melt pressed and thermally post-treated using the same method described in *Chapter* 2 (section 2.2.3).

3.2.4 Characterization

A Perkin Elmer Pyris Diamond TG/DTA was used to study the dynamic thermal stability. The polymers were initially heated to 370 °C and isothermally held at 370 °C for 1 h. under nitrogen to ensure full polymerization. After cooling to 25 °C, the samples were analyzed using a heating rate of 10 °C·min^{-1} under a nitrogen atmosphere.

The melt behavior of the polymers was determined by differential scanning calorimetry (DSC) using a Perkin Elmer Sapphire DSC with a heating rate of 20 °C·min^{-1}. All measurements were conducted under a nitrogen atmosphere.

A Leica DMLM optical microscope equipped with a Linkham hot stage was used to investigate the melt behavior as a function of time and temperature. The samples were investigated between glass slides upon heating using a heating rate of 50 °C·min^{-1}.

The rheological behavior of the polymers was investigated using a Rheometric MARS Ⅲ rheometer equipped with a force-rebalanced transducer in a parallel plate geometry. Parallel plates of 8 mm diameter were used and samples were prepared by compression molding (8 mm in diameter and 0.2 mm thick). The samples were investigated under a nitrogen atmosphere with temperature ramping (5 °C·min^{-1}) from 150 °C to a predetermined temperature followed by an isothermal hold at that temperature for 1 h. All experiments were performed at a frequency of 1.0 Hz and a strain amplitude of 0.1%, which is well within the linear

viscoelastic range (frequency of 0.1–10 Hz and a strain amplitude of 0.001–1.0%).

X-ray diffraction (XRD) analysis was conducted on a Bruker AXS D8 Discovery diffractometer, using a Cu-Kα radiation source. Wide-angle X-ray diffraction (WAXD) was performed using a distance of 6 cm between the sample and the detector and the exposure time was set to 5 min. The degree of crystallinity (%) was calculated using eqn. 2.1 (*Chapter* 2).

Dynamic mechanical thermal analyses (DMTA) was performed with a Perkin Elmer Diamond DMTA in a tension mode, using thin films (20±0.2) mm × (5±0.2) mm × (0.25±0.05) mm under a nitrogen atmosphere and at a heating rate of 2 °C·min^{-1}. All experiments were performed at a frequency of 1.0 Hz, static tension force of 2,000 mN, minimum tension force of 200 mN, tension gain of 1.5 and length amplitude of 5 μm. The minimum recordable storage modulus (E') was set to 1×10^4 Pa. In order to study the onset of the flowing temperature, a minimum tension force of 100 mN was applied alternatively.

A Zwick 1445 tensile tester with a 1 kN force cell was used to investigate the stress-strain behavior of the polymer films. Tensile tests were performed by fixating the films with an adhesive onto a rectangular frame with the side arms cut. All experiments were performed at 25 °C at a strain rate of 1 mm·min^{-1}. The data were reported as an average of 5 samples. The elastic modulus was measured by calculating the slope of the stress-strain curve between 0.1% and 0.3% strain.

3.3 Results and discussion

3.3.1 Synthesis of the poly(esterimide)s and reactive oligomers thereof

All poly(esterimide)s and reactive oligomers with phenylethynyl end-groups could be synthesized using a simple environmentally benign one-pot melt condensation procedure. The polymerizations were straightforward and no premature cross-linking of the phenylethynyl end-groups could be observed. The oligomers were ground into a fine powder and this powder was solid-state post-condensed at 270 °C for 24 h. under vacuum to complete the polymerization. All oligomers were easily synthesized in high yields and the synthetic procedure is very amenable to scale-up.

To quantify the molecular weight of the polymers and reactive oligomers, we attempted to find suitable solvents or solvent mixtures, *e.g.* dimethylacetamide, trifluoroacetic acid, pentafluorophenol/hexafluoro-isopropanol (1:1 v/v). However, our polymers and oligomers appeared completely insoluble, at 25 °C and elevated temperature, in the solvent/solvent mixtures mentioned above. Therefore, no characterization was feasible in solution. Our observations are in agreement with the results reported by Kricheldorf.[4] Land and Gedan-Smolka, however, reported that poly(esterimide)s with IM/HBA molar ratio's of 0.5/0.5 and 0.7/0.3 are soluble in *p*-chlorophenol at 45 °C or pentafluorophenol/chloroform-mixtures (1:1 v/v) at 25 °C.[3,7] This indicates that depending on polymerization method used, even with the same monomer composition, we are able to prepare different polymers. Gedan-Smolka and co-workers demonstrated that the homopoly-condensation rate of HBA is distinctly higher than that of IM. With the aim to prepare poly(esterimide)s with a random backbone distribution of monomer sequences, the melt condensation temperature was raised immediately from 270 °C to 320 °C. The polymerization method we used (heating rate of 1 °C·min^{-1}) promotes the formation of polyHBA (pHBA) or polyIM (pIM) rich blocks. The pHBA or pIM rich blocks prevent our polymers from dissolving in any solvent.

3.3.2 Thermal properties

TGA The thermal stability of the polymers and cured thermosets were evaluated using dynamic thermogravimetric analysis (TGA) at a heating rate of 10 °C·min^{-1}. High decomposition values ($T_d^{5\%}$ = 447–460 °C) and high char yields (61–68 wt%) were found, indicating that the dynamic thermal stability of these polymers is similar to that of the semi-crystalline polyesterimide 3-IM/7-HBA reported in *Chapter 2*. The thermal properties of the poly(esterimide)s are summarized in Table 3.2.

DSC The thermal behavior of the polymers and reactive oligomers was investigated using differential scanning calorimetry (DSC). Figure 3.2 depicts the first and second heating scans of the polymers using a heating rate of 20 °C·min^{-1}. The polymers show a glass transition temperature (T_g) in the range of 235–243 °C and endothermic peaks in the range of 300–359 °C upon the first heat (Table 3.2). After erasing the thermal history by quenching the samples from 390 °C to 25 °C, the second heat of 4-IM/6-HBA shows one endothermic peak at 302 °C only instead of multiple endothermic peaks. With the exception of a T_g at 241 °C and 234 °C for 5-IM/5-HBA and 7-IM/3-HBA, respectively, no endothermic peak is observed in their second heating scan. Figure 3.2 shows that the thermal behavior of the polyesterimide rich in HBA monomer 4-IM/6-HBA is similar to that of 3-IM/7-HBA as discussed in *Chapter* 2, confirming the semi-crystalline nature of 4-IM/6-HBA. However, the crystallization ability of 5-IM/5-HBA and 7-IM/3-HBA is poor, and crystallinity is only detectable after long post-condensation times. They are considered to be amorphous poly(esterimide)s here. More details with respect to their morphology will be discussed in section 3.3.4 (X-ray diffraction experiments).

Table 3.2. Thermal properties of the poly(esterimide)s, the reactive oligomers and their cured thermosets.

Sample	T_g (°C)[a]	Endothermic peak maximum (°C)[a]	T_g (°C)[b]	E' (GPa) at 25 °C	$T_d^{5\%}$ (°C)[c]	Char yield (wt%)[d]
4-IM/6-HBA	235	302, 334	205	6	447	61
5-IM/5-HBA	243	300	228	5	444	66
7-IM/3-HBA	242	333, 359	230	6	454	62
7-IM/3-HBA–9K	209	342	230	7	453	64
7-IM/3-HBA–5K	207	-	230	7	454	65
7-IM/3-HBA–2K	200	-	238	7	460	68

[a]T_g and endothermic peak maximum values of poly(esterimide)s and reactive oligomers were obtained from the first heating scan of DSC experiments. Heating rate 20 °C·min⁻¹/nitrogen atmosphere.
[b]T_g data were obtained from DMTA experiments using melt pressed films at 370 °C for 45 min., defined by the maximum of the loss modulus (E") peak. Heating rate 2 °C·min⁻¹/nitrogen atmosphere and a frequency of 1 Hz.
[c]Thermal stability was evaluated using dynamic TGA. The sample was cured by isothermal holding at 370 °C for 1 h. before the actual measurement. Heating rate 10 °C·min⁻¹/nitrogen atmosphere.
[d]Char yield at 600 °C.
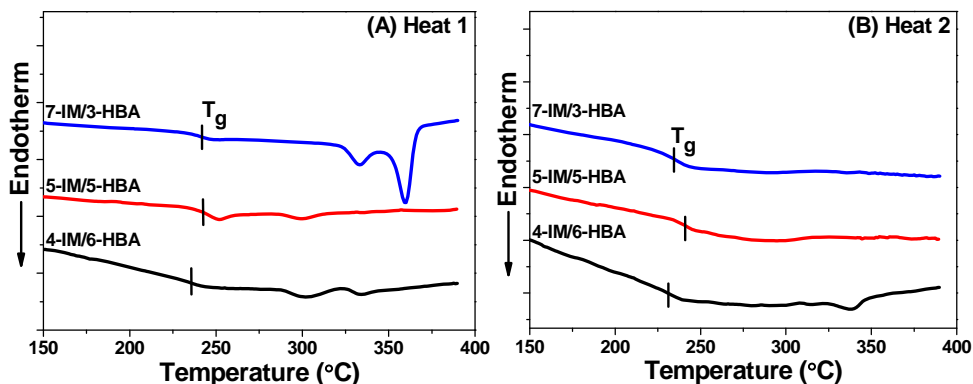
Figure 3.2. A- First and **B-** second DSC heating trace of the poly(esterimide)s after post-condensation (24 h. at 270 °C). Heating rate 20 °C·min^{-1}/nitrogen atmosphere.

All 7-IM/3-HBA reactive oligomers show a similar T_g at 200–209 °C upon the first heat (Table 3.2). Despite lowering the T_g by ~40 °C (upon the first heat), the incorporation of bulky phenylethynyl end-groups limits the molecular weight of the polymer and reduces the degree of crystallinity as compared to the polyesterimide parent polymer. For example, 7-IM/3-HBA–9K shows a single endothermic peak (T_m) at 342 °C, whereas 7-IM/3-HBA–5K and 7-IM/3-HBA–2K do not have any endothermic peak. In addition, all reactive oligomers show an increase by ~10 °C in T_g upon the second heat (Figure 3.3). This is attributed to polymerization (chain extension and/or crosslinking) via the reactive phenylethynyl end-groups during the first heat. All reactive oligomers appear to be amorphous after cure.
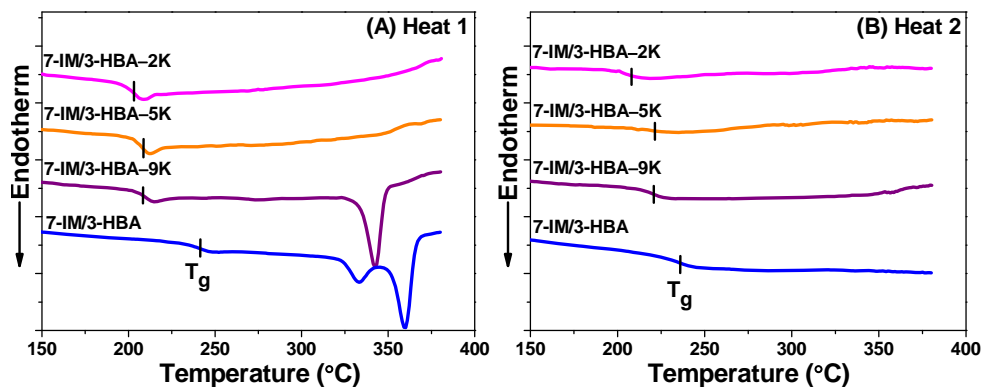
Figure 3.3. A- First and **B-** second DSC heating trace of the 7-IM/3-HBA parent polymer and reactive oligomers thereof after post-condensation (24 h. at 270 °C). Heating rate 20 °C·min^{-1}/nitrogen atmosphere.

Hot-stage optical microscopy Optical microscopy with crossed polarizers revealed another important difference between poly(esterimide)s poor and rich in imide-based monomer (IM). The 4-IM/6-HBA and 5-IM/5-HBA powders form a viscous biphasic melt at 370 °C. Polymer chains with a more random composition melt but polymer chains with a high HBA concentration do not melt. Shearing the biphasic melt of 4-IM/6-HBA and 5-IM/5-HBA at 370 °C reveals an immobile crystalline phase coexisting with a liquid crystalline phase (Figure 3.4A and 3.4B). A homogeneous, mobile, isotropic melt of 7-IM/3-HBA at 370 °C is shown in Figure 3.4C. This observation indicates that the IM unit is not mesogenic and the HBA unit is necessary to induce mesogenicity.[5] Reducing the molecular weight and introducing reactive end-groups gives a similar homogenous isotropic melt at 370 °C. The sample 7-IM/3-HBA–2K solidifies after a 5 min. isothermal hold due to curing, *i.e.* chain extension/crosslinking, of the reactive end-groups (Figure 3.4D).
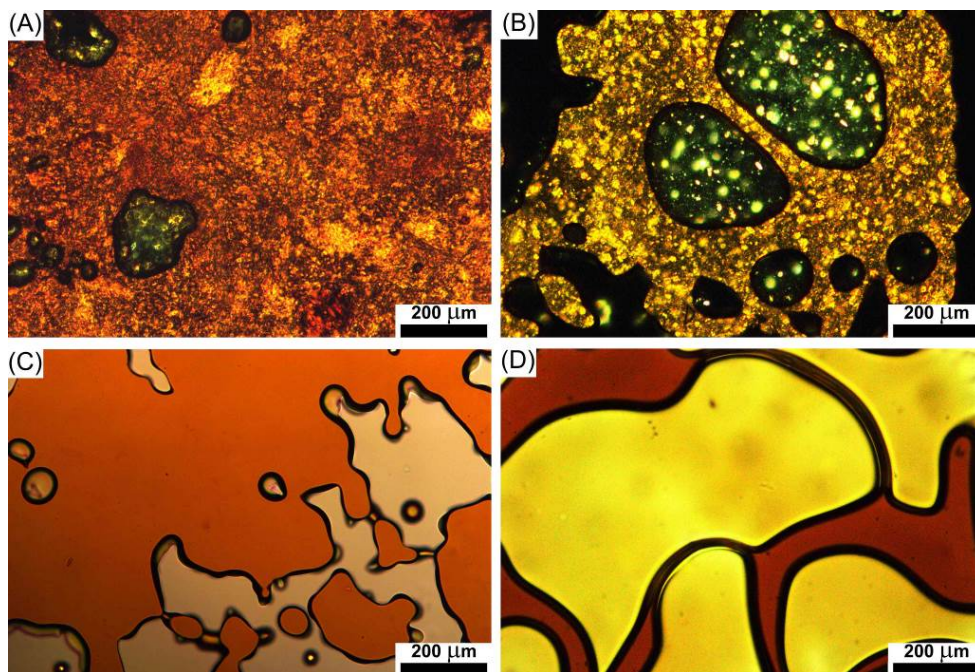
Figure 3.4. Microphotographs of the poly(esterimide)s powders (after solid-state post-condensation) at 370 °C. **A-** 4-IM/6-HBA forms a viscous biphasic melt (a liquid crystalline phase co-existing with a crystal phase). **B-** 5-IM/5-HBA forms a viscous biphasic melt (a liquid crystalline phase co-existing with a crystal phase). **C-** 7-IM/3-HBA forms a fluid homogenous isotropic melt. **D-** 7-IM/3-HBA–2K forms a homogenous isotropic melt, which solidifies after a 5 min. isothermal hold at 370 °C.

3.3.3 Rheology

Understanding the melt behavior of our polymers is critical in terms of defining the processing window. The storage modulus (G'), loss modulus (G") and complex melt viscosity ($|\eta^*|$) of the poly(esterimide)s and reactive oligomers as function of temperature and time were measured using a rheometer. Figure 3.5A shows that with temperature ramping

(5 °C·min^{-1}) from 150 °C to 370 °C the storage modulus of 7-IM/3-HBA shows two sharp drops, which occur at the T_g (235 °C) and T_m (330 °C), respectively. Both transitions are confirmed by the loss modulus peaks and are in a good agreement with the DSC results. After reaching the minimum value, the G' and G" of 7-IM/3-HBA start increasing and cross over after a 1 h. hold at 370 °C. It is evident that the increase is due to an increase in molecular weight and formation of chain entanglements.
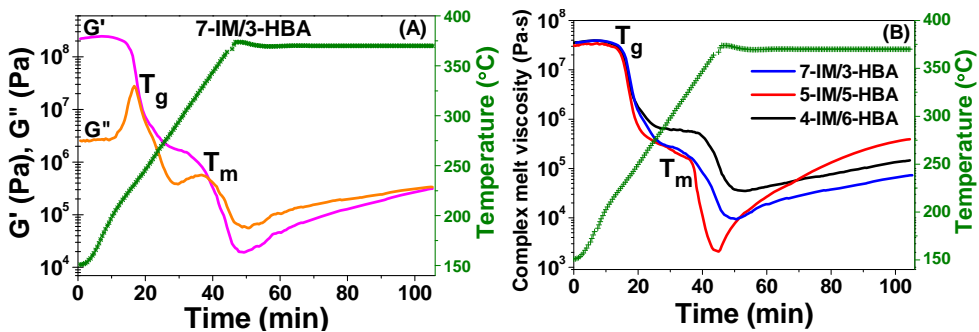
Figure 3.5. Rheological behavior of the poly(esterimide)s as function of temperature and a 1 h. hold at 370 °C. **A-** Storage modulus (G') and loss modulus (G") for 7-IM/3-HBA. **B-** Complex melt viscosities (|η*|) for all 3 poly(esterimide)s. Experiments were performed using a frequency of 1 Hz and heating rate of 5 °C min^{-1}/nitrogen atmosphere. The test specimens were prepared after the polymers were post-condensed at 270 °C for 24 h.

The plots of the complex melt viscosity (|η*|) as function of temperature and time allow us to quantify the processability of our polymers. Figure 3.5B shows that all poly(esterimide)s have an acceptable processing window of approximately 30 min. at 370 °C. Their melt viscosity reaches a minimum value at 370 °C. 5-IM/5-HBA exhibits the lowest viscosity (2×10^3 Pa·s), which is attributed to the most random IM/HBA sequence distribution. After reaching the minimum value, the

viscosity of all poly(esterimide)s starts increasing, which we believe is the result of transesterification and polymerization taking place during the 1 h. hold at 370 °C (effectively post condensing the polymer).

Figure 3.6A shows the complex melt viscosity of the reactive oligomer series (7-IM/3-HBA–2K, –5K and –9K). As could be anticipated, all oligomers display broader processing windows when compared with the polyesterimide parent compound (Figure 3.6B). After reaching a minimum value, the viscosity of the reactive oligomers increases, but this time the increase corresponds to curing of the phenylethynyl end-groups during temperature ramping.[3] For example, chain extension and cross-linking starts to take place at 350 °C for 7-IM/3-HBA–2K, leading to an increase in molecular weight and hence a rapid increase in |η*|.
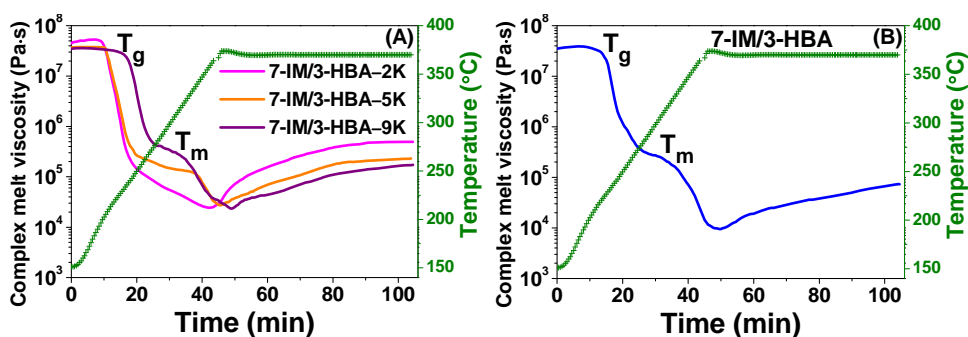
Figure 3.6. Rheological behavior of the 7-IM/3-HBA series as function of temperature and a 1 h. hold at 370 °C. **A-** 7-IM/3-HBA reactive oligomers and **B-** 7-IM/3-HBA high molecular weight parent polymer. Experiments were performed using a frequency of 1 Hz and heating rate of 5 °C·min^{-1} /nitrogen atmosphere. The test specimens were prepared after the polymers were post-condensed at 270 °C for 24 h.

3.3.4 X-ray diffraction (XRD) analysis

71

Wide-angle X-ray diffraction (WAXD) studies were performed to investigate the morphology of the polymer powders and melt pressed films. Figure 3.7 shows that the WAXD patterns of 4-IM/6-HBA and 5-IM/5-HBA powders after post-condensation (24 h. at 270 °C) show similar features as observed for poly(oxybenzoate) (pHBA). The characteristic 2θ = 15.8°, 19.5°, 23.1° and 29.1° peaks for pHBA are clearly visible and confirm the presence of pHBA blocks.[8-11] From the XRD data it is clear that incorporation of 40–50 mol% co-monomer in pHBA reduces the perfection of crystallites but the pHBA still dominates the crystal structure of 4-IM/6-HBA and 5-IM/5-HBA. These results are in contrast with 7-IM/3-HBA. This WAXD pattern shows a strong resemblance to the homopolymer of IM (pIM). 7-IM/3-HBA possesses a degree of crystallinity of 13%, which is 4% lower than that of pIM. This explains the sharp endothermic peaks of 7-IM/3-HBA observed in the DSC experiment (first heat).
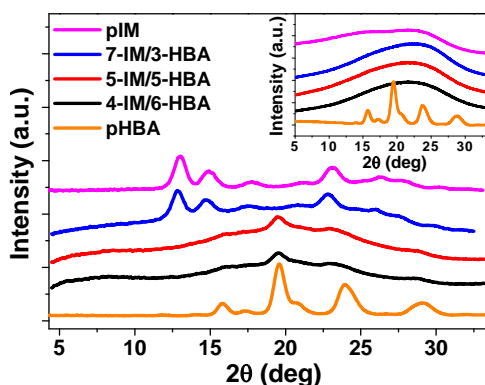
Figure 3.7. XRD analyses of the polyesterimide polymer powders (after post-condensation at 270 °C for 24 h.). All diffraction patterns were recorded at 25 °C. Also shown are the homopolymers of IM (pIM) and HBA (pHBA) for reference purposes. The inset shows the WAXD pattern of poly(esterimide)s films that were prepared using a hot press at 370 °C for 45 min.

Processing the powders into films using a hot press at 370 °C, results in stiff and brittle films. The inset of Figure 3.7 shows clear characteristic peaks of pHBA and no characteristic reflections from the crystals of poly(esterimide)s and pIM, which suggests that the poly(esterimide)s and pIM films have become amorphous.[12-13] This indicates that the crystallinity of the poly(esterimide)s and pIM, induced during the post condensation step, is mostly lost during the high temperature film processing step. Either the polymers have transesterified, resulting in a more random monomer sequence, or the rate of cooling is too fast, which prevents crystallization. However, melt pressing and fast cooling only lowers the crystallinity of pHBA from 82% to 48%, the WAXD pattern is unchanged because the pseudohexagonal chain packing of pHBA is stable up to 500 °C.[11] With respect to the endothermic peak of 4-IM/6-HBA in the second heat of the DSC, this peak might correspond to the remaining crystallites (∼4%), which did not completely melt in the first heat. The thermal and mechanical properties of the amorphous poly(esterimide)s films have been measured and the results will be discussed in the following sections.

3.3.5 Dynamic mechanical thermal analysis (DMTA)

In order to explore the thermomechanical properties of our polymers, the storage modulus (E') and loss modulus (E") as function of temperature were studied using dynamic mechanical thermal analysis (DMTA). Thin films of the poly(esterimide)s and cured thermosets were used for these DMTA experiments and the results are summarized in Figure 3.8 and Table 3.2.

The high storage moduli of 6 GPa (25 °C) for all poly(esterimide)s (Figure 3.8A) are relatively constant up to their T_gs. 4-IM/6-HBA shows a T_g at ∼205 °C, which is identical to that of 3-IM/7-HBA in *Chapter* 2.

However, most copolyesters of HBA only possess T_gs in the range of 100–140 °C.[14-18]. This demonstrates that incorporation of imide-based monomers is very efficient in increasing the T_g of HBA-based polyesters. When the molar fraction of imide monomer exceeds 50%, as for 5-IM/5-HBA and 7-IM/3-HBA, the T_g increases to ~230 °C. The increase in T_g is associated with an increase in larger (3-ring) IM monomeric units, a decrease in chain mobility and stronger chain–chain interactions (imide-imide π–π interactions).
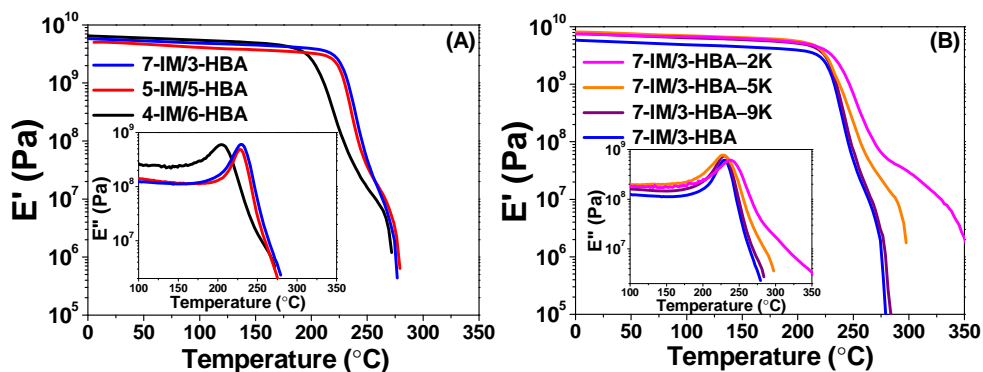
Figure 3.8. DMTA analysis of the poly(esterimide)s and cured thermoset films. **A-** Storage moduli (E') as function of temperature for the poly(esterimide)s films. **B-** Storage moduli (E') as function of temperature for the cured 7-IM/3-HBA films. The insets show the loss modulus (E") near the glass transition. Heating rate 2 °C·min^{-1}/nitrogen atmosphere and a frequency of 1 Hz.

The incorporation of small concentrations of phenylethynyl reactive end-groups does not lead to a significant improvement in the thermomechanical properties of the final after cure films (Figure 3.8B). For instance, the storage modulus (7 GPa) and T_g (230 °C) of 7-IM/3-HBA–5K and 7-IM/3-HBA–9K are similar to that of 7-IM/3-HBA. However,

7-IM/3-HBA–2K, with the largest concentration of phenylethynyl end-groups, displays a T_g of 238 °C. This is reasonable because the phenylethynyl end-groups cross-linking during the curing process and form a partially cross-linked network, which typically increases the T_g due to a reduction in chain mobility.

During the DMTA experiments we noticed that the polyesterimide films show a distinct transition in storage modulus when heated well above their T_g (Figure 3.8A). This thermodynamic transition has been designated as T_{ll}, a liquid-liquid transition by Boyer in 1970s.[19-22] It was observed in some traditional amorphous polymers, *i.e.* atactic polystyrene, polybutadiene and random copolymers thereof.[23] Lobanov *et al.* suggest that this transition is associated with an increase in chain mobility and a decrease in segment-segment associations.[24] We believe that reporting this transition as a flow point (T_f) is more appropriate, since T_{ll} suggests a transition between two different fluid states.[25] Figure 3.9 shows the T_f of the 7-IM/3-HBA film at 270 °C (blue line) where the segments of the macromolecules tend to exhibit liquid–like behavior with segmental contacts. The T_f of the 7-IM/3-HBA film shifts from 270 °C to 305 °C when 100 mN of minimum static tension force is applied instead of 200 mN. Because the tension force is reduced, the system needs more thermal energy to disrupt the segment–segment associations. In addition, a same transition is observed in Figure 3.8B for the 7-IM/3-HBA–9K film. Because 7-IM/3-HBA–9K has relatively low concentration of phenylethynyl end-groups, chain extension occurs rather than cross-linking during film melt pressing. In comparison to 7-IM/3-HBA and 7-IM/3-HBA–9K, the transition of 7-IM/3-HBA–5K and 7-IM/3-HBA–2K is more pronounced due to the presence of chemical cross-links and the formation of a distinct rubber plateau. The subsequent drop of E' for 7-IM/3-HBA–5K and 7-IM/3-HBA–2K at 300 °C and 350 °C suggests that our thermoset films were not fully cured under the conditions used (370 °C for 45 min.).
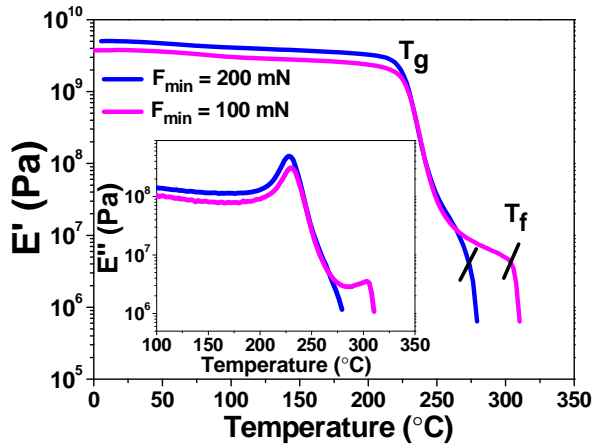
Figure 3.9. Storage moduli (E') and loss moduli (E") as function of temperature for the 7-IM/3-HBA film at two different minimum static tension forces (100 and 200 mN).

We learned from the previous chapter that the static thermal post treatment results in a dramatic increase in T_g for semi-crystalline polyesterimide films. Herein, a same thermal treatment (heating rate of 2 °C·min⁻¹) was performed on the amorphous poly(esterimide)s films to increase T_g. With an increase in thermal treatment temperature, the T_gs of 7-IM/3-HBA and 7-IM/3-HBA–9K show a similar increasing trend (Figure 3.10). Due to the large concentration of phenylethynyl reactive end-groups, 7-IM/3-HBA–2K benefits most from the heat treatment in terms of increasing the T_g. The higher the thermal treatment temperature, the larger the improvement in T_g. When the as-pressed films were thermally treated from 25 °C to 380 °C using a heating rate of 2 °C·min⁻¹, 7-IM/3-HBA and 7-IM/3-HBA–9K films show an increase in T_g of ~30 °C, whereas 7-IM/3-HBA–2K film exhibits an increase in T_g of ~50 °C. The thermally treated films are brittle, and could not be used for stress-strain experiments.
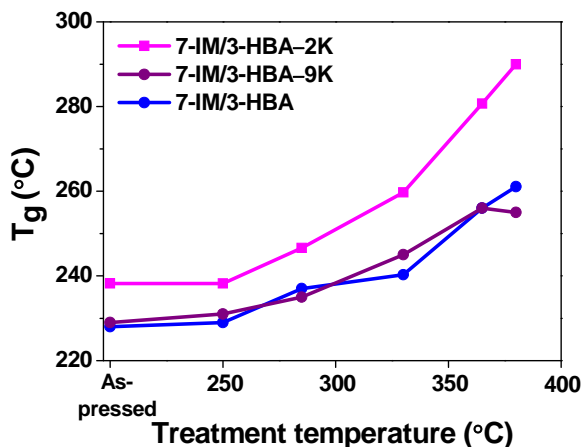
Figure 3.10. The T_g of 7-IM/3-HBA and thermoset films plotted as function of thermal treatment temperature. All films were thermally treated from 25 °C to the predetermined temperatures with a heating rate 2 °C·min⁻¹/nitrogen atmosphere and immediately cooled down to 25 °C (cooling rate ~3 °C·min⁻¹). T_gs were measured using DMTA (maximum of E") with a heating rate 2 °C·min⁻¹/nitrogen atmosphere and a frequency of 1 Hz.

3.3.6 Origin of the T_g increase

The increase in T_g of the semi-crystalline polyesterimide 3-IM/7-HBA has been explained by an increase in polymer molecular weight and the removal of small molecule plasticizing species in *Chapter 2*. As the polymer cannot be dissolved, measuring the zero-shear viscosity using a rheometer is an alternative way to probe whether the thermal post treatment has an effect on the polymer molecular weight. Because 3-IM/7-HBA remains biphasic (a liquid crystal phase coexists with a crystalline phase) until decomposition, this polymer is not suitable for zero-shear viscosity measurements. 7-IM/3-HBA is a better candidate as this polymer is amorphous. Therefore, the as-pressed and thermally

77

treated films of 7-IM/3-HBA were used to study the effect of thermal treatment on the molecular weight.

From a series of frequency scans the complex viscosity data was collected at different temperatures (240–280 °C, $\Delta T = 5$ °C) and used to construct a master curve ($T_{reference} = 260$ °C) using a temperature-time-superposition tool. Figure 3.11 shows that the complex melt viscosity decreases in a linear fashion as a function of frequency (10^{-4}–10 Hz). The complex melt viscosity shows no plateau (zero-shear viscosity) in the low frequency region, indicating that little or no entanglements exist in the polymer melt. With an increase in thermal treatment temperature, an obvious increasing trend in complex viscosity of the thermally treated films is observed. For instance, the as-pressed 7-IM/3-HBA film shows a complex viscosity of 8.5×10^4 Pa·s at 1 Hz. The complex viscosity of the 7-IM/3-HBA iii film (thermally treated from 25 °C to 365 °C) is 8.8×10^5 Pa·s at 1 Hz, which is an increase by a factor of 10 as compared to that of the as-pressed film. This observation reflects that the molecular weight of the film was indeed increased by the thermal treatment method used.[26] Of course, the removal of small molecules or by-products also contributes to the increase in complex viscosity.
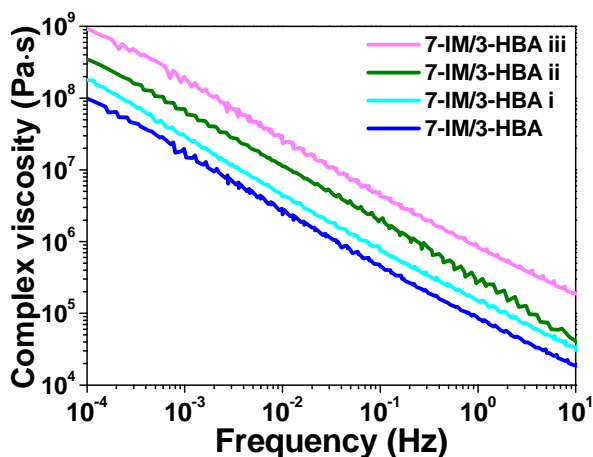
Figure 3.11. Complex viscosity (master curve) of 7-IM/3-HBA films plotted as function of frequency. The as-pressed film is labeled 7-IM/3-HBA. The films were thermally treated from 25 °C to 285 °C, 330 °C and 365 °C with a heating rate 2 °C·min⁻¹/nitrogen atmosphere and were labeled i, ii and iii, respectively.

3.3.7 Tensile properties

The polyesterimide films and the cured thermoset films prepared by melt pressing are brittle (Table 3.3), and show poor tensile properties, *i.e.* tensile strengths are in the range of 35–49 MPa and an elongation at break of 1.5–2.2%. These results indicate that the tensile properties are independent of the molar composition whether or not the polymers were prepared via the reactive oligomer route.

Table 3.3. Tensile properties of the polyesterimide– and cured thermoset films. The data shown is an average of 5 tensile specimens.

Sample	Tensile strength (MPa)	Elastic modulus (GPa)	Elongation at break (%)
4-IM/6-HBA	45±8	2.0±0.4	2.1±0.4
5-IM/5-HBA	49±5	2.0±0.2	2.0±0.3
7-IM/3-HBA	49±7	2.0±0.3	2.2±0.3
7-IM/3-HBA–9K	46±6	2.0±0.2	2.0±0.2
7-IM/3-HBA–5K	48±5	2.0±0.3	1.9±0.3
7-IM/3-HBA–2K	35±6	2.1±0.1	1.5±0.5

Upon thermal stretching above T_g the brittle films tend to become much more flexible and easier to handle. Figure 3.12 shows that the tensile strength of the thermally stretched films 7-IM/3-HBA SR1 and SR4 increased by a factor of 3.0 and 3.4, respectively, compared to the as-pressed films. Their elastic modulus increased from 2.0 GPa to 3.8 and 5.4 GPa, respectively. With the largest concentration of reactive end-groups, one can anticipate an obvious improvement in the tensile properties for 7-IM/3-HBA–2K. This will be aided by additional chain extension and cross-linking during the thermal stretching procedure. The thermally stretched films 7-IM/3-HBA–2K SR1 and SR4 indeed show an increasing trend, but the increase is less than that for 7-IM/3-HBA. Typically, when polymer fibers or films are stretched, the tensile strength increases and the elongation at break decreases.[27] However, the elongation at break of our thermally stretched 7-IM/3-HBA films showed a moderate increase from 2.2% to 3.3%. The elongation at break for the 7-IM/3-HBA–2K samples remained roughly the same. In terms of optimal properties, the 7-IM/3-HBA film shows the best overall performance after stretching the film once (entry 2, Table 3.4) The data of tensile properties are summarized in Table 3.4.
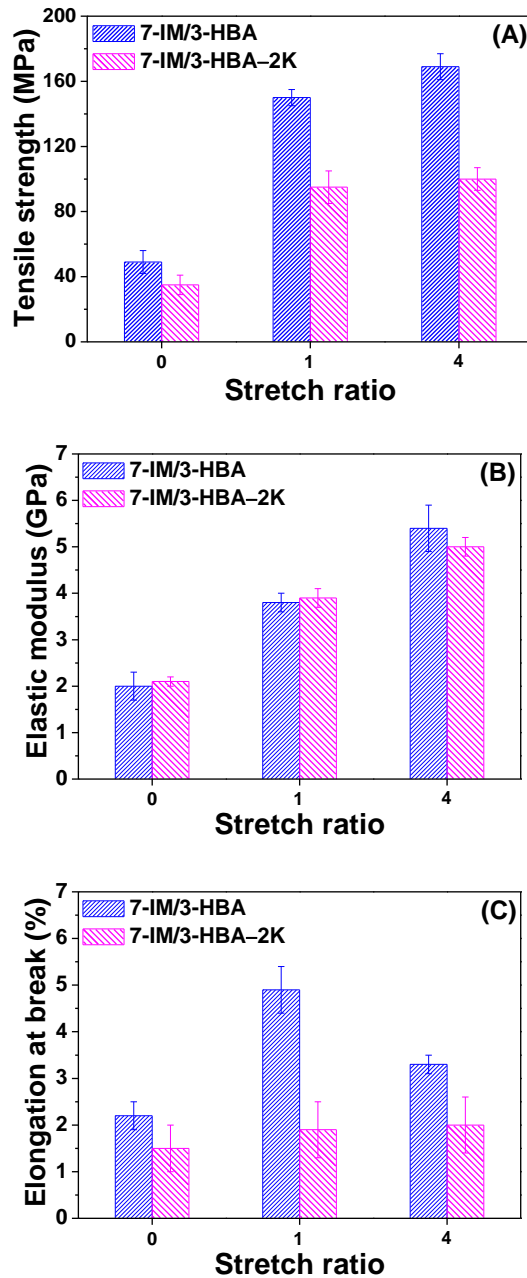
Figure 3.12. The tensile properties of 7-IM/3-HBA and cured thermoset films (5 samples) as function of stretch ratio. **A-** Tensile strength. **B-** Tensile modulus. **C-** Elongation at break.

Table 3.4. Tensile properties of the as-pressed and stretched films. The as-pressed films are labeled SR0. Films stretch by 100% and 400% were labeled SR1 and SR4, respectively. The data shown is an average of 5 tensile specimens.

Entry	Sample	Tensile strength (MPa)	Elastic modulus (GPa)	Elongation at break (%)
1	7-IM/3-HBA SR0	49±7	2.0±0.3	2.2±0.3
2	7-IM/3-HBA SR1	150±5	3.8±0.2	4.9±0.5
3	7-IM/3-HBA SR4	169±8	5.4±0.5	3.3±0.2
4	7-IM/3-HBA–2K SR0	35±6	2.1±0.1	1.5±0.5
5	7-IM/3-HBA–2K SR1	95±10	3.9±0.2	1.9±0.6
6	7-IM/3-HBA–2K SR4	100±7	5.0±0.2	2.0±0.6

3.4 Conclusions

We have systematically studied how the molar ratio of N-(3'-hydroxyphenyl)trimellitimide (IM) and 4-hydroxybenzoic acid (HBA) affects the bulk properties of IM/HBA–based poly(esterimide)s. High molecular weight poly(esterimide)s (4-IM/6-HBA, 5-IM/5-HBA and 7-IM/3-HBA) and an analogous series of reactive esterimide oligomers (7-IM/3-HBA–2K, 5K, and 9K) were synthesized using a one-pot melt condensation method. The as-synthesized poly(esterimide)s tend to crystallize during post-condensation. The observation of endothermic peaks in DSC scans and crystalline reflections observed by XRD confirms the existence of pHBA or pIM blocks depending on whether the polymer is poor or rich in IM monomer. Processing the powders into films using a hot press at 370 °C, results in amorphous films with poor stress-strain behavior. However, upon thermal stretching above T_g, 7-IM/3-HBA and 7-IM/3-HBA–2K films show acceptable stress-strain properties, *i.e.* tensile

strength of 170 and 100 MPa and strain at break of ~2–3%. A transition above T_g, designated by us as the flow point (T_f) was observed for all 3 poly(esterimide)s films and the 7-IM/3-HBA–9K film with a low concentration of reactive end-groups. The 7-IM/3-HBA–2K film exhibits a rubbery plateau instead of T_f above T_g, which is due to the presence of chemical cross-links. A static thermal treatment results in a T_g of 260 °C for 7-IM/3-HBA and 290 °C for 7-IM/3-HBA–2K. Our results suggest that an appropriate post-treatment could be very beneficial toward improving the thermal and mechanical properties of this family of poly(esterimide)s.

3.5 References

[1]   S. Chang, C. D. Han, *Macromolecules* **1996**, *29*, 2103.

[2]   P. K. Bhowmik, H. Han, *Macromolecules* **1993**, *26*, 5287.

[3]   M. Gedan-Smolka, D. Jehnichen, Hartmut Komber, D. Voigt, F. Böhme, M. Rätzsch, *Angew. Makromol. Chem.* **1995**, *229*, 159.

[4]   H. R. Kricheldorf, V. Linzer, C. Bruhn, *Eur. Polym. J.* **1994**, *30*, 549.

[5]   A. Knijnenberg, E. S. Weiser, T. L. StClair, E. Mendes, T. J. Dingemans, *Macromolecules* **2006**, *39*, 6936.

[6]   R. J. Young, P. A. Lovell, *Introduction to Polymer*, 2nd ed. Chapman and Hall, London, **2000**.

[7]   H. Land, M. Gedan, M. Rätzsch, F. Böhme (Hoechst Aktiengesellschaft), EP0582220 A2, **1994**.

[8]   J. Economy, W. Volksen, C. Viney, R. Geiss, R. Siemens, T. Karis, *Macromolecules* **1998**, *21*, 2777.

[9]   M. Nolan, J. C. Greer, *J. Phys. Chem. B* **1999**, *103*, 7111.

[10]   D. Y. Yoon, N. Masciccochi, L. E. Depero, C. Viney, W. Parrish, *Macromolecules* **1990**, *23*, 1793.

[11]   H. R. Kricheldorf, G. Schwarz, *Polymer* **1990**, *31*, 481.

[12]   V. Lehto, M. Tenho, K. Vähä-Heikkilä, P. Harjunen, M. Päällysaho, J.

Välisaari, P. Niemelä, K. Järvinen, Powder Technol. **2006**, *167*, 85.

[13] L. Červinka. J. Non-Cryst. Solids **1976**, *21*, 125.

[14] E. W. Choe, G. W. Calundann (Celanese Co.), *Ger. Pat.* 3015386, **1980**.

[15] G. W. Calundann (Celanese Co.), *US. Pat.* 4395513, **1983**.

[16] H. R. Kricheldorf, F. Ruhser, *Polymer* **1992**, *33*, 2431.

[17] *H. R.* Kricheldorf, V. Döring, *Polymer* **1992**, *33*, *5321.*

[18] H. R. Kricheldorf, G. Schwarz, *Makromolek. Chem., Rapid Commun.* **1989**, *10*, 243.

[19] S. J. Stadnicki, J. K. Gillham, R. F. Boyer, *J. Appl. Polym. Sci.* **1976**, *20*, 1245.

[20] R. F. Boyer, *J. Appl. Polym. Sci.* **1987**, *33*, 955.

[21] C. M. Warner, R. F. Boyer, *J. Polym. Sci., Part B: Polym. Phys.* **1992**, *30*, 1177.

[22] J. Chen, C. Kow, L. J. Fetters, D. J. Plazek, *J. Polym. Sci., Polym. Phys. Ed.* **1985**, *23*, 13.

[23] R. F. Boyer, *J. Macromol. Sci.-Phys.,* **1980**, B18, 461.

[24] A. M. Lobanov, S. Y. Frenkel, *Polym. Sci. USSR*, **1980**, *22*, 1150.

[25] C. D. Han, K. Y. Lee, N. C. Wheeler, *Polym. Eng. Sci.* **1996**, *36*, 1360.

[26] S. B. Warner, J. Lee, *J. Polym. Sci., Part B: Polym. Phys.* **1994**, *32*, 1759.

[27] N. S. Yoon, Y. J. Lim, M. Tahara, T. Takashi, Textile Res. J. **1996**, 66, 329.

CHAPTER 4

All-aromatic Liquid Crystal (block) Copoly(esterimide)s

Abstract

In order to improve the processability of 4-hydroxybenzoic acid (HBA), N-(3'-hydroxyphenyl)trimellitimide (IM) based poly(esterimide)s we introduced 6-hydroxy-2-naphthoic acid (HNA) into the polymer backbone. Due to the low reactivity of IM an ABA-triblock copolymer with two distinct T_gs was obtained. The first T_g at ~120 °C can be assigned to an HBA/HNA block (block B) and the second T_g at ~220 °C can be assigned to an HBA/IM block (block A). This is the first example, to the best of our knowledge, of a main-chain LC block copolymer prepared *via* a simple one-pot melt polymerization method. Dynamic mechanical thermal analysis (DMTA) of cured films confirms the formation of an ABA-triblock structure, with the HBA/HNA block located at the center of the polymer chain and HBA/IM phenylethynyl-terminated blocks positioned at the chain-ends. Scanning electron microscopy (SEM) experiments show a gradual change in morphology, from a typical fibrous LCP texture for the HBA/HNA rich polymers to a more consolidated morphology for the HBA/IM rich polymers. At low IM concentrations very little phase separation seems to occur, confirming a high degree of compatibility between the A- and B-block. All LC copolymers and reactive oligomers possess stable melt behavior and good processability.

4.1 Introduction

In previous chapters we concentrated on understanding the structure-property relationship of all-aromatic poly(esterimide)s and cross-linkable oligomers based on N-(3'-hydroxyphenyl)trimellitimide (IM) and 4-hydroxybenzoic acid (HBA), as shown in Figure 4.1. We specifically targeted this family because introducing imide moieties with a kinked structure in a polyester host polymer allows us to increase the T_g (> 200 °C) and lower T_m of the final polymer. Similar IM/HBA formulations were explored in the 90s,[1-4] but our main interest is in understanding how IM, an AB-type imide monomer, affects the overall polymer morphology (amorphous, semi-crystalline or liquid crystalline), processing characteristics and the final thermomechanical properties. Imide-based monomers are interesting building blocks as they introduce strong chain-chain interactions via imide-imide π-π stacking interactions. This could be used as a tool to control the liquid crystal phase type in this family of polymers.
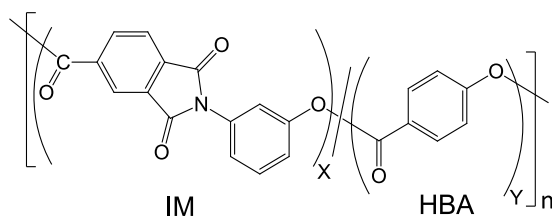
Figure 4.1. Representative backbone structure of non-linear IM/HBA poly(esterimide)s based on *N*-(3'-hydroxyphenyl)trimellitimide (IM) and 4-hydroxybenzoic acid (HBA) as systematically studied in *Chapters 2 and 3*.

Initially introducing 30 mol% IM into a rigid highly crystalline polyHBA (pHBA) host results in a complex multi-phase polymer composite

(*Chapter 2*). It is important to note that the formation of pHBA blocks is problematic, even at IM concentrations as high as 70% (*Chapter 3*). Because HBA is often employed as mesogenic building block for preparing thermotropic liquid crystalline polymers (TLCPs), the presence of HBA tends to induce high crystal-to-nematic melting points (T_{K-N}).[5-8] For example, Xydar™, which is prepared from HBA, 4,4'-biphenol (BP) and terephthalic acid (TA) exhibits excellent thermomechanical properties but this polymer is difficult to process due to the high T_{K-N} (> 390 °C) (Figure 4.2A).[9-10] To disrupt crystallinity and suppress the T_{K-N}, 2,6-naphthalene moieties such as 2,6-naphthoyl or 2,6-dioxynaphthalene were introduced into main-chain TLCPs.[11] The success of this approach is perhaps best illustrated by the following two examples: the T_{K-N} of the copolymer of HBA, 2,6-naphthoic acid and hydroquinone was reported to be 325–340 °C[12] and the T_{K-N} of a TA and 2,6-dihydroxynaphthalene copolymers was reported to be as low as 210 °C.[13]
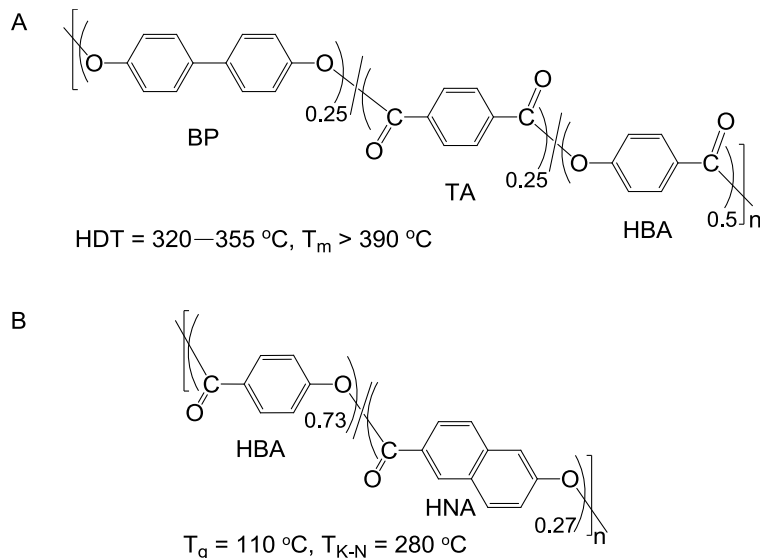
Figure 4.2. Examples of commercially available thermotropic liquid crystalline polyesters Xydar™ and Vectra-A™.

The most successful example to date must be the LC copolyester of HBA and 6-hydroxy-2-naphthoic acid (HBA$_{0.73}$/HNA$_{0.27}$) that has been commercialized under the trade name Vectra-A™ (Figure 4.2B).[14-15]

With the aim to further improve the processability and promote the formation of a stable liquid crystal phase in IM/HBA–based poly(esterimide)s, we introduced HNA into the backbone. A series of 3-component poly(esterimide)s with different molar ratio's of IM, HBA and HNA will be presented and the processability, morphology and thermomechanical properties of the all-aromatic LC poly(esterimide)s will be discussed. The effects of introducing phenylethynyl end-groups will be discussed as well.

4.2 Experimental

4.2.1 Materials

4-Hydroxybenzoic acid (4-HBA) and acetic anhydride were purchased from Aldrich (Zwijndrecht, The Netherlands). 6-Hydroxy-2-naphthoic acid (HNA) was purchased from Ueno Fine Chemicals Ltd and potassium acetate was purchased from Acros Organics (Geel, Belgium). 4-Phenylethynylphthalic anhydride (PEPA) was obtained from Hangzhou Chempro Tech Co., Ltd. The synthesis of the reactive end-groups, *i.e.* N-(4-carboxyphenyl)-4-phenylethynylphthalimide (PE-COOH) and N-(4-acetoxyphenyl)-4-phenylethynylphthalimide (PE-OAc) were reported elsewhere.[16] The detailed synthetic procedure for N-(3'-hydroxyphenyl)trimellitimide (IM) has been described in *Chapter* 2.

4.2.2 Synthesis of LC poly(esterimide)s and reactive oligomers

A series of LC poly(esterimide)s based on N-(3'-hydroxyphenyl)-trimellitimide (IM), 4-hydroxybenzoic acid (HBA) and 6-Hydroxy-2-naphthoic acid (HNA) was synthesized using standard melt condensation techniques as shown in Scheme 4.1. The samples were labeled LCP-xxIM according to the feed ratio of IM in the polymerization, so LCP-22IM refers to a IM/HBA/HNA molar ratio of 0.22/0.51/0.27. An all ester-based reference polymer, with a HBA/HNA molar ratio of 0.73/0.27, was synthesized according to an identical procedure but without IM and labeled "LC-Polyester".

In order to study the effect of reactive end-groups on the processability and thermomechanical properties of HBA-rich and IM-rich poly(esterimide)s, we selected the LCP-22IM and LCP-51IM formulations as representative backbones for our thermoset series. Two reactive oligomers based on each formulation with a target number average molecular weight M_n of 5,000 and 9,000 g·mol^{-1} were prepared by controlling the concentration of the reactive end-groups using Carothers equation.[17] The samples were labeled, LCP-22IM–5K, LCP-22IM–9K, LCP-51IM–5K and LCP-51IM–9K, respectively. The integers refer to the polymer molecular weight, *i.e.* 5K = 5,000 g·mol^{-1}.

The LC poly(esterimide)s and reactive oligomers were prepared using the method described in *Chapter* 2 (section 2.2.2). The polymer backbone compositions are summarized in Table 4.1.
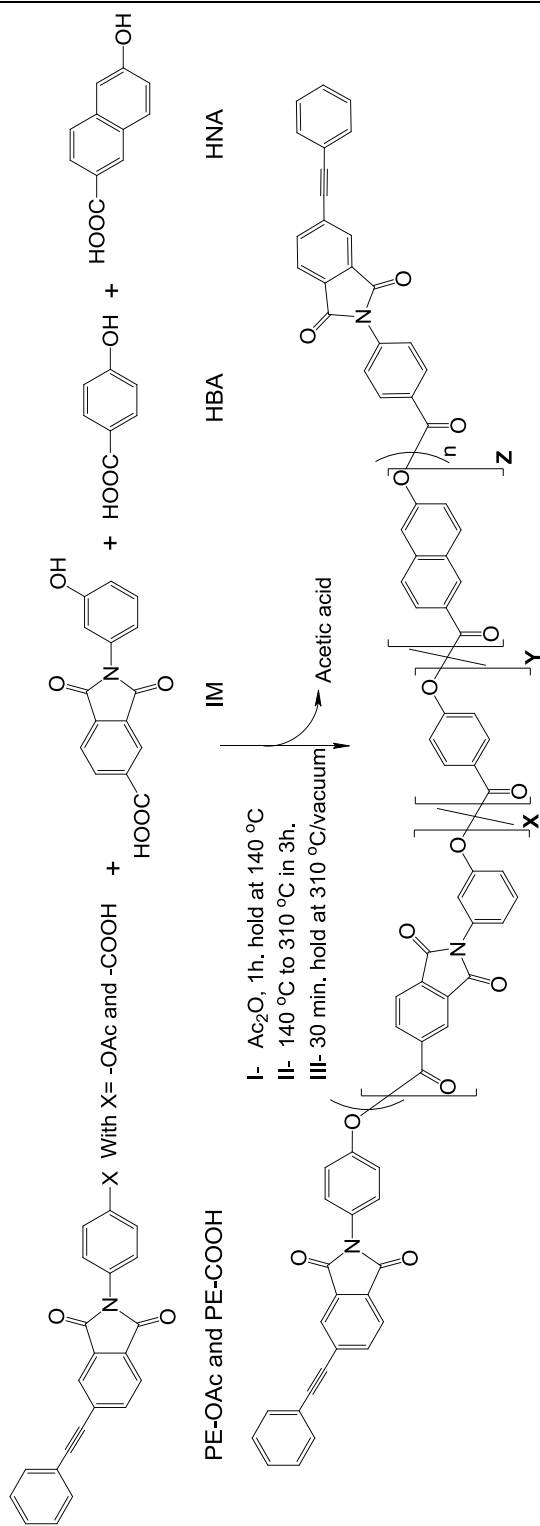
Scheme 4.1. Synthesis of the all-aromatic LC esterimide-based reactive oligomers with phenylethynyl end-groups. The high molecular weight polymers were synthesized according to an identical procedure but without reactive end-groups.

Table 4.1. Backbone composition of the LC poly(esterimide)s.

Sample	IM mol%	HBA mol%	HNA mol%
LC-Polyester	0	73	27
LCP-22IM	22	51	27
LCP-29IM	29	44	27
LCP-37IM	37	36	27
LCP-44IM	44	29	27
LCP-51IM	51	22	27
LCP-58IM	58	15	27
LCP-65IM	65	8	27
LCP-73IM	73	0	27
LCP-22IM–9K	22	51	27
LCP-22IM–5K	22	51	27
LCP-51IM–9K	51	22	27
LCP-51IM–5K	51	22	27

4.2.3 Preparation of thin films

Melt pressed thin films were prepared using standard melt pressing techniques. Post-condensed LC polyesterimide powder was placed between two Kapton™ films and consolidated in a preheated Joos hot press at 320 °C for 20 min. with 5 kN force. The reactive oligomer powder was pressed under similar conditions but cured at 370 °C for 45 min.

The polyesterimide thermoset films were thermal post-treated using the same method as described in *Chapter* 2 (section 2.2.3).

4.2.4 Injection molded tensile specimens

Dog bone-shaped tensile bars (75 × 12.5 × 2 mm^3, ISO 527-2, type 5A) were prepared using a DSM Xplore Micro 15cc Twin Screw Compounder and a DSM Xplore Micro 4cc injection molding machine. The extruder was filled with polymer and heated to 320 °C to melt the polymer in air atmosphere. The charge (10 g) was held for 5 min. at this temperature in order to obtain a uniform melt, after which pressure was applied to transfer the melt to the mold. The melt was injection molded at 320 °C with a mold temperature of 150 °C, injection pressure 7.5 bar. The nozzle diameter was 3 mm.

4.2.5 Characterization

Inherent viscosity measurements for imide-free polymers were performed using an Ubbelohde capillary viscometer. Solutions of 0.25 g/dL were prepared by dissolving the polymer in pentafluorophenol at 60 °C, followed by filtration of the solution (pore size 0.45 µm, Teflon). The M_v was calculated using the Mark-Houwink relationship, where $K = 2.36 \times 10^{-4}$ and $a = 0.98$.[18] For practical purposes, the intrinsic viscosity was assumed to be equal to the inherent viscosity, which results in a lower M_v value.

A Perkin Elmer Pyris Diamond TG/DTA was used to study the dynamic thermal stability. The polymers were initially heated to 370 °C and isothermally held at 370 °C for 1 h. under nitrogen to ensure full polymerization. After cooling to 25 °C, the samples were analyzed using a heating rate of 10 °C·min^{-1} under a nitrogen atmosphere.

The melt behavior of the polymers was determined by differential scanning calorimetry (DSC) using a Perkin Elmer Sapphire DSC with a

heating rate of 20 °C·min^{-1}. All measurements were conducted under a nitrogen atmosphere.

A Leica DMLM optical microscope equipped with a Linkham hot stage was used to investigate the melt behavior as a function of time and temperature. The samples were investigated between glass slides upon heating using a heating rate of 50 °C·min^{-1}.

The rheological behavior of the polymers was investigated using a Thermofisher Haake MARS Ш rheometer equipped with a force-rebalanced transducer in a parallel plate geometry. Parallel plates of 8 mm diameter were used and samples were prepared by compression molding (8 mm in diameter and 0.2 mm thick). The samples were investigated under a nitrogen atmosphere with temperature ramping (5 °C·min^{-1}) from 80 °C to a predetermined temperature followed by an isothermal hold at that temperature for 1 h. All experiments were performed at a frequency of 1.0 Hz and a strain amplitude of 0.1%, which is well within the linear viscoelastic range (frequency of 0.1–10 Hz and a strain amplitude of 0.001–1.0%).

X-ray diffraction (XRD) analysis was conducted on a Bruker AXS D8 Discovery diffractometer, using a Cu-Kα radiation source. Wide-angle X-ray diffraction (WAXD) was performed using a distance of 6 cm between the sample and the detector and the exposure time was set to 5 min.

Dynamic mechanical thermal analyses (DMTA) was performed with a Perkin Elmer Diamond DMTA in tension mode, using thin films (20±0.2) mm × (5±0.2) mm × (0.25±0.05) mm under a nitrogen atmosphere and at a heating rate of 2 °C·min^{-1}. All experiments were performed at a frequency of 1.0 Hz, static tension force of 2,000 mN, minimum tension force of 200 mN, tension gain of 1.5 and length amplitude of 5 μm. The minimum recordable storage modulus (E') was set to 1×10^4 Pa.

A high-resolution JEOL scanning electron microscope (HR-SEM) operating at 5 kV was employed to study the fracture surfaces of the as-pressed films. After sputtering with gold, the samples were placed in the SEM vacuum chamber, and the electron beam was focused on the cross-sectional area of the fractured edge.

A Zwick 1445 tensile tester with a 10 kN force cell was used to investigate the stress-strain behavior of the tensile specimens (75 × 12.5 × 2 mm^3). All experiments were performed at 25 °C at a strain rate of 1 mm·min^{-1}. The data were reported as an average of 5 samples. The elastic modulus was measured by calculating the slope of the stress-strain curve between 0.1% and 0.3% strain.

4.3 Results and discussion

4.3.1 Synthesis of the LC poly(esterimide)s and reactive oligomers thereof

All LC poly(esterimide)s and reactive oligomers with phenylethynyl end-groups could be synthesized using a simple environmentally benign one-pot melt condensation procedure. The polymerizations were straightforward and no premature cross-linking could be observed, indicating that the phenylethynyl end-groups remain latent during the polymerization. The resulting LC poly(esterimide)s and reactive oligomers were ground into a fine powder and this powder was solid-state post-condensed at 260 °C for 24 h. under vacuum to complete the polymerization. All polymers and reactive oligomers were easily synthesized in high yields and the synthetic procedure is very amenable to scale-up.

The LC-Polyester reference polymer (Vectra-A^{TM}), synthesized using an identical melt condensation procedure, dissolved slowly in penta-fluorophenol (PFP) at 25 °C and formed a clear solution. The M_v of 30,800 g·mol^{-1} was estimated using the Mark-Houwink equation,[19] which is in the

same molecular weight range of commercial Vectra-A™. To quantify the molecular weight of the LC poly(esterimide)s and reactive oligomers, we attempted to find suitable solvents or solvent mixtures, *e.g.* penta-fluorophenol (PFP), PFP/hexafluoroisopropanol (1:1 v/v), dimethyl-acetamide, and trifluoroacetic acid. However, all LC poly(esterimide)s appeared completely insoluble at 25 °C and elevated temperature, which precludes size exclusion chromatography (SEC) and inherent viscosity measurements. This means no information could be obtained with respect to the molecular weight of our new LC poly(esterimide)s.

4.3.2 Thermal properties

TGA The thermal stability of the LC polymers and cured thermosets were evaluated using dynamic thermogravimetric analysis (TGA) at a heating rate of 10 °C·min^{-1}. High decomposition values ($T_d^{5\%}$ ~450 °C) and high char yields (~65 wt%) were found, indicating that the dynamic thermal stability of this polymer series is similar to that of the semi-crystalline and amorphous poly(esterimide)s described in previous chapters. The char yield of the LC poly(esterimide)s is higher than that of the LC-Polyester (54 wt%), which results from the excellent thermal stability of the imide-based moiety (IM).[20] The thermal properties of the LC poly(esterimide)s are summarized in Table 4.2.

Table 4.2. Thermal properties of the LC-polyester, LC poly(esterimide)s, the reactive oligomers and their cured thermosets.

Sample	T_{K-N} (°C)[a]	T_{g1} (°C) DSC[b]	T_{g2} (°C) DSC[b]	T_{g1} (°C) DMTA[c]	T_{g2} (°C) DMTA[c]	E' at 25 °C (GPa)	$T_d^{5\%}$ (°C)[c]	Char yield (wt%)[e]
LC-Polyester	280	-	-	111	-	5	480	54
LCP-22IM	280	120	222	124	200	6	450	63
LCP-29IM	300	119	229	124	220	6	449	65
LCP-37IM	310	121	226	129	221	7	447	65
LCP-44IM	300	-	221	139	219	8	445	63
LCP-51IM	300	-	225	143	216	7	448	65
LCP-58IM	290	-	233	-	224	5	453	64
LCP-65IM	290	-	234	-	230	5	448	65
LCP-73IM	300	-	235	-	228	5	446	66

Table 4.2. Continued.

Sample	T_{K-N} (°C)[a]	T_{g1} (°C) DSC[b]	T_{g2} (°C) DSC[b]	T_{g1} (°C) DMTA[c]	T_{g2} (°C) DMTA[c]	E' at 25 °C (GPa)	$T_d^{5\%}$ (°C)[c]	Char yield (wt%)[e]
LCP-22IM-9K	280	118	250	123	225	8	458	63
LCP-22IM-5K	270	118	254	127	243	10	458	64
LCP-51IM-9K	300	-	236	142	223	4	450	61
LCP-51IM-5K	300	-	240	-	233	5	458	63

[a]T_{K-N} values were obtained from the hot-stage optical microscopy study. Heating rate 50 °C·min⁻¹/air atmosphere.

[b]T_g values were obtained from the second heating scan of DSC experiments. Heating rate 20 °C·min⁻¹ /nitrogen atmosphere.

[c]T_g data were obtained from DMTA experiments using melt pressed films, defined by the maximum of the loss modulus (E'') peak. Heating rate 2 °C·min⁻¹/nitrogen atmosphere and a frequency of 1 Hz.

[d]Thermal stability was evaluated using dynamic TGA. The sample was isothermal held at 370 °C for 1 h. before the actual measurement. Heating rate 10 °C·min⁻¹/nitrogen atmosphere.

[e]Char yield at 600 °C.

DSC The thermal behavior of the LC polymers and reactive oligomers was investigated using differential scanning calorimetry (DSC). Figure 4.3 depicts the first and second heating scans of the polymers using a heating rate of 20 °C·min^{-1}. With regard to the LC-Polyester, no glass transition temperature (T_g) but a crystal-to-nematic transition (T_{K-N}) at 283 °C is observed. All LC poly(esterimide)s show high T_gs at 210–230 °C, which are in the same range as for the IM/HBA-based poly(esterimide)s as reported by Kricheldorf and Gedan-Smolka.[3-4] It is noteworthy to mention that the LC poly(esterimide)s with small IM concentrations (22–37 mol%) exhibit an additional T_g at 110 °C.
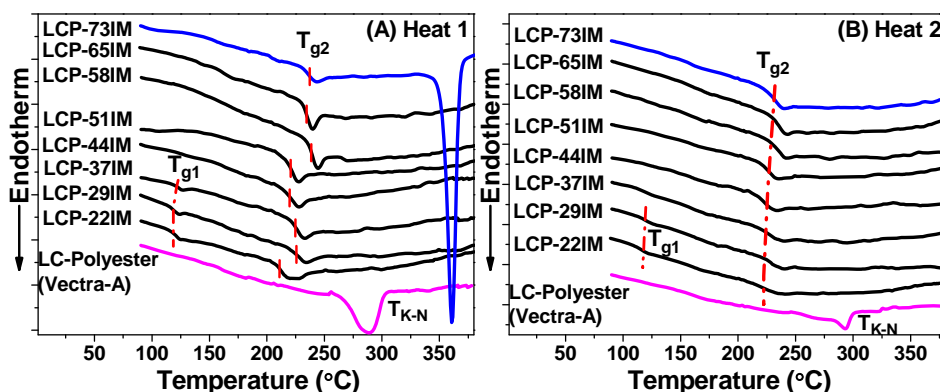
Figure 4.3. A- First and **B-** second DSC heating trace of the LC polyesterimide series after post-condensation (24 h. at 260 °C). Heating rate 20 °C·min^{-1}/nitrogen atmosphere.

When 4-hydroxybenzoic acid (HBA) in the LC-Polyester parent polymer is completely replaced by IM, as is the case for LCP-73IM, a polymer is obtained with a T_g of 235 °C and a sharp melting peak (T_{K-N}) at 355 °C (Figure 4.3A). Upon quenching LCP-73IM from 370 °C to 25 °C, the effect of the prior annealing history is erased, with only a T_g remaining in the second heating trace (Figure 4.3B). The DSC results indicate that incorporation of IM effectively prevents crystallization of the LC-Polyester. Eventually a new crystal structure dominated by the IM unit can be

formed. More details with respect to the polymer morphology will be discussed in section 4.3.5 (X-ray diffraction experiments).

Incorporating phenylethynyl reactive end-groups limits the molecular weight of the polymer and allows the short oligomeric chains to crystallize. This is evidenced by a broad T_{K-N} at 266 °C for LCP-22IM–9K and a slightly lower value (258 °C) for LCP-22IM–5K (Figure 4.4A). In addition, the T_gs of LCP-51IM–9K and LCP-51IM–5K show an increase of ~30 °C upon the second heat (Figure 4.4D). This is attributed to chain extension and/or cross-linking *via* the reactive phenylethynyl end-groups during the first heat.
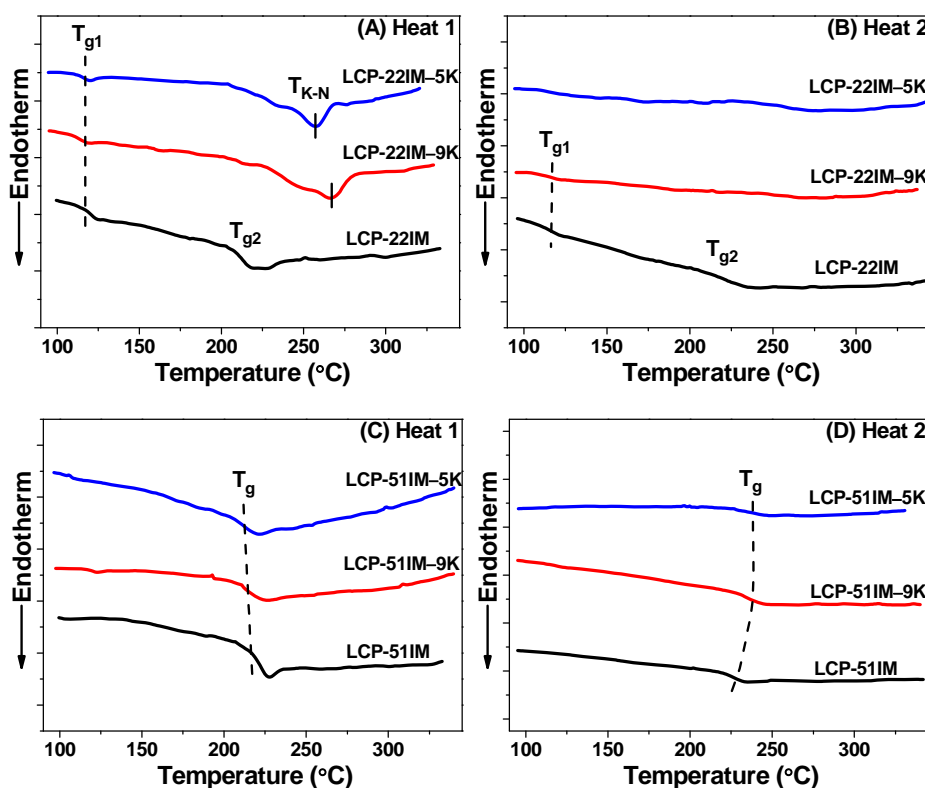
Figure 4.4. DSC measurements of the LC polymers and their reactive 5K and 9K oligomer analogs after post-condensation (24 h. at 260 °C). **A-** First

and **B-** second DSC heating trace of the LCP-22IM series. **C-** First and **D-** second DSC heating trace of the LCP-51IM series. Heating rate 20 °C·min^{-1} /nitrogen atmosphere.

Hot-stage optical microscopy In order to understand the phase behavior in more detail the LC polymers and reactive oligomers were investigated using hot-stage optical microscopy. All LC poly(esterimide)s exhibit a stable nematic phase from ~300 °C up to the decomposition temperature (~450 °C). This suggests that the LC polymers and reactive oligomers are processable over a broad temperature range. The T_{K-N} values are summarized in Table 4.2.

The textures for LCP-22IM and its reactive analog LCP-22IM–9K are shown in Figures 4.5A and 4.5C. Both textures were labeled as grainy or polydomain nematic textures and this texture is typical for high molecular weight or thick samples.[21] The textures observed for LCP-51IM and LCP-51IM–9K, Figures 4.5B and 4.5D, resemble nematic marbled textures.

All textures appear to be nematic in nature, which is typical for main chain thermotropic LCPs.[22] However, we do note a difference in texture formation going from imide-poor compositions to imide-rich compositions, *i.e.* [IM] >37 mol%. Interpretation of optical textures, especially high molecular weight main-chain LCPs is challenging because of the polydispersity, high melt viscosity, surface anchoring effects and presence of (nano)crystallites (pHBA). When going from an ester-based LCP to an esterimide-based LCP we change the backbone structure from linear to kinked (bend-core!) and introducing imides will change the local electrostatics. The imide functionality has a strong dipole moment and is able to associate with adjacent chains *via* π-π stacking. The presence of imide groups, however, does not result in the formation of higher ordered smectics, as confirmed by XRD experiments (section 4.3.5). Our evaluation

100

of the LC textures should therefore be considered a preliminary study only. A more detailed investigation is needed in order to understand the nature of the observed textures.
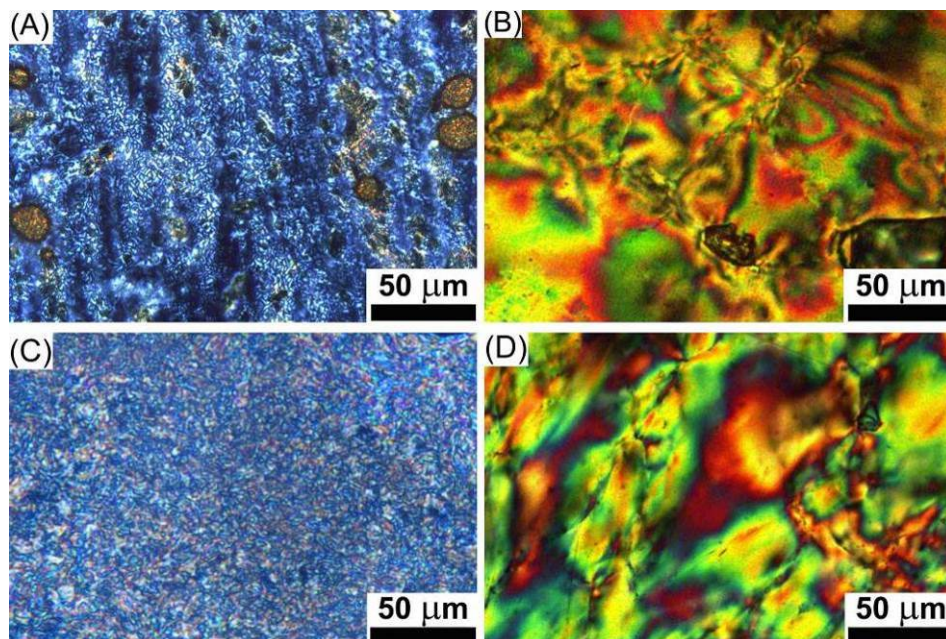
Figure 4.5. Microphotographs of the LC polyesterimide melts (after post-condensation for 24 h. at 260 °C), between cross polarizers. **A-** LCP-22IM and **B-** LCP-51IM at 330 °C. **C-** LCP-22IM–9K and **D-** LCP-51IM–9K solidified nematic textures after a 1 h. isothermal hold at 370 °C.

Phase diagram Based on the DSC and optical microscopy results, we are able to construct a phase diagram for the LC poly(esterimide)s as function of the IM concentration. This phase diagram is shown in Figure 4.6 and the literature T_g (103 °C) of LC-Polyester (HBA/HNA) is included for reference purposes.[23] For the LC poly(esterimide)s with an IM concentration between 22 mol% and 37 mol%, two distinct T_gs could be

observed at 110 °C and 220 °C. The T_gs can be assigned to HBA/HNA-rich segments and HBA/IM-rich segments, respectively, and implies that esterimide block copolymers can be obtained using a simple one-pot melt polymerization method. The origin of block copolymer formation will be discussed in section 4.3.3 (Kinetics of melt polycondensation). When the concentration of IM exceeds 37 mol%, the LC poly(esterimide)s exhibit a single T_g at ~230 °C. When the temperature reaches ~300 °C (T_{K-N}), the polymers melt into a nematic phase. Above the isotropization temperature (~450 °C), a homogeneous isotropic melt is obtained for all LC poly(esterimide)s. The phase diagram clearly illustrates that by adding IM there is a modest increase in T_{K-N} and a modest drop in T_{N-I}. As discussed already, when the IM concentration is below 37 mol% a grainy polydomain nematic texture is obtained and at IM concentrations exceeding 37 mol% a marbled nematic texture is observed. Both textures are included in the phase diagram and the 37 mol% IM concentration is marked with a vertical dashed line.
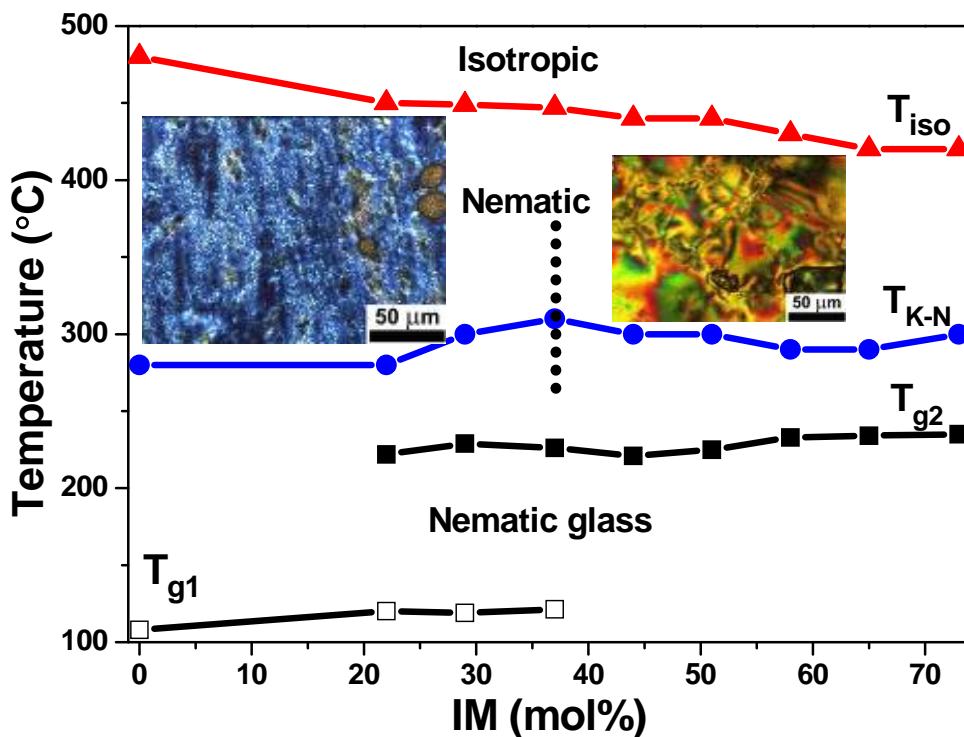
Figure 4.6. Phase diagram of the LC poly(esterimide)s as function of the IM concentration (mol%). The crystal-to-nematic transition temperature (T_{K-N}) and isotropization temperature (T_{iso}) were obtained from the hot-stage optical microscopy study. Heating rate 50 °C·min⁻¹/air atmosphere. The T_{g1} and T_{g2} values were obtained from the second heating scan of DSC experiments. Heating rate 20 °C·min⁻¹/nitrogen atmosphere.

4.3.3 Kinetics of melt polycondensation

Vectra-A, a commercial LC-Polyester, is prepared in the melt state by the reaction of acetoxy groups and carboxylic acid groups with the elimination of acetic acid.[24-27] Understanding the reaction kinetics is the first step towards understanding why the copolymerization of HBA, HNA and IM favors the formation of a block copolymer.

Prior to the actual polycondensation, HBA, HNA and IM are converted into 4-acetoxybenzoic acid (ABA), 6-acetoxy-2-naphthoic acid (ANA) and N-(3'-acetoxyphenyl)trimellitimide (AIM) by acetylation at 140 °C for 1 h. The acidolysis reaction involves a nucleophilic addition reaction, consisting of two steps (Scheme 4.2). Step 1, the carboxylic acid dissociates to the carboxylate anion. The predicted pK_a value of AIM (3.31±0.20) is smaller than that of ABA (4.05±0.10) and ANA (4.11±0.30), indicating that AIM is a stronger acid.[28] Because $k_{AIM1} > k_{ANA1} \approx k_{ABA1}$, the dissociation equilibrium of AIM is shifted more to the right than ANA and ABA, resulting in a higher concentration of carboxylate anion of AIM. The presence of the electron-poor imide group stabilizes the AIM carboxylate making the AIM carboxylate anion much less reactive than the ANA and ABA carboxylate anions. This means that the AIM-based monomer reacts much slower in step 2 ($k_{AIM2} << k_{ANA1} \approx k_{ABA2}$). This agrees well with the findings of Gedan-Smolka *et al.* They found that the conversion of ABA reaches 90% at 300 °C for 20 min. The conversion of AIM only reaches 65% under the same reaction conditions, indicating that the reaction rate of ABA to polymer is distinctly higher. In order to reach 90% AIM conversion, the polymerization temperature needs to be 330 °C.[4] Hence, the one-pot melt condensation of ABA, ANA and AIM starts with the polymerization of ABA and ANA *via* the acidolysis route since AIM is significantly less reactive than ABA and ANA.

Step 1

ABA pK_a = 4.05±0.10

ANA pK_a = 4.11±0.30

AIM pK_a = 3.31±0.20
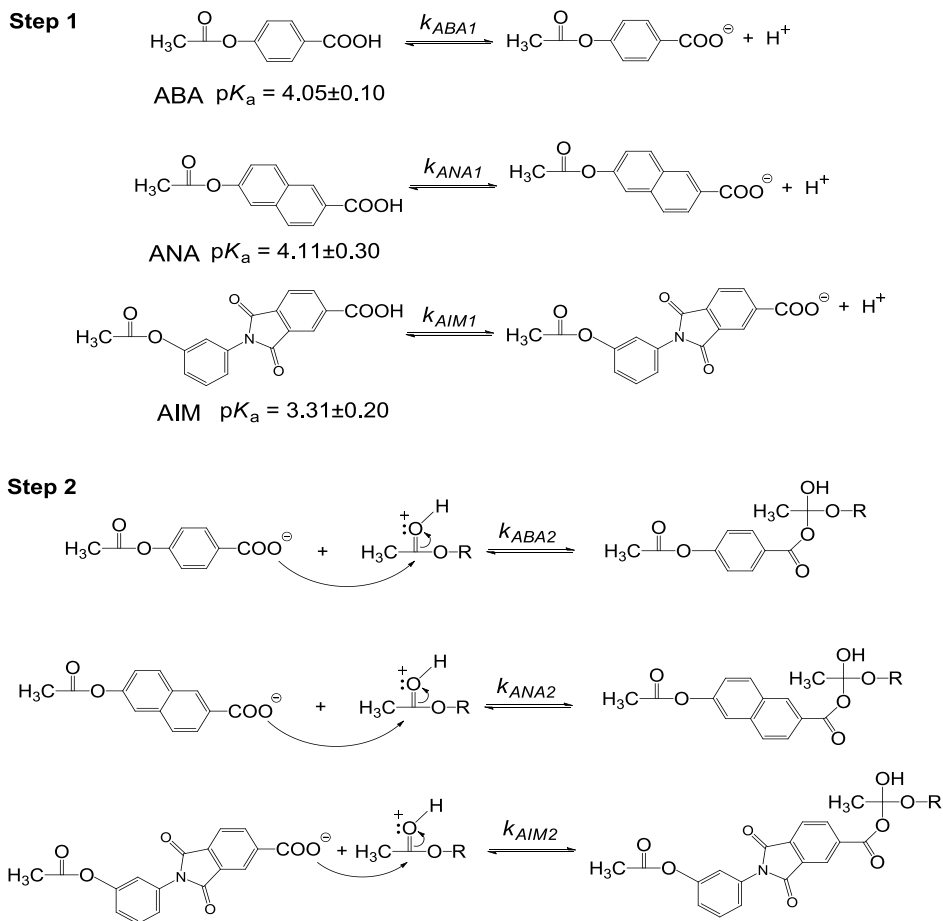
Step 2

Scheme 4.2. Partial mechanism of the acidolysis reaction showing the rate-determining steps.[25,27] **Step 1-** Dissociation of the carboxylic acid. **Step 2-** Nucleophilic addition of the carboxylate anion to the carbonyl group of the acetate. Note: the pK_a values are predicted using Advanced Chemistry Development (ACD/Labs) Software V11.02.

Although the melt polymerization takes place in one-pot, several reactions take place that follow different kinetic pathways –the polymerization mechanism of HBA/HNA is shown in Scheme 4.1S. For

polymers with a low concentration of IM (*e.g.* LCP-22IM), ANA will initially be consumed to form mostly oligomeric HBA/HNA with a small amount of IM incorporated into the backbone. As the polymerization temperature increases, IM becomes more reactive and becomes part of the growing polymer backbone, forming a triblock copolymer with an HBA/HNA-rich central core and HBA/IM-rich terminal blocks. The transition from HBA/HNA-rich to HBA/IM-rich is expected to be gradual (tapered) as illustrated in Figure 4.7.
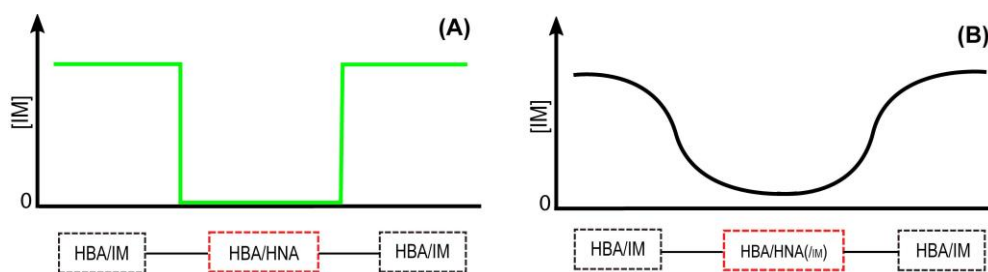
Figure 4.7. The IM monomer distribution of corresponding blocks in the copolymer. **A-** An ideal ABA-triblock copolymer. **B-** Proposed ABA-triblock copolymer in present work.

Based on the kinetics, as discussed above, and the DSC results we feel confident that we have prepared an ABA-triblock copolymer where the B-block is composed of HBA/HNA and the A-blocks are composed of HBA/IM. The two T_gs observed by DSC at 110 °C and 220 °C, as shown in Figure 4.3, can be assigned to the HBA/HNA and HBA/IM blocks, respectively.

4.3.4 Rheology

Understanding the melt behavior of our polymers is critical in terms of defining the processing window. The complex melt viscosity ($|\eta^*|$) of the

LC-Polyester sample shows a very typical behavior; a T_g at 110 °C and a sharp decrease at T_{K-N} (300 °C) where the polymer chains become mobile.[29] During the 1 h. hold at 320 °C the viscosity of LC-Polyester showed an increase from 4.5×10^3 Pa·s to 1.1×10^4 Pa·s (Figure 4.8A), which is due to an increase in molecular weight (post condensation). LCP-29IM, and LCP-44IM, as representative LC poly(esterimide)s examples, show a drop in viscosity at T_{g1} (130 °C) and a large drop in viscosity at T_{g2} (210 °C), which is in agreement with a blocky backbone structure. LCP-73IM, on the other hand, shows one T_g only (~210 °C) as this polymer has a high concentration of IM. Figure 4.8B shows the melt behavior of LCP-44IM including a 1h. isothermal hold at 370 °C. Both glass transition temperatures are clearly visible including the melt transition (T_{K-N}) at 320 °C. Holding LCP-44IM at 370 °C for 1h. results in an increase in viscosity, suggesting that additional polymerization is taking place (effectively post condensing the polymer).
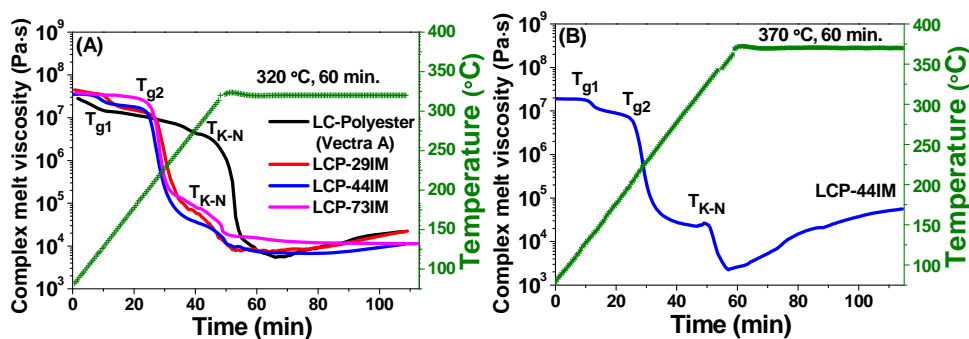
Figure 4.8. Rheological behavior of the LC poly(esterimide)s as function of temperature and a 1 h. isothermal hold. **A-** LC-Polyester, LCP-29IM, LCP-44IM and LCP-73IM held at 320 °C for 1 h. and **B-** LCP-44IM held at 370 °C for 1 h. Experiments were performed using a frequency of 1 Hz and heating rate of 5 °C·min^{-1}/nitrogen atmosphere. The test specimens were prepared after the polymers post-condensed at 260 °C for 24 h.

Due to the large concentration of IM, the minimum viscosity of LCP-73IM is slightly higher than that of the others. The rheology results show that all LC poly(esterimide)s have a broad processing window of approximately 1 h. at 320 °C. It must be pointed out, however, that the rheology studies were performed using a rheometer in a parallel plate geometry. This has to be considered as a preliminary study only.

The incorporation of reactive phenylethynyl end-groups limits the molecular weight of the polymer and reduces the melt viscosity. Figure 4.9 shows that LCP-22IM reaches a minimum melt viscosity 1.2×10^4 Pa·s at 350 °C whereas LCP-22IM–5K reaches 0.4×10^4 Pa·s at the same temperature. After reaching the minimum value, the viscosity of LCP-22IM starts increasing and leveling off after a 50 min. (post condensation) hold at 370 °C. Although LCP-22IM–9K contains cross-linkable end-groups, only chain extension is expected to occur due to the low concentration of end-groups and therefore the viscosity profile shows a trend similar to that of LCP-22IM. In the case of LCP-22IM–5K, chain extension and cross-linking are taking place at 350 °C resulting in an increase in molecular weight and hence a rapid increase in $|\eta^*|$. After a 50 min. hold at 370 °C, the chain extension and cross-linking chemistry is mostly complete and the viscosity levels off. Similar results were reported by Iqbal *et al.*[30] From the rheology experiments it is clear that an isothermal hold at 370 °C for 1 h. can cure the reactive oligomers to form cross-linked thermosets.
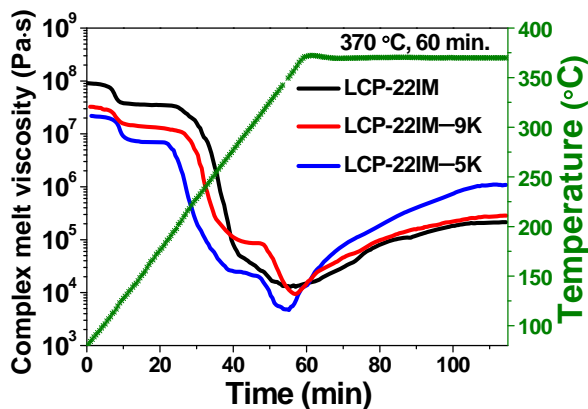
Figure 4.9. Rheological behavior of LCP-22IM and reactive oligomers thereof as function of temperature and a 1 h. hold at 370 °C. Experiments were performed using a frequency of 1 Hz and heating rate of 5 °C·min^{-1} /nitrogen atmosphere. The test specimens were prepared after the polymers were post-condensed at 260 °C for 24 h.

4.3.5 X-ray diffraction (XRD) analysis

A wide-angle X-ray diffraction (WAXD) study was performed to investigate the morphology of the LC poly(esterimide)s. In the diffraction pattern of the LC-Polyester in Figure 4.10A, a sharp peak is present centered at the 2θ angle of 20.0° and a weak shoulder peak at 26.5°, which are the typical feature peaks of main-chain nematic LC polymers.[31] Using the Bragg equation, the *d*-spacing (2θ = 20.0°) is calculated to be 4.5 Å, which corresponds to the average intermolecular spacing between the rod-like liquid crystalline mesogens. The *d*-spacing of 3.3 Å (2θ = 26.5°) was also observed in other WAXD studies. According to reports of Acierno *et al.*[32] and Wei *et al.*,[33] the 3.3 Å peak belongs to the (211) crystallographic plane of pHBA, implying the presence of pHBA (nano)crystallites.

109
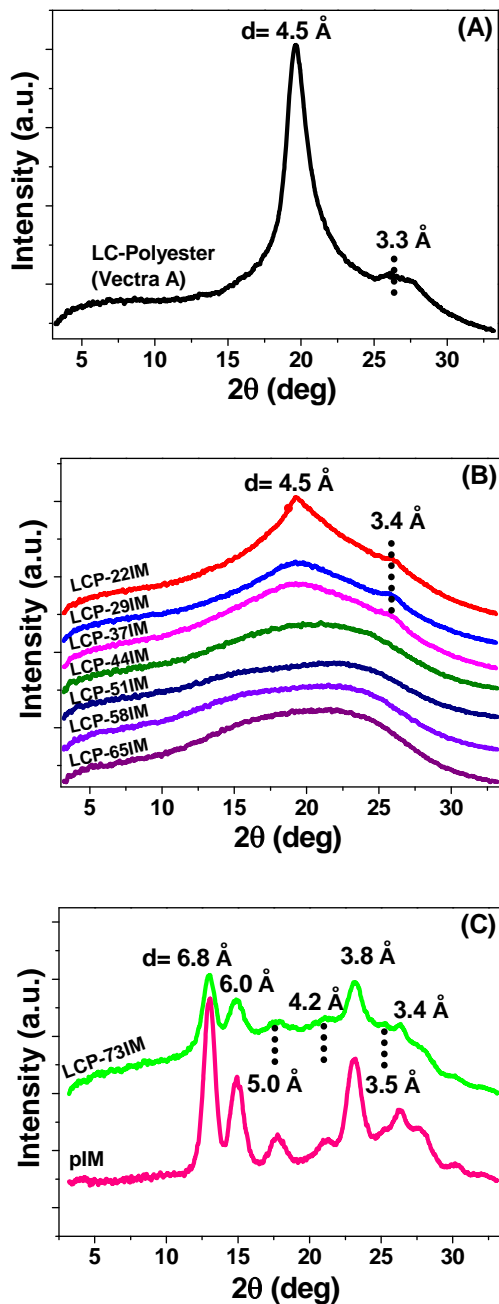
Figure 4.10. XRD analyses of the polymer powders at 25 °C (after post-condensation at 260 °C for 24 h.) **A-** LC-Polyester. **B-** Poly(esterimide)s

with an IM concentration ≤ 65 mol%. **C-** Polyesterimide with an IM concentration of 73 mol%. Also shown is the homopolymer of IM (pIM) for reference purposes.

From the XRD data it is evident that introducing IM into the HBA/HNA backbone is very effective in reducing the intensity of the $2\theta = 20.0°$ peak (Figure 4.10B). The reason for this is that the presence of the HBA/IM blocks hinders the crystallization of HBA/HNA. Upon incorporation of IM, broad asymmetric WAXD patterns are observed, which agrees with the presence of a block copolymer rather than that of a random amorphous copolymer. The broad WAXD patterns confirm the lack of crystallinity and this explains the absence of crystal-to-nematic transitions in the DSC thermograms. The WAXD pattern of LCP-73IM is shown in Figure 4.10C. This semi-crystalline polymer has a high concentration of IM (73%) and the diffraction pattern resembles that of the IM homopolymer (pIM).[4]

4.3.6 Dynamic mechanical thermal analysis (DMTA)

In order to explore the thermomechanical properties of the LC poly(esterimide)s, the storage modulus (E') and loss modulus (E") as function of temperature were studied using dynamic mechanical thermal analysis (DMTA). Thin films were used for these DMTA experiments and the results are summarized in Figure 4.11 and Table 4.2.

Figure 4.11A shows that the LC-Polyester parent polymer has a T_g at 110 °C, after which E' starts to decrease significantly and the experiment terminates at the melting point (T_{K-N}). Incorporation of kinked imide moieties (IM) into the LC-Polyester backbone changes the nature of the parent polymer significantly. Chain-chain interactions are enhanced via imide-imide π–π stacking interactions, the backbone becomes more kinked and this will increase the possibility of forming chain

111

entanglements. Now, if IM becomes randomly distributed into the HBA/HNA backbone all of the above-mentioned interactions will just increase the T_g and E' of the resulting HBA/HNA/IM random copolymers. However, the DMTA results show a different behavior. Upon introducing IM, two distinct T_gs become clearly visible, as shown in Figures 4.11C and 4.11D. This confirms the formation of a block copolymer and the T_gs can be assigned to an HBA/HNA-rich block (T_{g1} ~120 °C) and an HBA/IM-rich block (T_{g2} ~220 °C), respectively. When the IM concentration increases, more HBA/IM blocks are obtained and this shifts T_{g1} to higher temperatures and increases the rubber plateau between T_{g1} and T_{g2}. T_{g2} is similar to that of the 2-component HBA/IM poly(esterimide)s discussed in the previous chapters. For the high IM concentration systems (58, 65 and 73 mol% IM), LC poly(esterimide)s with a random backbone composition are obtained with a single T_g at 230 °C (Figures 4.11E and 4.11F).

It is noteworthy to mention that all poly(esterimide)s with a high IM concentration ([IM] > 37 mol%) exhibit a flow point (T_f) at 252–278 °C (Figures 4.11C and 4.11E). Flow points were also observed for the 2-component poly(esterimide)s discussed in *Chapter 3*. This thermodynamic transition is associated with an increase in chain mobility and a decrease in segment-segment associations.[34] It should not be confused with the T_{K-N} transition, which is a first-order transition. The T_{K-N} (melt) transition can be identified by a change in E" (280 °C in Figure 4.11B). There is no change in E" at T_f (Figure 4.11D and 4.11F).
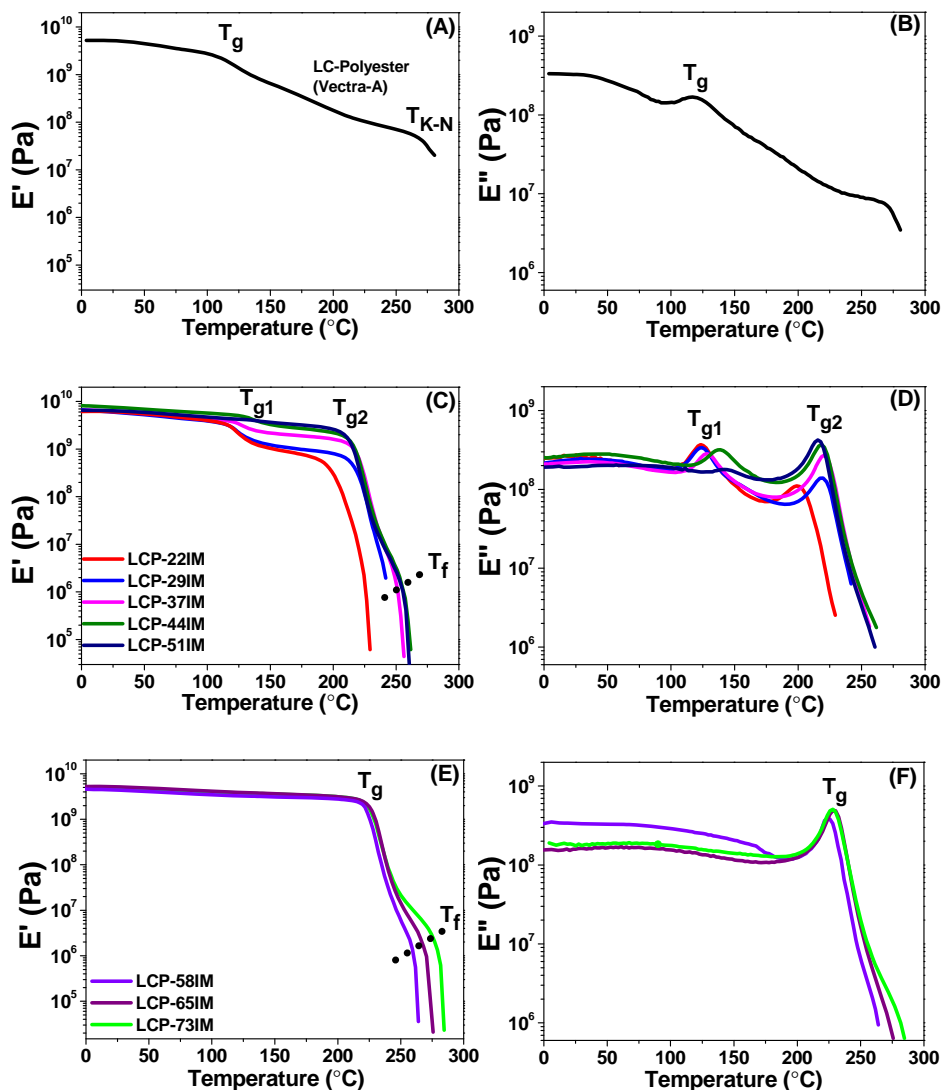
Figure 4.11. DMTA analysis of the LC poly(esterimide)s melt pressed films. **A-** Storage modulus (E') and **B-** Loss modulus (E") as function of temperature for LC-Polyester. **C-** Storage modulus (E') and **D-** Loss modulus (E") as function of temperature for the polymers with [IM] ≤ 51 mol%. **E-** Storage modulus (E') and **F-** Loss modulus (E") as function of temperature for the polymers with [IM] ≥ 58 mol%. Heating rate 2 °C· min^{-1}/nitrogen atmosphere and a frequency of 1 Hz.

113

The incorporation of phenylethynyl reactive end-groups leads to an improvement in the thermomechanical properties of the cured films. The storage modulus plateau with a high modulus (E' = 2 GPa) between the two T_gs is extended and a stable rubber plateau above T_{g2} is observed. The LCP-22IM parent polymer and thermoset films share the same T_g event at 120 °C (T_{g1}) (Figure 4.12) but the second T_g (T_{g2}) shows a dramatic upward shift from 200 °C (LCP-22IM) to 254 °C and 250 °C, for LCP-22IM–9K and LCP-22IM–5K, respectively. As discussed above, T_{g1} is assigned to the HBA/HNA block and T_{g2} to the HBA/IM block. The T_g of the HBA/IM-block shows an increase of ~50 °C and the T_g of the HBA/HNA remains virtually the same. This strongly suggests that we are dealing with an ABA-triblock copolymer structure. The central B-block is based on HBA/HNA and the terminal A-blocks are comprised of HBA/IM. Crosslinking the terminal A-blocks via phenylethynyl reactive groups results in an increase in T_g of the HBA/IM fraction only. The increase in T_{g2} (~50 °C) is reasonable as similar increases in T_g have been observed for other phenylethynyl crosslinked systems.[16]
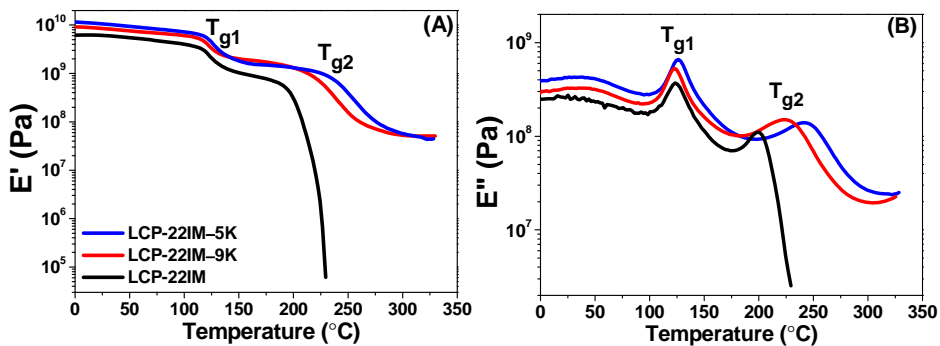
Figure 4.12. A- Storage moduli (E') and **B-** Loss moduli (E") as function of temperature for the LCP-22IM parent polymer and cured thermoset films thereof. Heating rate 2 °C·min⁻¹/nitrogen atmosphere and a frequency of 1 Hz.

Thermally post-treating the LCP-22IM–5K thermoset films at different temperatures, *i.e.* 330, 350 and 370 °C results in a dramatic increase in T_{g2} from 243 °C to 349 °C (Figure 4.13 and entry 4, Table 4.3) but does not change T_{g1}. The higher the thermal post treatment temperature, the larger the increase in T_{g2}, indicating that additional cross-linking and chain extension has occurred. This again confirms that the reactive phenylethynyl end-groups reside on the HBA/IM terminal blocks and not on the HBA/HNA blocks.
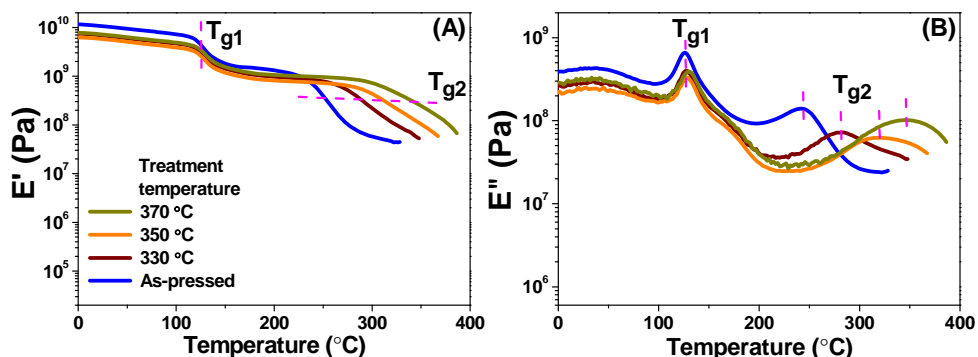
Figure 4.13. A- Storage moduli (E') and **B-** Loss moduli (E") for LCP-22IM–5K films after different post-treatment temperatures. Heating rate 2 °C·min^{-1}/nitrogen atmosphere and a frequency of 1 Hz. The films were post-treated from 25 °C to the predetermined temperatures with a heating rate 2 °C·min^{-1}/nitrogen atmosphere and immediately cooled down to 25 °C (cooling rate ~3 °C·min^{-1}).

Table 4.3. Summary of the DMTA results of the post-treated LCP-22IM–5K films. All data collected under a nitrogen atmosphere and a heating rate of 2 °C·min^{-1} and 1 Hz.

Entry	Post-treatment temperature (°C)	T_{g1} (°C)[a]	T_{g2} (°C)[a]	E' at 25 °C (GPa)
1	-	126	243	10
2	330	128	281	7
3	350	127	319	6
4	370	129	349	7

[a]T_g is reported at the maximum of E".

4.3.7 Scanning electron microscopy (SEM)

Poly(esterimide)s with low concentrations of IM (22-37 mol%) clearly show the presence of two distinct T_gs when analyzed with DSC and DMTA. This means that the A- and B-blocks are phase separated into two different domains. An initial assessment of the morphology was made using high-resolution scanning electron microscopy (HR-SEM). The morphology of several cryogenically fractured LC poly(esterimide)s films was studied and the results are summarized in Figure 4.14. All specimens were sputter coated with a 15 nm layer of gold before SEM analysis.

SEM analysis allows us to check whether phase separation takes place on a length scale of ~50 nm. For the LC-Polyester reference polymer a single-phase morphology with a typical LCP fibrous structure is observed (Figure 4.14A). The second block copolymer in the series, LCP-29IM, shows a change in morphology. Fibrils (0.16–0.6 µm) seem to co-exist with a matrix but the fibrils appear well embedded (Figure 4.14B). Increasing the IM concentration to 44 mol% results in a similar morphology but in this case fibril pullout (fibrils have a diameter in the range 0.1–0.27 µm) seems to occur as can be concluded from the voids

clearly visible in Figure 4.14C. At this IM concentration the two phases become incompatible and phase separation takes place. Increasing the IM concentration even further (LCP-58IM) results in a complete loss of the fibrilar structure and a brittle fracture surface is observed. This is remarkable as the polymer is still LC and most LCPs show a fibrilar fracture surface (Figure 4.14D).
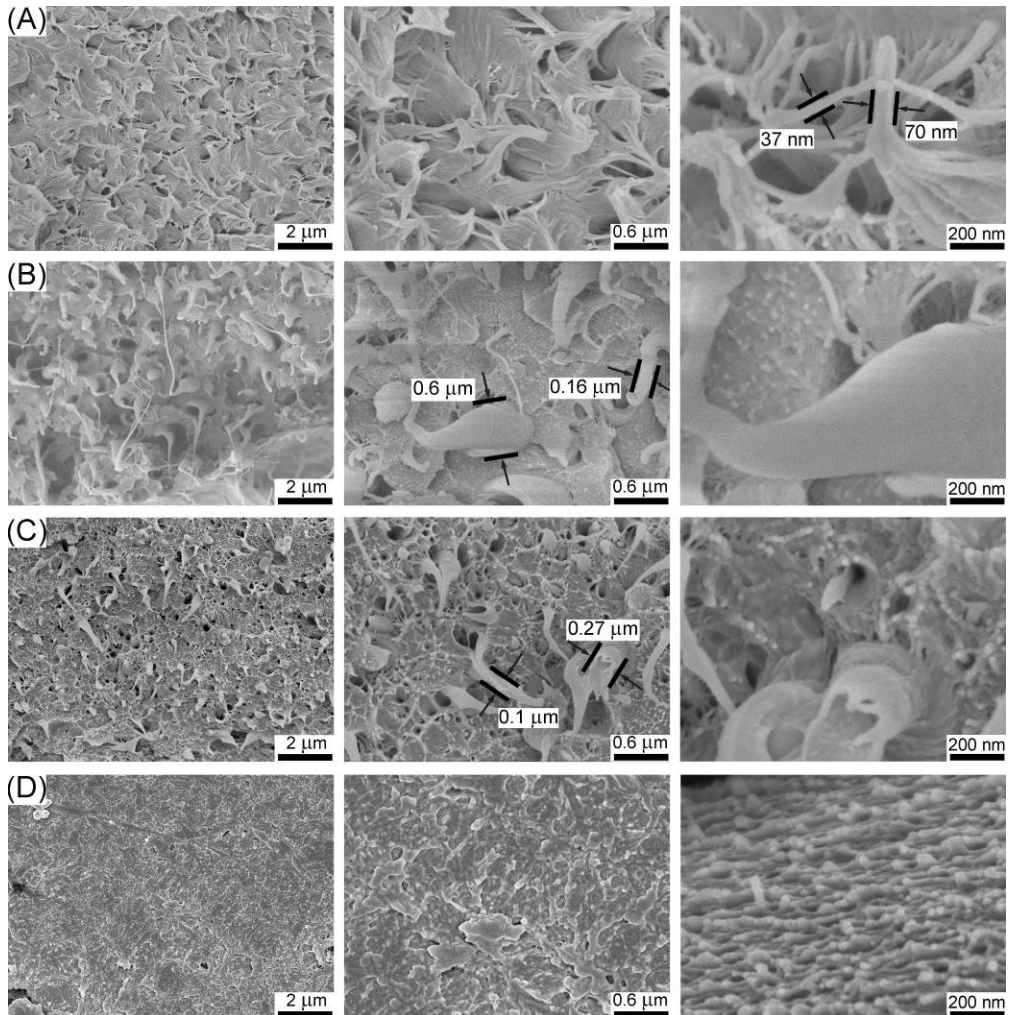
Figure 4.14. SEM images of the LC poly(esterimide)s melt pressed films fracture surface. **A-** LC-Polyester. **B-** LCP-29IM. **C-** LCP-44IM. **D-** LCP-58IM.

In order to place our results in the context of high-performance polymer blends we want to contrast our results with a known polyetherimide (Ultem™)/LC polyester (Vectra-A™) blend. In general, microphase separation is observed in 2-polymer blend systems, despite the efforts of researchers to improve compatibility between the two polymers using compatibilizers.[35-38] For example, in Figure 4.15A microphase separation is clearly observed in a Ultem™/Vectra-A™ blend.[39] Vectra-A™ fibrils with an average diameter of 0.3 µm are dispersed in the PEI matrix and increasing the extruder speed improves the dispersion but does not improve miscibility (Figure 4.15B). Our ABA-triblock copolymer with a low concentration IM (LCP-29IM) seems to show little or no phase separation at a length scale of 50 nm, which is indicative that a good compatibility of the HBA/HNA and HBA/IM blocks.
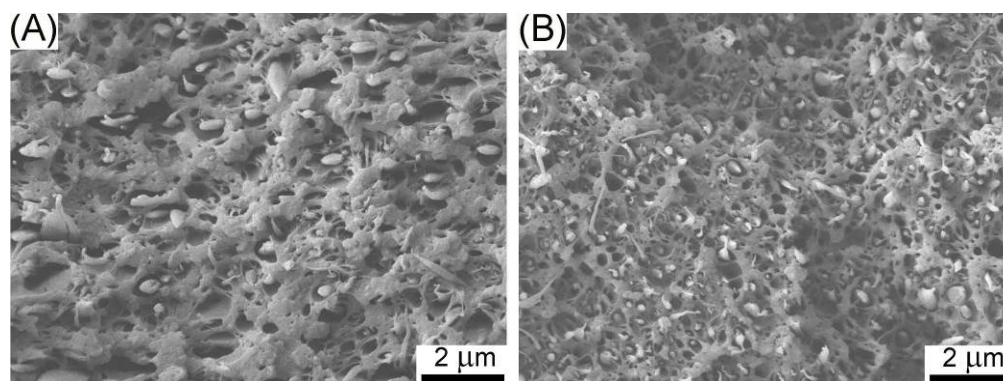
Figure 4.15. SEM images of the polyetherimide/LC polyester (80 wt% Ultem™/20 wt% Vectra-A™) blend fracture surface. The polymers were blended at 350 °C for 5 min. with different extruder speeds, **A-**100 RPM, **B-**150 RPM. (Reproduced from reference[38] with permission.)

Based on the HR-SEM results it is not possible to say anything conclusive with respect to the morphology and whether we can recognize

the two different phases. Additional transmission electron microscopy (TEM) and atomic force microscopy (AFM) experiments might be needed.

4.3.8 Tensile properties

Attempts were made to injection mold all LC poly(esterimide)s into tensile bars. Only the LC poly(esterimide)s with an IM concentration equal or less than 37 mol% were successfully injection molded at 320 °C. The tensile properties of the molded specimens (75 × 12.5 × 2 mm^3, ISO 527-2, type 5A) are shown in Figure 4.16 and the results are listed in Table 4.4. The LC-Polyester reference polymer exhibits good tensile properties, *i.e.* a tensile strength of 122 MPa, an elastic modulus of 3.6 GPa, and elongation at break of 7.3%. LCP-22IM shows slightly better tensile properties in terms of a tensile strength of 126 MPa and an elastic modulus of 4.8 GPa. However, the elongation at break drops to 3.3%. The tensile strength and elongation at break of LCP-29IM and LCP-37IM show a decreasing trend whereas the elastic modulus remains high (~5 GPa). These results agree with the HR-SEM results. LCP-29IM shows little or no phase separation and the fibrilar structure seems to have a positive effect on the tensile strength and elastic modulus. Increasing the IM concentration results in phase separation (LCP-44IM) and this agrees with the deterioration in mechanical properties observed in the high IM content polymers.
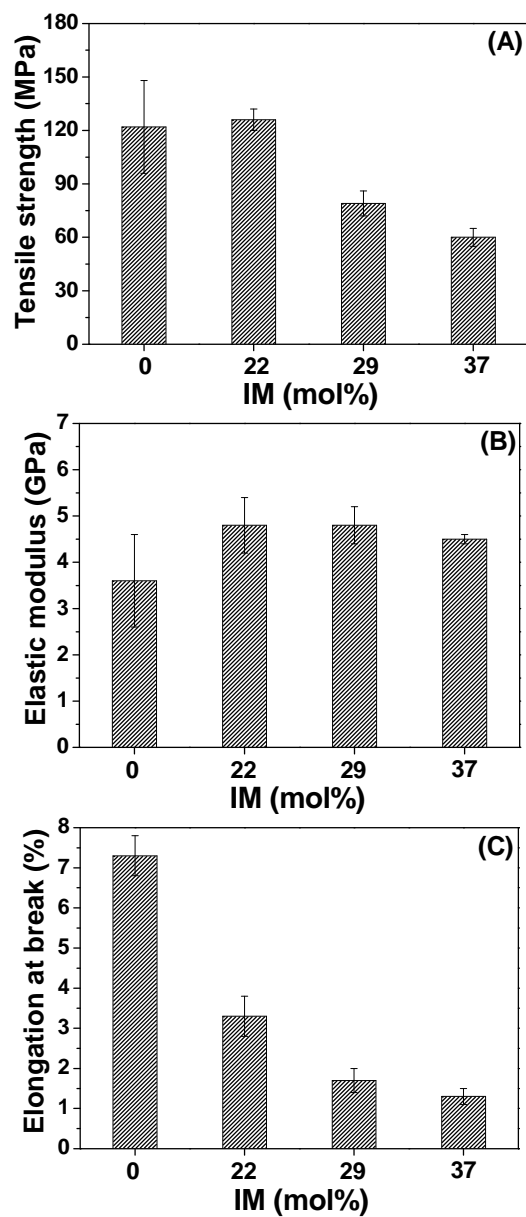
Figure 4.16. Tensile properties of the LC poly(esterimide)s tensile specimens (5 samples). **A-** Tensile strength. **B-** Elastic modulus. **C-** Elongation at break.

The order parameter of all test specimens was measured and the results are listed in Table 4.4. The results confirm that injection molding under said conditions results in LC tensile bars where the mesogens exhibit the same degree of orientation, *i.e.* $<P_2>$ for all samples is between 0.43–0.47. This means a fair comparison among all tensile specimens can be made.

Table 4.4. Tensile properties of the LC poly(esterimide)s tensile bars. The data shown is an average of 5 tensile specimens.

Sample	Tensile strength (MPa)	Elastic modulus (GPa)	Elongation at break (%)	$<P_2>$[a]
LC-Polyester	122±26	3.6±1.0	7.3±0.5	0.47
LCP-22IM	126±6	4.8±0.6	3.3±0.5	0.47
LCP-29IM	79±7	4.8±0.4	1.7±0.3	0.43
LCP-37IM	60±5	4.5±0.1	1.3±0.2	0.43

[a]The scattering data on a ring along the 2θ direction containing the scattering peaks were integrated to get the scattering intensity, as a function of the Azimuthal angle. The intensity profiles (Figure 4.1S) were fitted using Maier-Saupe type function to calculate the order parameter.[40-41]

4.4 Conclusions

We have developed a new series of all-aromatic ABA-triblock poly(esterimide)s and thermosets with excellent thermomechanical properties. The new LC poly(esterimide)s based on N-(3'-hydroxyphenyl)trimellitimide (IM), 4-hydroxybenzoic acid (HBA) and 6-hydroxy-2-naphthoic acid (HNA) were synthesized using a one-pot melt condensation method. By replacing HBA with less reactive IM, ABA-

triblock copolymers can be prepared with two distinct T_gs (T_{g1} ~120 °C and T_{g2} ~220 °C). Introducing larger concentrations of IM (> 51 mol%) results in random copolymers with a single T_g of ~230 °C. The DMTA results of cured thermoset films further confirm the formation of ABA-triblock copolymers. The SEM images confirm that at low IM concentration the HBA/HNA and HBA/IM blocks are compatible as there is little microphase separation on the maximum observable length scale of 50 nm. All LC copolymers and reactive oligomers possess stable melt behavior and good processability.

The tensile behavior of the LC poly(esterimide)s is a strong function of the IM concentration. At concentrations below 37 mol% the injection molded tensile bars exhibit good tensile properties. In particular LCP-22IM has a tensile strength of 126 MPa, an elastic modulus of 4.8 GPa and elongation at break of 3.3%. Increasing the IM concentration results in rapid reduction in tensile strength, elastic modulus and elongation at break, and these finding are consistent with the polymer morphology.

4.5 References

[1]   H. R. Dicke, J. Genz, V. Eckhardt, L. Bottenbruch. C. A. (Bayer AG), DE 37 37 067, **1987**.

[2]   H. Land, M. Gedan, M. Rätzsch, F. Böhme (Hoechst Aktiengesellschaft), EP0582220 A2, **1994**.

[3]   H. R. Kricheldorf, V. Linzer, C. Bruhn, *Eur. Polym. J.* **1994**, *30*, 549.

[4]   M. Gedan-Smolka, D. Jehnichen, H. Komber, D. Voigt, F. Böhme, M. Rätzsch, *Angew. Makromol. Chem.* **1995**, *229*, 159.

[5]   J. Mark, K. Ngai, W. Graessley, L. Mandelkern, E. Samulski, J. Koenig, G. Wignall, *Physical Properties of Polymers*, Cambridge University Press, Cambridge UK **2004**, p. 362.

[6]   A. M. Donald, A. H. Windle, *Liquid Crystalline Polymers,* Cambridge University Press, Cambridge UK **1992**.

[7]   C. Lekakou, J. Cowley, C. E. Dickinson, *J. Mater. Sci.* **1997**, *32*, 1319.

[8]   T.-S. Chung, *Thermotropic Liquid Crystal Polymers*, Technomic Publishing Company, Inc., Basel Switzerland **2001**.

[9]   D. O. Hummel, U. Neuhoff, A. Bretz, H.-J. Düssel, *Makromol. Chem.* **1993**, *194*, 1545.

[10]   K. Sueoka, M. Nagata, H. Ohtani, N. Naga, S. Tsuge, *J. Polym. Sci., Part A: Polym. Chem.* **1991**, *29*, 1903.

[11]   X. Wang, Q. Zhou, Liquid Crystalline Polymers, World Scientific, Singapore, **2004**.

[12]   L. F. Charbonneau, G. W. Calundann, EP0067618 A2, **1982**.

[13]   J. F. Harris, Jr. US4391966 A, **1981**.

[14]   ''Ticona Vectra Liquid Crystal Polymer (LCP) Product Information,'' Ticona, Summit, NJ, 07901, **2000**.

[15]   S. Chandrasekhar, *Liquid Crystals*, Cambridge University Press, Cambridge, **1992**.

[16]   A. Knijnenberg, E. S. Weiser, T. L. StClair, E. Mendes, T. J. Dingemans, *Macromolecules* **2006**, *39*, 6936.

[17]   H. R. Allcock, F.W. Lampe, J. E. Mark, *Contemporary Polymer Chemistry*, Pearson Education, Inc., NJ USA, **2003**.

[18]   G. W. Calundann, M. Jaffe, Proceedings of the Robert, A. Welch Conferences on Chemical Research. *Synth. Polym.* **1982**, XXVI.

[19]   R. J. Young, P. A. Lovell, *Introduction to Polymers*, Chapman & Hall, London, **1991**.

[20]   F. W. Huang, F. R. Huang, Y. Zhou, L. Du. *Polym. J.* **2010**, *42*, 261.

[21]   N.J. Alderman, M.R. Mackley, *Faraday Discuss. Chem. Soc.* **1985**, *79*, 149.

[22]   D. Demus, J. Goodby, G. W. Gray, H.-W. Spiess, V. Vill, *Handbook of Liquid Crystals, High Molecular Weight Liquid Crystals,* **1998**, Vol 3. Chapter 2.

[23] R. A. Weiss, Y. Ghebremeskel, L. Charbonneau, *Polymer* **2000**, *41*, 3471.

[24] I. Vulić, T. Schulpen, *J. Polym. Sci., Part A: Polym. Chem.* **1992**, *30*, 2725.

[25] P. A. Williams, X. Han, A. B. Padias, H. K. Hall Jr. *Macromolecules* **1996**, *29*, 1874.

[26] X. Han, P. A. Williams, A. B. Padias, H. K. Hall Jr. *Macromolecules* **1996**, *29*, 8313.

[27] A. B. Padias, H. K. Hall Jr. *Polymer* **2011**, *3*, 833.

[28] J. E. McMurry, *Organic chemistry*, Cornell University, California, **1996**.

[29] C. D. Han, S. Chang, S. S. Kim, *Mol. Cryst. Liq. Cryst.* **1994**, *254*, 335.

[30] M. Iqbal, B. Norder, E. Mendes, T. J. Dingemans, *J. Polym. Sci., Part A: Polym. Chem.* **2009**, *47*, 1368.

[31] D. J. Wilson, C. G. Vonk, A. H. Windle, *Polymer* **1993**, *34*, 227.

[32] D. Acierno, F. P. La Mantia, G. Polizzotti, A. Ciferri, B. Valenti, *Macromolecules* **1982**, *15*, 1455.

[33] P. Wei, M. Cakmak, Y. Chen, X. Wang, Y. Wang, Y. Wang, *J. Appl. Polym. Sci.* **2014**, *131*, 40487.

[34] A. M. Lobanov, S. Y. Frenkel, *Polym. Sci. USSR*, **1980**, *22*, 1150.

[35] H. C. Jung, H. S. Lee, Y. S. Chun, S. Kim, W. N. Kim, *Polym. Bull.* **1998**, *41*, 387.

[36] J. He, W. Bu, *Polymer* **1994**, *35*, 5061.

[37] M. Garcia, J. I. Eguiazabal, J. Nazabal, *J. Appl. Polym. Sci.* **2004**, *91*, 52.

[38] F. Yazaki, A. Kohara, R. Yosomiya, *Polym. Eng. Sci.* **1994**, *34*, 1129.

[39] R. van de Watering, T. J. Dingemans, unpublished.

[40] C. D. Ruijter, E. Mendes, H. Boerstoel, S. J. Picken, *Polymer* **2006**, *47*, 8517.

[41] C. Sisbandini, H. A. Every, S. Viale, E. Mendes, H. Boerstoel, S. J. Picken, *J. Polym. Sci., Part B: Polym. Phys.* **2007**, *45*, 666.

CHAPTER 5

High-temperature Shape Memory Behavior of Main-chain Liquid Crystal Poly(esterimide)s

Abstract

Herein we demonstrate that main-chain liquid crystal (LC) ABA-triblock poly(esterimide)s can be used as single component high-temperature (≥ 250 °C) shape memory polymers (SMPs). Dual shape memory (SM), triple SM, and one-way reversible SM appear to be possible. The shape fixation (R_f) and shape recovery efficiency (R_r) of a thermoplastic (LCP-22IM) and thermoset (LCP-22IM–5K) triblock copolyesterimide film were investigated using a rheometer in torsion mode. This set-up allows for large deformations at moderate strains and is suitable for materials with a limited elastic strain region such as main-chain LC polymers. A rigid 4-hydroxybenzoic acid/N-(3'-hydroxyphenyl)-trimellitimide (HBA/IM) block was used to provide a stable elastic plateau, which effectively functions as a "permanent" physical network. Thermoplastic LCP-22IM shows excellent dual-SM behavior (R_f and R_r ~100%) at 170 °C. Upon crosslinking (LCP-22IM–5K), we obtain a SMP exhibiting a physical- and chemically-crosslinked network with a well-defined elastic and rubbery plateau. This material displayed high-temperature (≥ 250 °C) tunable triple SM and one-way reversible SM behavior with a single component system.

5.1 Introduction

Since the discovery of shape memory polymers (SMPs) in the 1980s, research interest in the shape memory effect (SME) in polymers has grown rapidly.[1-7] SMPs are stimuli-responsive materials with the ability to undergo a large recoverable deformation upon the application of an external stimulus such as heat, light, solvent, electrical and magnetic fields.[8] So far, thermally responsive SMPs are the most extensively investigated and widely used systems.[9–15]

SMPs can be categorized into one-way dual-SMP, one-way multi-SMP, and two-way SMP. In order to explain the basic molecular design rules and the SM mechanism, we will discuss the one-way dual-SMP. More elaborate SMP examples can be found in the literature.[16-19] A SMP is typically a rigid plastic that has its permanent shape at room temperature, as illustrated in Figure 5.1. The polymer strands of the SMP network are coiled, *i.e.* at their lowest energy (highest entropy) state. The SMP is first heated to a programming temperature (T_{prog}), which is typically above a glass-transition (T_g) and/or melting point (T_m), leading to material softening. An external strain is subsequently applied to the permanent shape, which causes extension of the polymer chains raising the energy state of the system. When cooled to a temperature below either T_g or T_m, the imposed strain will be quenched and maintained even after the removal of the external force. This so-called fixation of a temporary shape marks the completion of the shape programming step. At the molecular level, cooling leads to formation of a rigid scaffold, which constrain the segmental mobility and effectively lock the deformed chain conformation. When reheated to a certain recovery temperature (T_r) above T_g and T_m, the material restores its original permanent shape by releasing the stored free energy and relaxation of the network strands. As the scaffold is removed by melting of glassy and crystalline domains, the free energy is

released, thus driving the polymer chains back to its highest entropic state corresponding to the permanent shape.
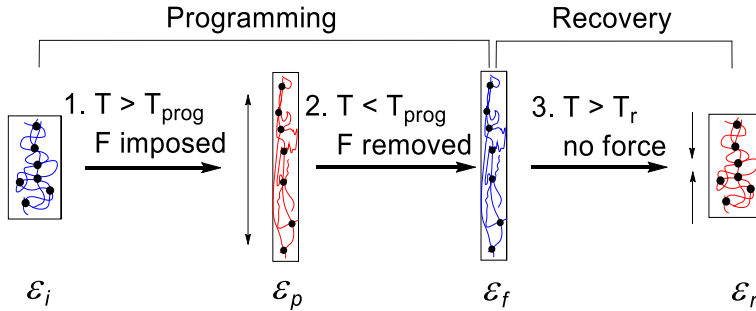
Figure 5.1. Schematic illustration of the dual-shape memory effect in tension mode. Black dots: network points; blue lines: molecular chains of low mobility below T_{prog}; red lines: molecular chains of high mobility above T_{prog} or T_r.

A SMP should meet two design requirements: (i) a permanent network is needed to define the permanent shape and ensure its recovery upon heating and (ii) a second temporary network is needed to enable fixation of a temporary shape. The temporary network can be made using physical interactions *e.g.* crystallites, glassy hard domains,[20] hydrogen bonding,[21] ionic assembly,[22–23] chain entanglements[24], or chemical covalent bonds.[25-26] For chemically cross-linked systems, the permanent network is indeed established by the formation of covalent crosslink points each of which connects more than two chains together. This network should be sufficiently stable to withstand the thermomechanical conditions encountered in the shape memory process without failing otherwise the permanent shape would not fully recover. The shape memory performance is characterized by two parameters: shape fixation (R_f) and shape recovery efficiency (R_r).[1]

$$R_f = \frac{\varepsilon_f}{\varepsilon_p} \times 100\% \qquad (5.1)$$

$$R_r = \frac{\varepsilon_p - \varepsilon_r}{\varepsilon_p} \times 100\% \qquad (5.2)$$

where ε_p represents the programmed strain under load, ε_f is the fixed strain after cooling and load removal, and ε_r is the strain after recovery.

T_{prog} and T_r, both named switching temperatures, can be the same or different, depending on the properties of the SMP. The switching temperature is usually equal to the glass transition temperature (T_g) for an amorphous SMP or melting point (T_m) for a semi-crystalline SMP. The development of thermal-responsive SMPs has primarily been focused on relatively low to medium switching temperatures (< 100 °C) and elastomeric polymers, such as thermoplastic polyurethanes (PU), cross-linked polyethylene (PE), poly-ε-caprolactone, and polynorbornene. Said polymers are appropriate for biomedical and surgical applications, smart fabrics, and heat shrinkable tubing.[27–30] However, SMPs envisioned for aerospace, under the hood automotive or micro-electronic applications often require much higher switching temperatures and more functionality when it comes to shape change and actuation.

In recent years, there have been several reports about semi-crystalline and amorphous high-temperature SMPs, such as polyimides, poly(etheretherketone)s (PEEK) and cyanate esters.[31–33] Gao *et al.*[34] reported on an amorphous SMP made of an epoxy resin blended with PEEK. The cured epoxy domain exhibits a T_g of 223 °C and serves as chemical network to set the permanent shape while PEEK shows a lower T_g (130 °C) and is used as the switching phase.

We note that most high-temperature SMPs are composed of multiple components because the switching temperature of the neat polymer is

relatively low. A recently reported amorphous fluorinated polyimide (Figure 5.2A) that exhibits the highest T_r of 320 °C is a single component system. At the absence of chemical cross-linking, chain entanglements are regarded as physical cross-links resulting in a quasi-permanent network. Excellent SMP properties with the R_f of 97% and R_r of 91% were achieved.[35] Although only simple dual-SM behaviour was demonstrated, this is the first example of a high-temperature SMP based on a single component system. This study also implies that most all-aromatic high-performance polymers are potential high-temperature dual-SMPs.
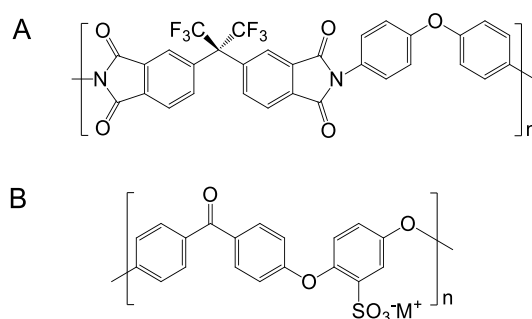
Figure 5.2. Examples of high-temperature SMPs. **A-** Amorphous fluorinated polyimide.[35] **B-** Metal salts of sulfonated PEEK.[40]

Known high-tempertature multi-SMP, mainly triple SMP, blends or composites are composed of at least two well separated components, such as polymer matrices combined with thermal reversible fillers or metal salts.[23, 36-39] Shi *et al.*[40] developed semi-crystalline triple SMPs (Figure 5.2B) based on metal salts of sulfonated PEEK (M-SPEEK) ionomers with T_r as high as 250 °C. The ionomers prepared with multivalent cations display R_f and R_r values greater than 90%, but the maximum temperature for processing and shape memory was limited by the desulfonation of the ionomers, which occurred above 300 °C. Tuning the triple SME for multi-

component systems requires varying the contribution of the reversible phase, which cannot be realized without changing the material composition. This brings up the question whether a high-temperature triple SMP can be designed based on a single component system, which requires a polymer with two thermal transitions, e.g. glass-transition and crystallization.

Main-chain thermotropic liquid crystalline polymers (TLCPs) are a well-known class of high-temperature polymers. They possess excellent properties such as easy processing, high tensile strength and modulus, and excellent solvent resistance, which make them attractive materials for aerospace, electronics, and automotive applications.[41-42] However, to date there has been no report of high-temperature SMPs based on main-chain TLCPs. This is mainly attributed to a lack of an appropriate physical or chemical network in TLCPs to ensure that any macroscopic deformation is the result of molecular chain conformation change, that is, deformation should lead to an entropic change as the necessary driving force for recovery. The presence of a useful physical or chemical network above T_g or T_m can be confirmed by dynamic mechanical thermal analysis (DMTA) of the polymer. Most TLCPs, however, have a high storage modulus (E') but do not exhibit a well-defined rubbery plateau above T_g or T_m. For example, the storage modulus (E') of the LC polyester Vectra-A™ is 5 GPa at 25 °C, but it drops constantly above T_g (Figure 5.3). This means that the conformation of the polymer chains during shape programming cannot be fixed efficiently.
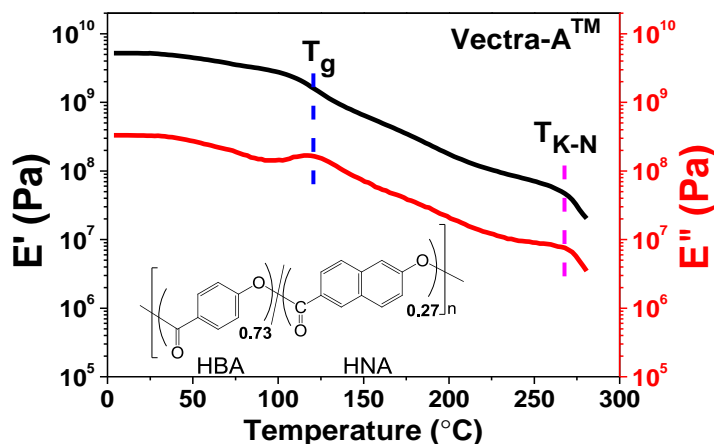
Figure 5.3. Storage modulus (E') and loss modulus (E") as function of temperature for LC polyester Vectra-A™. Heating rate 2 °C·min⁻¹/nitrogen atmosphere and a frequency of 1 Hz. The inset shows the chemical structure of Vectra-A™.

A novel family of LC ABA-triblock poly(esterimide)s with a stable intermediate elastic plateau between two distinct T_gs at ~120 °C and ~200 °C was introduced in *Chapter 4*. Motivated by the unique thermomechanical properties of this new family LCPs , we have explored the feasibility of using the LC poly(esterimide)s as high-temperature single component SMPs. The dual-SME of the LC polyesterimide and cured thermoset will be investigated at elevated temperatures (> 200 °C) and contrasted with the parent LC polyester, Vectra-A™. In addition, more sophisticated SMP forms, such as triple and one-way reversible shape memory behavior and kinetics will be explored using a single component LC ABA-triblock polyesterimide instead of a conventional multi-component system.

5.2 Design

Nematic LCPs are different from amorphous and semi-crystalline polymers in that the molecular chains are easy to align above T_g, which cause significant plastic (unrecoverable) deformation.[42] The alignment is particularly strong upon tensile deformation (Figure 5.1), which is a conventional SMP test. In order to circumvent this problem we have performed shape programming in torsion mode (Figure 5.4). This allows for monitoring large shape transformations, but with only moderate local strains. Accordingly, from the cyclic shape memory torsion test R_f and R_r can be calculated using the following equations:

$$R_f = \frac{\varphi_f}{\varphi_p} \times 100\% \qquad (5.3)$$

$$R_r = \frac{\varphi_p - \varphi_r}{\varphi_p - \varphi_r} \times 100\% \qquad (5.4)$$

where φ_p, φ_f, and φ_r denote the degree of rotation after the torsion step, the degree of rotation of the fixed temporary shape, and the degree of rotation after recovery, respectively.
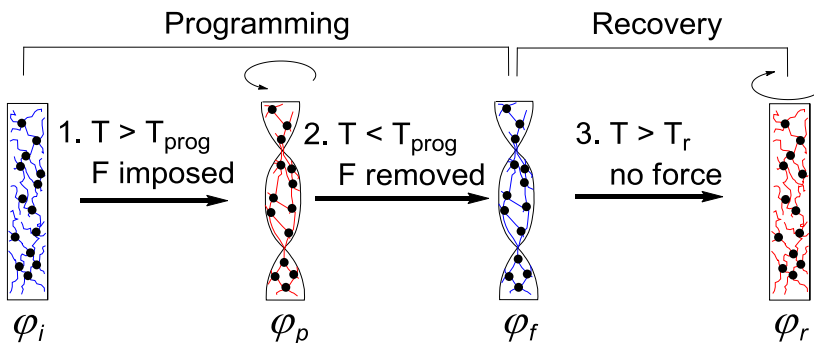
Figure 5.4. Schematic illustration of a dual-SMP experiment performed using a rheometer in controlled torsion mode. Samples under investigation are rotated between 90–180°. In this set-up samples can be exposed the large deformations but they experience little strain.

5.3 Experimental

5.3.1 Materials

The synthesis of the all-aromatic liquid crystal (LC) ABA-triblock polyesterimide LCP-22IM and its reactive oligomer LCP-22IM–5K have been described in *Chapter 4*. The structures of LCP-22IM and LCP-22IM–5K are shown in Figure 5.5.
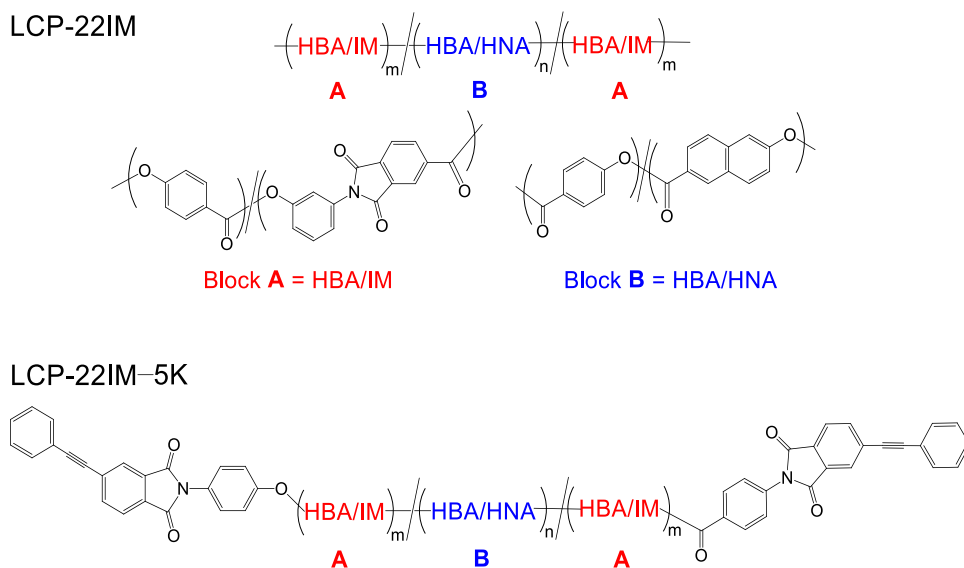
Figure 5.5. Structures of the all-aromatic liquid crystal ABA-triblock polyesterimide LCP-22IM and its reactive oligomer LCP-22IM–5K.

133

5.3.2 Preparation of thin films

The LC thermoplastic and thermoset films were melt pressed using the same method as described in *Chapter 4* (Section 4.2.3).

5.3.3 Characterization

The thermal and mechanical properties of LC polyester Vectra-A™, ABA-triblock polyesterimide LCP-22IM and its reactive oligomer LCP-22IM–5K were reported in *Chapter 4* (Section 4.2.5).

The shape fixation (R_f) and recovery efficiencies (R_r) were determined from shape memory cycles carried out using rectangular thin films with the dimension of (25 ± 1) mm × (4 ± 0.2) mm × (0.25 ± 0.05) mm in controlled torsion mode. The torsion tests were performed using a Thermofisher Haake MARS Ш rheometer equipped with a solid clamp geometry (Figure 5.6). All experiments were performed under a nitrogen atmosphere and at a constant strain rate of $0.001\%{\cdot}s^{-1}$, equivalent to a rotation speed of $0.9°{\cdot}s^{-1}$. The procedure for the cyclic torsion tests includes the following steps: (1) heating the sample to the programming temperature (T_{prog}) at 10 °C·min^{-1}, rotating the sample to a predetermined angle followed by a isothermal hold at T_{prog} for 10 min.; (2) reduce the temperature at 10 °C·min^{-1} followed by removing the stress; (3) heating the sample to the recovery temperature (T_r) at 10 °C·min^{-1}.

Figure 5.6. The torsion mode test setup in a Thermofisher Haake MARS Ш rheometer equipped with a solid clamp geometry.

5.4 Results and discussion

5.4.1 Thermomechanical properties of the ABA-triblock copoly(esterimide)s

The key challenge in the design of thermally activated single component shape memory polymers (SMPs) is to maintain a balance of a permanent network allowing for large and reversible strain and a strong temporary network for shape fixation, which can be released at a specific temperature. To satisfy this requirement, the neat polymer has to possess distinct rubbery property at the fixation temperature and viscoelastic properties in the glassy state,. To evaluate the viscoelasticity of the LC polyester reference polymer (Vectra-A™) and the ABA-triblock copoly(esterimide)s, the storage modulus (E') and loss modulus (E") as function of temperature were studied using dynamic mechanical thermal analysis (DMTA). Thin films were used for the DMTA experiments and the results are shown in Figure 5.7 and summarized in Table 5.1. Reference polymer LC polyester Vectra-A™ has a glass transition temperature (T_g) at 111 °C where the mobility of the polymer segments increases significantly. Vectra-A™ behaves like a typical thermoplastic polymer. E'

135

drops continuously till T_m (T_{K-N} in this case), at which point the experiment terminates. The viscoelastic behavior of Vectra-A™ suggests that it may exhibit shape memory (SM) behavior by taking vitrification as the dual-SMP mechanism.[13,43]
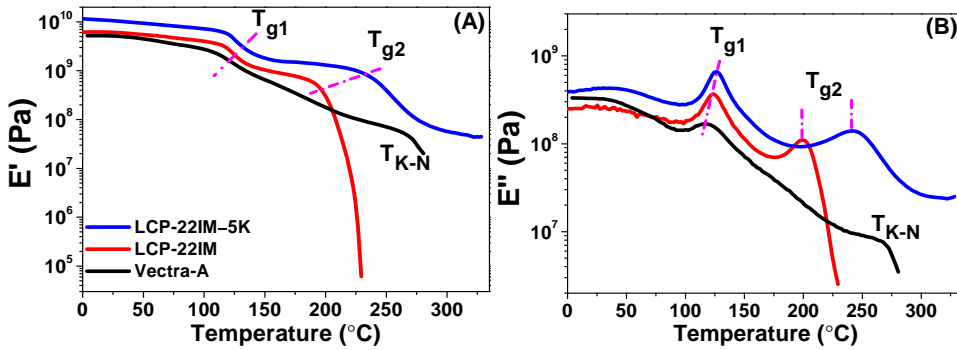
Figure 5.7. DMTA results of the LC polyester reference (Vectra-A™) and triblock poly(esterimide)s melt pressed films. **A-** Storage moduli (E') and **B-** Loss moduli (E") as function of temperature for Vectra-A™, LCP-22IM and LCP-22IM–5K. Heating rate 2 °C·min^{-1}/nitrogen atmosphere and a frequency of 1 Hz. The T_gs were defined by the maximum of the E" peak.

Table 5.1. Thermomechanical and tensile properties of the LC polyester reference polymer (Vectra-A™) and the thermoplastic and thermoset triblock poly(esterimide)s.

Sample	Behavior[a]	T_{g1} (°C)[b]	T_{g2} (°C)[b]	E' (GPa)[b] at 25 °C	Tensile strength (MPa)[c]	Elastic modulus (GPa)[c]	Elongation at break (%)[c]
Vectra-A™	TP	111	-	5	122±26	3.6±1.0	7.3±0.5
LCP-22IM	TP	124	200	6	126±6	4.8±0.6	3.3±0.5
LCP-22IM–5K	TS	126	242	10	103±10	6.8±0.5	1.7±0.2

[a]TP = thermoplastic; TS = thermoset.
[b]T_g and storage modulus (E') data were obtained from DMTA experiments using melt pressed films. The T_g is defined by the maximum of the loss modulus (E'') peak. Heating rate 2 °C·min⁻¹ /nitrogen atmosphere and a frequency of 1 Hz.
[c]From stress-strain experiments. Tensile specimens (75 × 12.5 × 2 mm³, ISO 527-2, type 5A). All experiments were performed at 25 °C at a strain rate of 1 mm·min⁻¹. The data were reported as an average of 5 samples.

The ABA-triblock polyesterimide LCP-22IM consists of 4-hydroxybenzoic acid/N-(3'-hydroxyphenyl)-trimellitimide (HBA/IM) as block A, and 4-hydroxybenzoic acid/6-hydroxy-2-naphthoic acid (HBA/HNA) as block B (Figure 5.5). This polymer shows two distinct T_gs at 124 °C and 200 °C, as shown in Figure 5.7, and the T_gs can be assigned to block B and block A, respectively. A stable intermediate elastic plateau with E' of ~1 GPa between two T_gs is observed, suggesting that LCP-22IM may exhibit SM behavior if the HBA/IM block can effectively function as a "permanent" network. The programming temperature (T_{prog}) is set between the two T_gs. Also, an efficient shape recovery process may be anticipated because the E' of LCP-22IM drops rapidly above T_{g2}, which can be the recovery temperature (T_r). Besides the same T_{g1} at 124 °C, the triblock polyesterimide thermoset LCP-22IM–5K displays a much higher T_{g2} at 254 °C, which is due to the presence of a chemical cross-linked network. The elastic plateau between the two T_gs (E' of ~2 GPa) is broadened compared to LCP-22IM. Moreover, a stable rubbery plateau (E' ~60 MPa) above T_{g2} is observed. This suggests that LCP-22IM–5K may exhibit not only dual-SM behavior but possibly also triple SM using physical and chemical cross-links as the permanent network structure.

An additional advantage of developing SMPs from LC ABA-triblock poly(esterimide)s is their ease of processing and excellent mechanical properties. Both high molecular weight polymer LCP-22IM and low molecular weight (5,000 g·mol^{-1}) reactive oligomer LCP-22IM–5K can be processed like thermoplastics using conventional polymer processing techniques such as extrusion, compression molding, and injection molding. Injection molded tensile specimens of LCP-22IM and LCP-22IM–5K exhibited good tensile properties. For both polymers the tensile strength values are in the range of 100–130 MPa, elastic moduli 5–7 GPa and elongation at break of 1.7–3.3% (Table 5.1), which are comparable to commercial available Vectra™.[44] The outstanding thermomechanical

properties of ABA-triblock poly(esterimide)s makes them potential candidates for high-performance/high-temperature SM applications.

5.4.2 Dual-shape memory behavior

Our materials allow programming different types of shape memory transformations including (i) the conventional dual-shape SM, i.e. a transformation between a temporary and permanent shapes, (ii) triple-shape SM, i.e. one-way sequential transformation between two temporary and one permanent shapes, and (iii) one-way reversible SM, i.e. triple shape memory, where the second temporary shape is identical to the permanent shape. We first present our findings on the dual-shape memory behavior. The thermally activated dual-SM behavior of LC thermoplastics Vectra-A™ and LCP-22IM is shown in Figure 5.8. The shape fixation (R_f) and recovery efficiencies (R_r) were measured from shape memory cycles carried out using a film fixture in the controlled torsion mode of the rheometer.
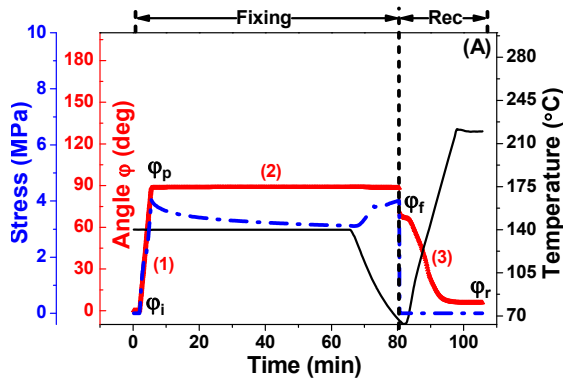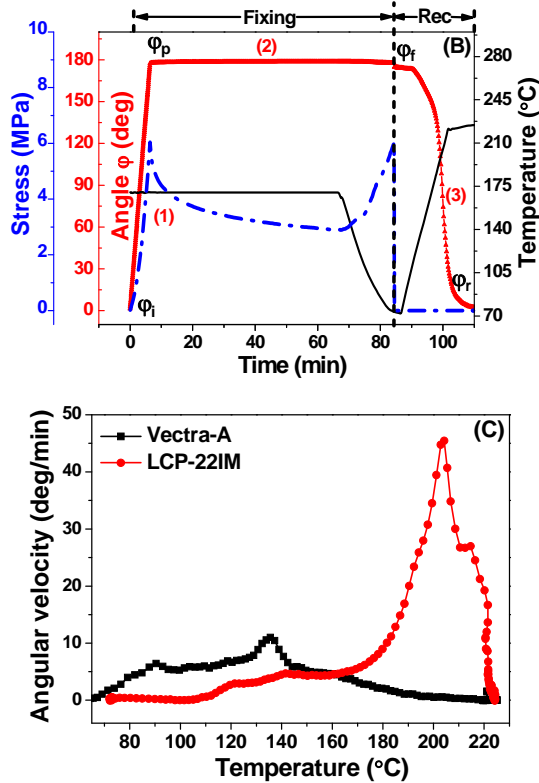
Figure 5.8. SM torsion test of LC thermoplastics polyester (Vectra-A™) and triblock polyesterimide melt pressed films. **A-** Vectra-A™. The degree of rotation = 90°, T_{prog} = 140 °C, T_r = 220 °C. **B-** LCP-22IM. The degree of rotation = 180°, T_{prog} = 170 °C, T_r = 225 °C. To compare the viscoelasticity of Vectra-A™ and LCP-22IM, the samples were isothermally held at T_{prog} for 1 h. For practical purposes, the samples of the torsion tests in all other experiments were isothermally held at T_{prog} for 10–15 min. and the test results were not affected. **C-** Angular velocity of shape recovery as function of temperature during stress-free heating for Vectra-A™ and LCP-22IM. Cooling and heating rate 10 °C·min⁻¹ /nitrogen atmosphere.

In order to avoid local alignment of the samples, only a rotation that could be recovered greater than 90% was chosen for our experiments. For example, the torsion test of the Vectra-A[TM] film with an angle of 90° (rotation rate of ~0.9°·s^{-1}) was performed at 140 °C, which is well above the T_g of the polymer. With the presence of an intermediate elastic plateau between two T_gs, a larger rotation (180°) could be applied to the LCP-22IM film at higher T_{prog} (170 °C).

In the case of Vectra-A[TM], the temporary shape is fixed after initial deformation and isothermally held at 140 °C for 1 h. An external stress of 4 MPa on the sample was generated due to the rotation (Figure 5.8A, step 1). The stress shows a slight decrease at the beginning of step 2 and then levels off at 3 MPa during the isothermal hold step, indicative of the viscoelastic behavior of Vectra-A[TM] at T_{prog}. The stress keeps increasing during the cooling step, which is a stress restoring process, storing the entropy for later shape recovery. The external stress is removed at the end of step 2 where rotation relaxation takes place. Upon heating the temporary shape, recovery starts to take place close to the T_g of Vectra-A[TM], up to 220 °C where the shape recovery finishes. R_f and R_r can be calculated according to eqns. 5.3 and 5.4, and the results are summarized in Table 5.2. Vectra-A[TM] exhibits a moderate R_f value of 77% and high R_r value of 93%. The nematic order (anisotropy, *i.e.* long range order) of Vectra-A[TM], minimal chain entanglements and vitrification help to hold the temporary shape. However, this is not sufficient to fix the deformation (rotation) as the internal stress increased, followed by a large rotation relaxation. This was also observed in other systems which possess only physical cross-links.[45-48]

In contrast to Vectra-A[TM], the torsion test was performed on LCP-22IM at higher T_{prog} (170 °C) and larger rotation (180°). A deformation of 98% could be fixed and the R_r obtained was 100% (Figure 5.8B). The shape fixation was significantly improved due to the existence of the rigid

HBA/IM-blocks and chain entanglements present in LCP-22IM, which play the role of a physical scaffold to hold the temporary shape. Upon cooling below T_{g1}, the shape could be efficiently fixed by both rigid and soft blocks. Investigating the recovery kinematics gives information with respect to the kinetics of recovery (Figure 5.8C). These results show that the shape recovery is triggered by the activation of molecular mobility, which is consistent with a change in viscoelastic properties of the polymers.[49] For example, the HBA/HNA blocks become mobile when the temperature approaches T_{g1} of LCP-22IM, the shape recovery starts with low angular velocity and then reaches a maximum at T_{g2} where the rigid HBA/IM-blocks are softening as well. LCP-22IM exhibits better SM behavior than Vectra-A™ and this can be attributed to the more distinct thermodynamic transitions of the former. Finally, we have looked at the experimental reproducibility. For LCP-22IM we performed 5 consecutive SM cycles under said conditions and found an identical R_f of 95% and R_r of 100% for each SM cycle (Figure 5.9). Single component high-temperature dual-SMPs reported so far, all suffer from a rapid decrease in either R_f or R_r after 5 consecutive cycles.[23,35]

Table 5.2. Shape fixation and recovery efficiencies of the LC polyester reference (Vectra-A™) and the ABA-triblock poly(esterimide)s films.

Sample	T_{prog} (°C)[a]	T_r (°C)[a]	E′ at T_{prog} (MPa)	E′ at T_r (MPa)	Rotation deg (°)	R_f (%)[b]	R_r (%)[b]
Vectra-A™	140	220	827	118	90	77	93
LCP-22IM	170	225	820	50	180	98	100
LCP-22IM –5K	180	275	1480	102	120	91	95
	250	285	400	75	120	90	90

[a]T_{prog} and T_r refer to the programming temperature and recovery temperature, respectively.

[b]R_f and R_r refer to shape fixation and recovery efficiencies, respectively.
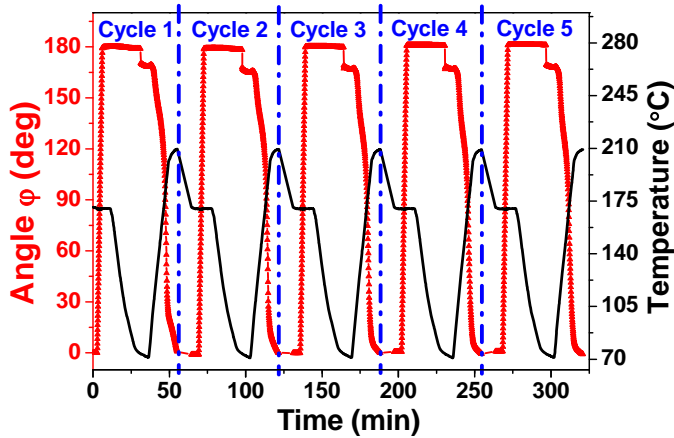
Figure 5.9. Five consecutive shape memory cycles for LCP-22IM. The degree of rotation = 180°, T_{prog} = 170 °C, isothermal hold at T_{prog} for 10 min., T_r = 210 °C. Cooling and heating rate 10 °C·min^{-1}/nitrogen atmosphere.

Unlike the physical scaffold present in the LC thermoplastics Vectra-A™ and LCP-22IM, a different mechanism is at work in the cured LCP-22IM analog (LCP-22IM–5K). Here we have the same rigid HBA/IM-blocks but they (partially) crosslinked into a permanent covalently linked network. Both the physical and chemical cross-links act as a scaffold and prevent polymer chain slippage. The same shape change (degree of rotation = 120°) for LC-22IM–5K was programmed at 180 °C and 250 °C, respectively. The high E' in the glassy state gives rise to a large increase in internal stress during cooling, resulting in a rotation relaxation when the external stress is removed. Both tests exhibit good shape fixation and recovery efficiency (≥ 90%) as shown in Figures 5.10A and 5.10B.
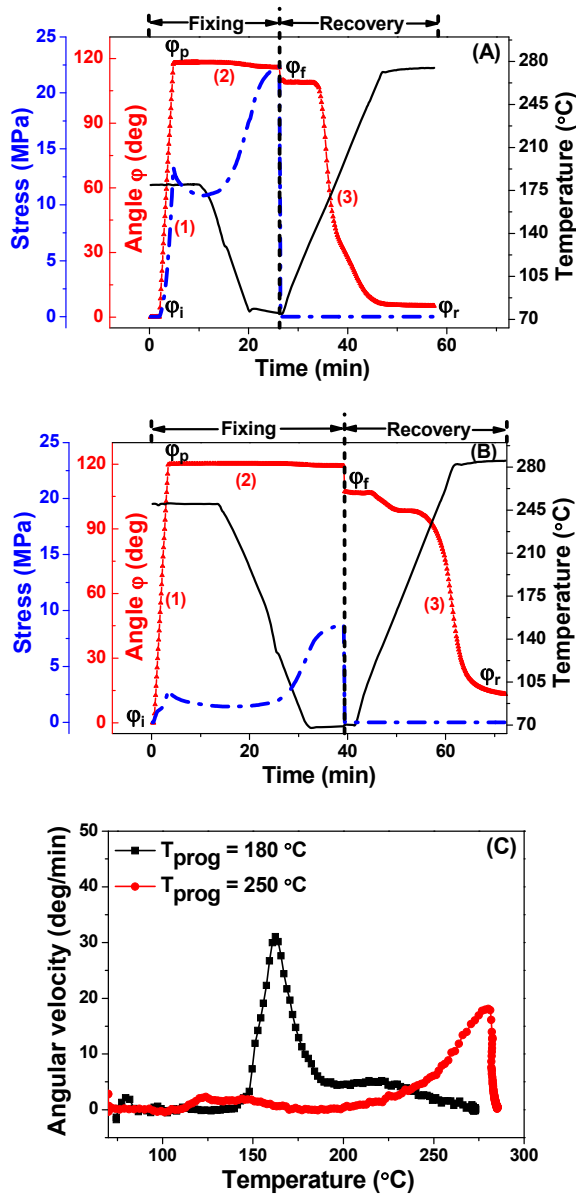
Figure 5.10. SM torsion test of LCP-22IM–5K cured thermoset films. **A-** The degree of rotation = 120°, T_{prog} = 180 °C, T_r = 275 °C. **B-** The degree of rotation = 120°, T_{prog} = 250 °C, T_r = 285 °C. **C-** Angular velocity of shape recovery as function of temperature during stress-free heating for the

experiments shown in Figures **A** and **B**. Cooling and heating rate 10 °C·min^{-1}/nitrogen atmosphere.

Figure 5.10C displays two different shape recovery processes, depending on the program temperature used. For the shape programming at 180 °C, the rotation was applied to the entire sample, but only the HBA/HNA block contributed to the deformation. The temporary shape was fixed by both the HBA/IM- and HBA/HNA-blocks during cooling. The shape recovery took place between 150–190 °C, which is lower than that of LCP-22IM due to the presence of a larger internal stress in LCP-22IM–5K. With respect to the shape programming at 250 °C, both HBA/HNA- and HBA/IM-blocks yield under the applied stress field. Upon heating (recovery phase), a small portion of the initial shape is recovered at 125 °C, which is driven by the entropy stored in the HBA/HNA-blocks whereas the main shape recovery at 230–285 °C is driven by the entropy stored in the (crosslinked) HBA/IM-blocks. To the best of our knowledge, this is the first demonstration of a high-temperature LC dual-SMP.

5.4.3 Triple shape memory behavior

In the previous section we discussed the dual-SM behavior of the LC thermoplastics, Vectra-A™ and LCP-22IM, and thermoset LCP-22IM–5K. The latter exhibits dual-shape recovery at two distinct temperature ranges due to the co-existence of a high intermediate elastic plateau (E′ = ~2 GPa) between the two T_gs (T_{g1} = 126 °C and T_{g2} = 242 °C, respectively) with a stable rubbery plateau (E′ = ~60 MPa) above T_{g2}. This unique viscoelastic behavior encourages us to explore whether it's possible to design a triple SMP based on LCP-22IM–5K.

The LCP-22IM–5K film was first heated to 250 °C, which is above both

T_gs, and the film was rotated to 30° (temporary shape B). The sample was isothermally held at 250 °C for 15 min. and then cooled to 180 °C to fix the temporary shape B (Figure 5.11A). A second rotation of 90° was then applied to program temporary shape C at 180 °C. This resulted into a significant increase in stress since the chemically crosslinked HBA/IM-block are difficult to deform. The sample was isothermally held at 180 °C for 15 min. and then cooled to 70 °C to fix temporary shape C. The external stress was then removed, resulting in a small rotation relaxation. Similar strain contraction was observed in other triple SMP systems.[50–52]
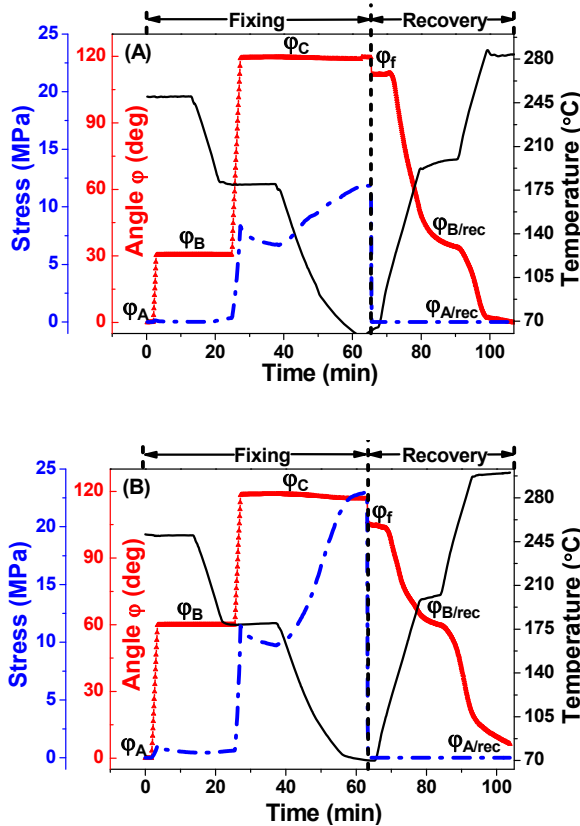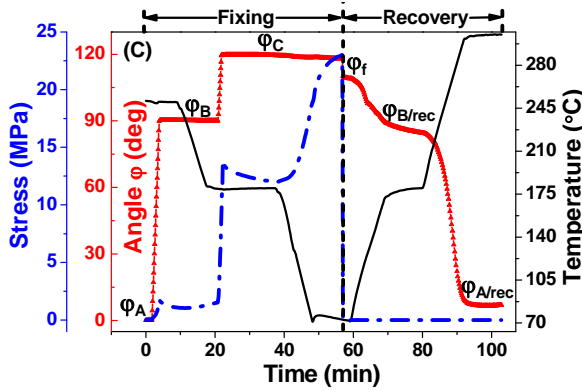
Figure 5.11. Triple SM torsion test of LCP-22IM–5K with various partitionings. **A-** The degree of rotation = 30° + 90°, $T_{prog(A\rightarrow B)}$ = 250 °C, $T_{prog(B\rightarrow C)}$ = 180 °C, $T_{r(C\rightarrow B)}$ = 200 °C, $T_{r(B\rightarrow A)}$ = 280 °C. **B-** The degree of rotation = 60° + 60°, $T_{prog(A\rightarrow B)}$ = 250 °C, $T_{prog(B\rightarrow C)}$ = 180 °C, $T_{r(C\rightarrow B)}$ = 200 °C, $T_{r(B\rightarrow A)}$ = 295 °C. **C-** The degree of rotation = 90° + 30°, $T_{prog(A\rightarrow B)}$ = 250 °C, $T_{prog(B\rightarrow C)}$ = 180 °C, $T_{r(C\rightarrow B)}$ = 180 °C, $T_{r(B\rightarrow A)}$ = 300 °C. Cooling and heating rate 10 °C·min^{-1}/nitrogen atmosphere.

A shape fixation (R_f) of 95% was calculated using eqn. 5.5. Sequential shape recovery was achieved by heating the sample that was in the temporary shape C to 200 °C to recover the temporary shape B, followed by heating to 280 °C to recover the permanent shape A (Figure 5.11A). Shape recoveries $R_{r(C\rightarrow B)}$ of 94% and $R_{r(B\rightarrow A)}$ of 98% were obtained based on eqns. 5.6 and 5.7, respectively.[52]

$$R_f = \frac{\varphi_f}{\varphi_C} \times 100\% \qquad (5.5)$$

$$R_{r(C\rightarrow B)} = \frac{\varphi_C - \varphi_{B/rec}}{\varphi_C - \varphi_B} \times 100\% \qquad (5.6)$$

147

$$R_{r(B \to A)} = \frac{\varphi_B - \varphi_{A/rec}}{\varphi_B - \varphi_A} \times 100\% \qquad (5.7)$$

where φ_A is the degree of permanent shape A (0°), φ_B and φ_C denote the degree of rotation of the two temporary shapes B and C, respectively, $\varphi_{A/rec}$ and $\varphi_{B/rec}$ are the degree of recovery.

The experimental results, as shown in Figure 5.11A, suggest that LCP-22IM–5K can memorize two metastable shapes in a single shape memory cycle, which means triple shape memory is indeed possible.[53] Unlike the traditional high-temperature triple SMP composed of multiple components, LCP-22IM–5K, as a single component system possesses multiple phase switches which are possible because of a well-defined elastic and rubbery plateau (see DMTA results, Figure 5.7). This provides controllable and complex shape morphing ability, which is clearly demonstrated by the triple SM torsion tests using different partitioning schemes (Figures 5.11B and 5.11C). The triple SM test results are summarized in Table 5.3. The triple SME of LCP-22IM–5K, therefore, is highly tunable within a broad temperature regime (110–300 °C), as shown in Figure 5.12A. It is interesting to note that the absolute angular velocity ($V_a = d\varphi/dt$) of each triple SM test cycle is proportional to the programmed rotation. This can be confirmed by the near identical relative recovery rate (V_r) values in Figure 5.12B. The V_r is defined as:

$$V_r = \frac{\frac{d\varphi}{dt}}{\varphi_p} \qquad (5.8)$$

where φ_p is the programmed rotation. This provides a convenient method to program the triple SM behavior of a polymer for desired applications.
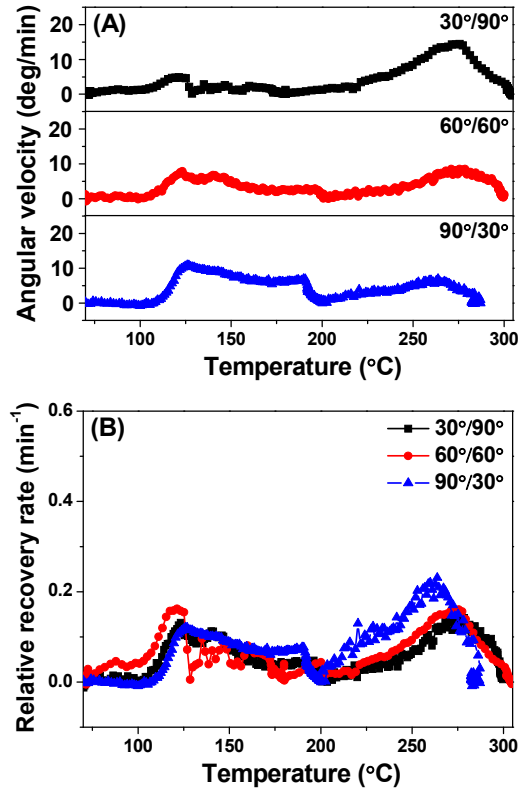
Figure 5.12. Kinetics of the shape recovery as function of temperature during stress-free heating for triple SM torsion tests of LCP-22IM–5K. **A-** Absolute angular velocity of shape recovery. **B-** Relative shape recovery rate.

Table 5.3. Summary of the triple SM test results using LCP-22IM–5K.

Partitioning (deg/deg)	$T_{prog(A \to B)}$ (°C)[a]	$T_{prog(B \to C)}$ (°C)[a]	$T_{r(C \to B)}$ (°C)[a]	$T_{r(B \to A)}$ (°C)[a]	Rotation degree$_{(A \to B)}$ (°)	Rotation degree$_{(B \to C)}$ (°)	R_f (%)[b]	$R_{r(C \to B)}$ (%)[b]	$R_{r(B \to A)}$ (%)
30/90	250	180	200	280	30	90	95	94	98
60/60	250	180	200	295	60	60	88	100	89
90/30	250	180	180	300	90	30	93	100	93

[a]T_{prog} and T_r refer to the fixing temperature and recovery temperature, respectively.

[b]R_f and R_r refer to the shape fixation and recovery efficiencies, respectively.

5.4.4 One-way reversible shape memory behavior

The SM behavior discussed so far, dealt with shapes that were programmed to deform in one direction, either forward or backward, and then the shapes were recovered by heating in the reverse direction. When both forward and backward deformations are programmed into one shape memory cycle, theoretically the corresponding temporary shapes would recover in the reverse direction. To demonstrate the feasibility of such a process our LCP-22IM–5K crosslinked sample was programmed forward to 90° at T > T_{g2} and back to 0° (by $\Delta\varphi = -90°$) *via* the intermediate elastic plateau, as described in more detail below. This programs the sample to perform a shape reversible transition in the shape memory cycle. As shown in Figure 5.13, a sample having a permanent shape A (0°) was heated to $T_{prog(A\to B)} = 250$ °C and applied a forward rotation to 90° (temporary shape B, $\Delta\varphi = +90°$).
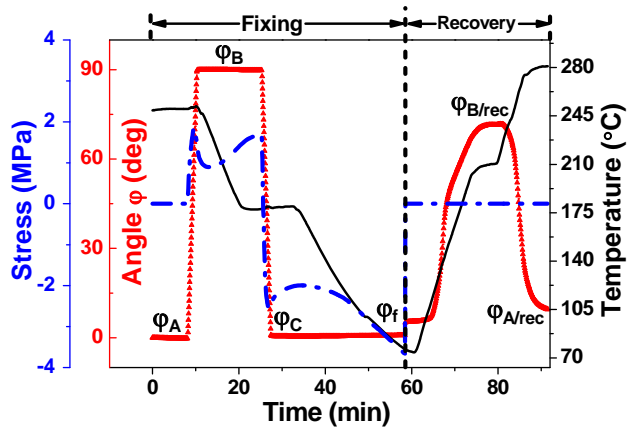
Figure 5.13. One-way reversible shape memory test of LCP-22IM–5K. The degree of rotation = +90°/–90°, $T_{prog(A\to B)} = 250$ °C, $T_{prog(B\to C)} = 180$ °C, $T_{r(C\to B)} = 210$ °C, $T_{r(B\to A)} = 280$ °C. Cooling and heating rate 10 °C·min⁻¹ /nitrogen atmosphere.

The sample was cooled to $T_{prog(B \to C)}$ = 180 °C and rotated back to 0° ($\Delta\varphi$ = –90°), having a new temporary shape C. The sample was isothermally held at 180 °C for 15 min. and then fixed (R_f = 95%) by cooling to 70 °C. Subsequent heating from 70 °C to $T_{r(C \to B)}$ = 210 °C and then to $T_{r(B \to A)}$ = 280 °C, triggered a transition in the reverse direction from temporary shape C to temporary shape B and back to permanent shape A.

The shape recovery $R_{r(C \to B)}$ and $R_{r(B \to A)}$ are 80% and 90%, respectively. This can be understood when one considers the fact that the soft HBA/HNA-block that deformed together with the rigid HBA/IM-block at 250 °C was still mobile when the system was cooled to 180 °C. At this temperature, a backward rotation was applied to HBA/HNA-block, which results in a deformation of the film that is less than the programmed value of 90°. Despite the $R_{r(C \to B)}$ value of 80% our results demonstrate that LCP-22IM–5K could work in a one-way reversible SM system. Note that the reversible shape transformations in this experiment occurred without application of any external mechanical force. They were driven by internal stress of the oppositely strained sub-networks of glassy domains formed during the first and second fixation steps. Our results clearly demonstrate that tunable high-temperature SMEs can be designed based on our ABA-triblock poly(esterimide)s, both the thermoplastic LCP-22IM and the crosslinked analog LCP-22IM–5K are useful candidates.

5.5 Conclusions

In summary, our research demonstrates that our all-aromatic liquid crystal ABA-triblock copoly(etherimide)s can be used as high-temperature (≥ 250 °C) single component shape memory polymers. Although the LC polyester Vectra-A™ reference polymer exhibits dual-SM behavior only (rotation of 90°, T_{prog} = 140 °C and T_r = 220 °C), a novel LC ABA-triblock copolyesterimide LCP-22IM demonstrates more robust SM

performance. The rigid HBA/IM-blocks in conjunction with chain entanglements in LCP-22IM play the role of a physical scaffold and ensures that the temporary shape can be recovered after large deformations. Rotating a LCP-22IM film by 180° and recovering the original shape results in an R_f of 98% and R_r of 100% (T_{prog} = 170 °C and T_r = 225 °C). LCP-22IM–5K, a crosslinked analog of LCP-22IM, exhibits two distinct T_gs at 126 °C (T_{g1}) and 242 °C (T_{g2}), respectively. The elastic plateau and rubbery plateau above T_{g1} and T_{g2} allowed us to explore more elaborate SM designs. We demonstrated high-temperature (≥ 250 °C) LC dual-SM with good shape fixation and recovery efficiency in excess of 90% (rotation of 120°, T_{prog} = 140 °C and T_r = 220 °C). Tunable high-temperature triple SM and one-way reversible SM were also demonstrated using this single component LC ABA-triblock copolyesterimide.

5.6 References

[1]   M. Behl, A. Lendlein*, Mater. Today* **2007**, *10*, 20.

[2]   A. Lendlein, S. Kelch, *Angew. Chem. Int.* **2002**, *41*, 2034.

[3]   Y. J. Liu, H. B. Lv, X. Lan, J. S. Leng, S. Y. Du, *Compos. Sci. Technol.* **2009**, *69*, 2064.

[4]   I. S. Gunes, S .C. Jana, *J. Nanosci. Nanotechnol*. **2008**, *8*, 1616.

[5]   D. Ratna, J. Karger-Kocsis, *J. Mater. Sci.* **2008**, *43*, 254.

[6]   C. Liu, H. Qin, P. T. Mather, *J. Mater. Chem.* **2007**, *17*, 1543.

[7]   V. A. Beloshenko, V. N. Varyukhin, Y. V. Voznyak, *Russ. Chem. Rev.* **2005**, *74*, 265.

[8]   A. Nelson, *Nat. Mater.* **2008**, *7*, 523.

[9]   A. Khaldi, J. A. Elliott, S. K. Smoukov, *J. Mater. Chem. C* **2014**, *2*, 8029.

[10]   T. F. Scott, R. B. Draughon, C. N. Bowman, *Adv. Mater.* **2006**, *18*, 2128.

[11]   D. H. Yi, H. J. Yoo, S. S. Mahapatra, Y. A. Kim, J. W. Cho, *J. Colloid Interface Sci.* **2014**, *432*, 128.

[12] A. M. Schmidt, *Macromol. Rapid Commun.* **2006**, *27*, 1168.

[13] T. Xie, *Nature* **2010**, *464*, 267.

[14] J. Zhou, S. A. Turner, S. M. Brosnan, Q. Li, J.-M. Y. Carrillo, D. Nykypanchuk, O. Gang, V. S. Ashby, A. V. Dobrynin, S. S. Sheiko, *Macromolecules* **2014**, *47*, 1768.

[15] K. Kratz, S. A. Madbouly, W. Wagermaier, A. Lendlein, *Adv. Mater.* **2011**, *23*, 4058.

[16] Q. Zhao, H. Jerry Qi, T. Xie, *Prog. Polym. Sci.* **2015**, *49-50*, 79.

[17] M. Behl, M. Y. Razzaq, A. Lendlein, *Adv. Mater.* **2010**, *22*, 3388.

[18] T. Xie, *Polymer* **2011**, *52*, 4985.

[19] J. S. Leng, X. Lan, S. Y. Du, *Prog. Mater. Sci.* **2011**, *56*, 1077.

[20] A. Lendlein, S. Kelch, *Angew. Chem. Int. Ed.* **2002**, *41*, 2034.

[21] S. B. Zhou, X. T. Zheng, X. J. Yu, J. X. Wang, J. Weng, X. H. Li, *Chem. Mater.* **2007**, *19*, 247.

[22] J. Dong, R. A. Weiss, *Macromolecules* **2011**, *4*, 8871.

[23] Y. Shi, M. Yoonessi, R. A. Weiss, *Macromolecules* **2013**, *46*, 4160.

[24] X. Z. Gu, P. T. Mather, *Polymer* **2012**, *53*, 5924.

[25] J. H. Li, J. A. Viveros, M. H. Wrue, M. Anthamatten, *Adv. Mater.* **2007**, *19*, 2851.

[26] J. H. Li, C. L. Lewis, D. L. Chen, M. Anthamatten, *Macromolecules* **2011**, *44*, 5336.

[27] T. Defize, R. Riva, J.-M. Raquez, P. Dubois, C. Jérôme, M. Alexandre, *Macromol. Rapid Commun.* **2011**, *32*, 1264.

[28] Q. Ge, X. Luo, E. D. Rodriguez, X. Zhang, P. T. Mather, M. L. Dunn, H. J. Qi, *J. Mech. Phys. Solids* **2012**, *60*, 67.

[29] H. Luo, J. Hu, Y. Zhu, *Mater. Lett.* **2011**, *65*, 3583.

[30] W. B. Song, L. Y. Wang, Z. D. Wang, *Mater. Sci. Eng., A* **2011**, *529*, 29.

[31] M. Yoonessi, Y. Shi, D. A. Scheiman, M. Lebron-Colon, D. M. Tigelaar, R. A. Weiss, M. A. Meador, *ACS Nano* **2012**, *6*, 7644.

[32] H. Koerner, R. J. Strong, M. L. Smith, D. H. Wang, L. S. Tan, K. M. Lee, T. J. White, R. A. Vaia, *Polymer* **2013**, *54*, 391.

[33] F. Xie, L. N. Huang, Y. J. Liu, J. S. Leng, *Polymer* **2014**, *55*, 5873.

[34]   J. Gao, C. Zhang, X. He, H. Ma, X. An, G. Dang, C. Chen, *Adv. Mater. Res.* **2010**, *152–153*, 530.

[35]   X. L. Xiao, D. Y. Kong, X. Y. Qiu, W. B. Zhang, F. H. Zhang, L. W. Liu, Y. J. Liu, S. Zhang, Y. Hu, J. S. Leng, *Macromolecules* **2015**, *48*, 3582.

[36]   N. G. Sahoo, Y. C. Jung, H. J. Yoo, J. W. Cho, *Compos. Sci. Technol.* **2007**, *67*, 1920.

[37]   G. H. Pan, W. M. Huang, Z. C. Ng, N. Liu, S. J. Phee, *Smart. Mater. Struct.* **2008** ,*17*, 045007.

[38]   A. Balazs, T. Emrick, T. P. Russell, *Science* **2006**, *314*, 1107.

[39]   E. Manias, *Nat. Mater.* **2007**, *6*, 9.

[40]   Y. Shi, R. A. Weiss, *Macromolecules* **2014**, *47*, 1732.

[41]   J. Mark, K. Ngai, W. Graessley, L. Mandelkern, E. Samulski, J. Koenig, G. Wignall, *Physical Properties of Polymers*, Cambridge University Press, Cambridge UK **2004**, p. 362.

[42]   A. M. Donald, A. H. Windle, *Liquid Crystalline Polymers,* Cambridge University Press, Cambridge UK **1992**.

[43]   Y. Shao, C. Lavigueur, X. X. Zhu, *Macromolecules* **2012**, *45*, 1924.

[44]   ''Ticona Vectra Liquid Crystal Polymer (LCP) Product Information,'' Ticona, Summit, NJ, 07901, **2000**.

[45]   R. A. Weiss, E. Izzo, S. Mandelbaum, *Macromolecules* **2008**, *41*, 2978.

[46]   C. J. Kloxin, T. F. Scott, B. J. Adzima, C. N. Bowman *Macromolecules* **2010**, *43*, 2643.

[47]   R. J. Wojtecki, M. A. Meador, S. J. Rowan, *Nat. Mater.* **2011**, *10*, 14.

[48]   Y. Yang, M. W. Urban, *Chem. Soc. Rev.* **2013**, *42*, 7446.

[49]   F. Liu, M. W. Urban, *Prog. Polym. Sci.* **2010**, *35*, 3.

[50]   T. Chung, A. Rorno-Uribe, P. T. Mather, *Macromolecules* **2008**, *41*, 184.

[51]   J. Li, W. R. Rodgers, T. Xie, *Polymer* **2011**, *52*, 5320.

[52]   T. Xie, X. Xiao, Y. Cheng, *Macromol. Rapid Commun.* **2009**, *30*, 1823.

[53]   M. Behl, A. Lendlein, *J. Mater. Chem.* **2010**, *20*, 3335.

Summary

The main objective of this research is to understand the structure-property relationships of all-aromatic (multiblock) copoly(esterimide)s and crosslinkable oligomers thereof. A non-linear imide-based monomer, N-(3'-hydroxyphenyl)-trimellitimide (IM), was used to modify poly(4-hydroxybenzoic acid) (pHBA) and the effects on polymer morphology, processing characteristics and the final thermomechanical properties were investigated.

In *Chapter 2* we described the synthesis and properties of a semi-crystalline polyesterimide based on 30 mol% IM and 70 mol% 4-hydroxybenzoic acid (HBA). This approach resulted in a complex biphasic polymer composite, in which the crystalline, pHBA-rich phase co-exists with the liquid crystal (nematic) IM/HBA phase. Despite a high glass transition temperature (T_g) of 205 °C, the as prepared films display poor mechanical properties. However, upon thermal stretching above T_g, the films show a dramatic increase in thermal properties. The T_g of the polymer increased from 205 °C to 248 °C whereas the T_g of the thermoset increased from 207 °C to 284 °C. At the same time, the energy at break of the thermally treated films improved by a factor of 2.

With the aim to explore more processable IM/HBA formulations, analogous poly(esterimide)s with larger concentrations of IM, *i.e.* 40, 50 and 70 mol%, are discussed in *Chapter 3*. All as made poly(esterimide)s show a semi-crystalline morphology whereas all melt pressed films are amorphous. The thermomechanical properties are independent of the molar composition. Upon thermal post-treatment, T_g's of 260 °C and 290 °C are obtained for the parent polymer with 70 mol% IM (7-IM/3-HBA) and the cured thermoset (7-IM/3-HBA–2K), respectively. A thermally stretched 7-IM/3-HBA film shows a high tensile strength of 169 MPa and an elongation at break of 3.3%.

In *Chapter 4* liquid crystal formulations based on 6-hydroxy-2-naphthoic acid (HNA), HBA an IM are discussed. Due to the low reactivity of IM an ABA-triblock copolyesterimide with two distinct T_g's was obtained. The first T_g at ~120 °C can be assigned to the HBA/HNA block (block B) and the second T_g at ~220 °C can be assigned to the HBA/IM block (block A). This is the first example, to the best of our knowledge, of a main-chain LC ABA-triblock copolymer prepared *via* a simple one-pot melt polymerization method. HR-SEM studies showed that at low IM concentrations the HBA/HNA and HBA/IM blocks are compatible as there is little microphase separation on a length scale of 50 nm.

Finally, motivated by the unique thermomechanical properties of the LC ABA-triblock polymers, we explored their high-temperature (≥ 250 °C) shape memory behaviour and the initial results are presented in *Chapter 5*. The shape fixation (R_f) and shape recovery efficiency (R_r) of the ABA-triblock copolyesterimide films were investigated using a rheometer in torsion mode. Thermoplastic LCP-22IM shows excellent dual-SM behavior (R_f and R_r = ~100%) at 170 °C. Using LCP-22IM–5K, a crosslinked polymer analogous to LCP-22IM, a SMP could be prepared exhibiting a physical and chemically crosslinked network with a well-defined elastic and rubbery plateau. We demonstrated high-temperature (≥ 250 °C) LC dual-SM with R_f and R_r values in excess of 90% (rotation of 120°, T_{prog} = 140 °C and T_r =220 °C). Tunable high-temperature triple SM and one-way reversible SM were also demonstrated using this single component LC ABA-triblock copolyesterimide.

Samenvatting

Het hoofddoel van dit onderzoek is om de structuur-eigenschap relatie van geheel aromatisch (multiblok) copoly(esterimide)s en hun vernetbare oligomeren te begrijpen. We gebruikten een non-lineair imide monomeer, N-(3'-hydroxyphenyl)-trimellitimide (IM), om poly(4-hydroxybenzoic acid) (pHBA) te modificeren en keken daarbij naar wat de effecten op de polymeermorfologie, de verwerkingseigenschappen en de uiteindelijke thermomechanische eigenschappen zijn.

In *Hoofdstuk 2* worden de synthese en eigenschappen van een semi-kristallijn polyesterimide, gebaseerd op 30 mol% IM en 70 mol% 4-hydroxybenzoic acid (HBA), beschreven. Deze aanpak resulteerde in een complex twee fase polymeer composiet, waarbij de kristallijne pHBA fase co-existeert met de vloeibaar kristallijne (nematische) IM/HBA fase. Ondanks het feit dat polymeerfilmpjes een hoge glasovergangstemperatuur (T_g) hebben van 205 °C zijn de mechanische eigenschappen slecht. Echter, door de polymeerfilmpjes thermisch te verstrekken boven de T_g blijken de thermische eigenschappen sterk te verbeteren. De T_g van het polymeer stijgt van 205 °C naar 248 °C, en de T_g van de thermoharder gaat van 207 °C naar 284 °C. Tegelijkertijd gaat na de warmte behandeling de breukenergie van de filmpjes omhoog met een factor 2.

Om de verwerkbaarheid van IM/HBA te verbeteren hebben we een serie IM/HBA polymeren gesynthetiseerd met hogere concentraties IM, te weten: 40, 50 en 70 mol%. De resultaten worden besproken in *Hoofdstuk 3*. Alle gesynthetiseerde poly(etherimide)s zijn initieel semi-kristallijn, maar de vanuit de smelt verwerkte polymeerfilmpjes zijn amorf. De thermomechanische eigenschappen blijken onafhankelijk te zijn van de moleculaire compositie. Na een thermische behandeling heeft het referentiepolymeer met 70 mol% IM (7-IM/3-HBA) een T_g van 260 °C en heeft de 7-IM/3-HBA thermoset een T_g van 290 °C. Het 7-IM/3-HBA

referentiepolymeer heeft, nadat het thermisch verstrekt is, een treksterkte van 169 MPa en een breukrek van 3.3%.

In *Hoofdstuk* 4 worden vloeibaar kristallijne polymeren gebaseerd op 6-hydroxy-2-naphthoic acid (HNA), HBA en IM besproken. Vanwege de lage reactiviteit van IM verkregen we een ABA-triblok copolyesterimide met twee duidelijk van elkaar gescheiden T_g's. De eerste Tg bij ~120 °C kan worden toegekend aan het HBA/HNA blok (blok B) en de tweede T_g bij ~220 °C hoort bij het HBA/IM blok (blok A). Voor zover we weten, is dit het eerste voorbeeld waarbij een vloeibaar kristallijn ABA-triblok copolymeer gesynthetiseerd wordt via een eenvoudige één-stap smeltcondensatie methode. HR-SEM studies laten zien dat de HBA/HNA en HBA/IM blokken compatibel zijn met elkaar bij lage IM concentraties. Tot 50 nm is er weinig tot geen fasescheiding waarneembaar.

Tenslotte hebben we, gemotiveerd door de unieke thermomechanische eigenschappen van de vloeibaar kristallijne ABA-triblok copolymeren, de hoge temperatuur (≥ 250 °C) geheugen eigenschappen (*i.e.* de mogelijkheid om voorgeprogrammeerde vormen te onthouden) onderzocht. De eerste resultaten zijn gerapporteerd in *Hoofdstuk 5*. We onderzochten de vormfixatie (R_f) en vormherstel efficiency (R_r) van de ABA-triblok polyesterimide met een torsie rheometer. Het thermoplastisch LCP-22IM polymeer vertoont uitstekende geheugen eigenschappen (R_f en R_r = ~100%) bij 170 °C. Met LCP-22IM-5K, de thermoset analoog, bleek het mogelijk om een geheugenpolymeer te maken gebaseerd op een fysische en chemisch netwerkstructuur met een goed gedefinieerd elasticiteits en rubber plateau. Hoge temperatuur (≥ 250 °C) geheugen eigenschappen met hoge R_f en R_r waarden (>90%) (rotatie van 120°, T_{prog} = 140 °C en T_r =220 °C) konden worden gedemonstreerd. Complexe vorm programmering, zgn. "triple shape-memory" en "one-way reversible shape-memory", bleek ook mogelijk met deze vloeibaar kristallijn ABA-triblok poly(esterimide)s.

Appendix
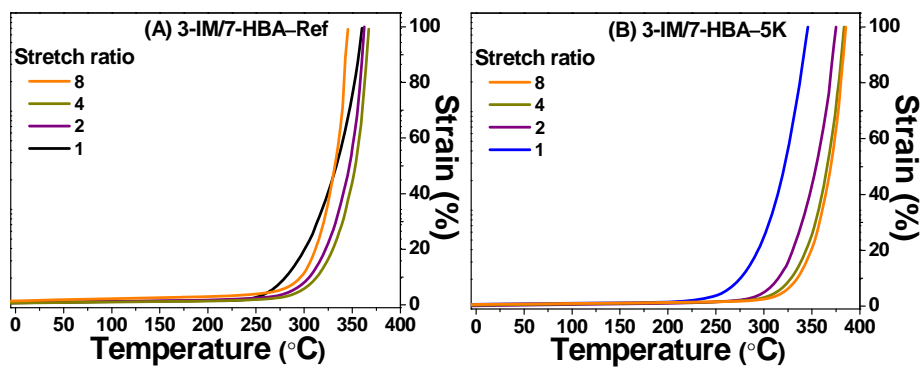
Figure 2.1S. Stretch behaviors of **A-** 3-IM/7-HBA–Ref and **B-** 3-IM/7-HBA–5K films as function of temperature.
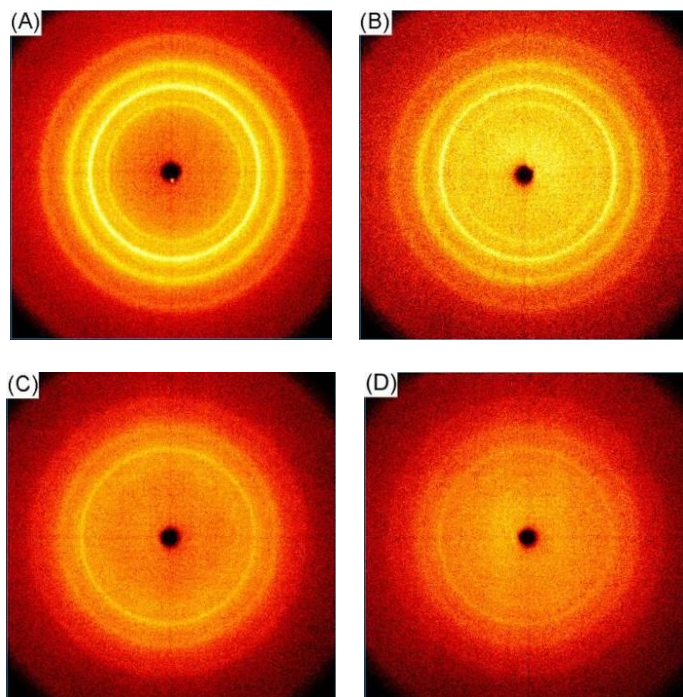
Figure 2.2S. Diffraction pattern recorded on a two dimensional detector for the reference polymer and cured thermoset films at 25 °C. **A-** 3-IM/7-HBA–Ref SR1, **B-** 3-IM/7-HBA–Ref SR16, **C-** 3-IM/7-HBA–5K SR1, **D-** 3-IM/7-HBA–5K SR16.
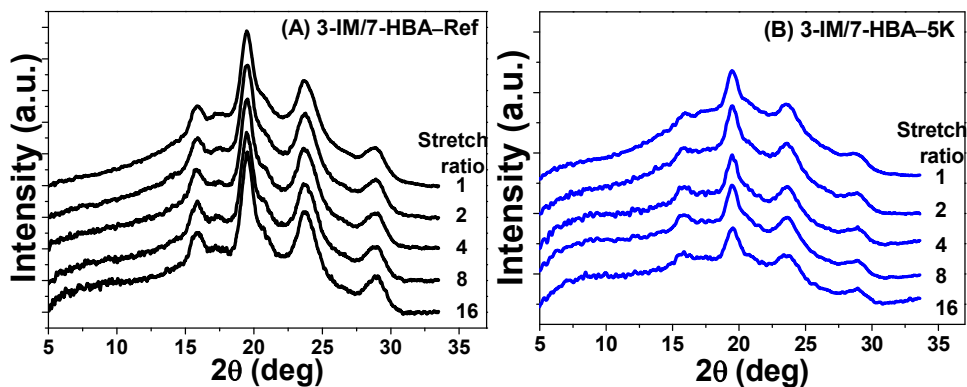
Figure 2.3S. XRD patterns of **A-** 3-IM/7-HBA–Ref and **B-** 3-IM/7-HBA–5K films with different stretch ratios.
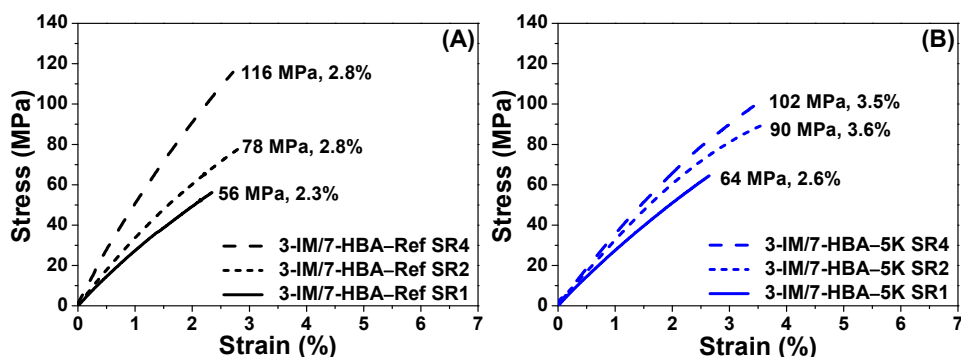
Figure 2.4S. Stress-strain curves of the as-pressed and stretched films of **A-** 3-IM/7-HBA–Ref and **B-** 3-IM/7-HBA–5K. The as-pressed films are labeled SR1. Films stretch by 100% and 300% were labeled SR1 and SR4, respectively. Shown are the best results only from each series.

Table 2.1S. Tensile properties of the as-pressed and stretched films

Sample	Tensile strength (MPa)	Elastic modulus (GPa)	Elongation at break (%)
3-IM/7-HBA–Ref SR1	47±7	2.9±0.2	2.3±0.4
3-IM/7-HBA–Ref SR2	73±5	3.5±0.1	2.9±0.5
3-IM/7-HBA–Ref SR4	108±7	3.9±0.2	3.0±0.3
3-IM/7-HBA–5K SR1	52±12	2.9±0.1	2.3±0.5
3-IM/7-HBA–5K SR2	83±8	3.5±0.2	3.1±0.6
3-IM/7-HBA–5K SR4	98±3	4.0±0.2	3.0±0.6
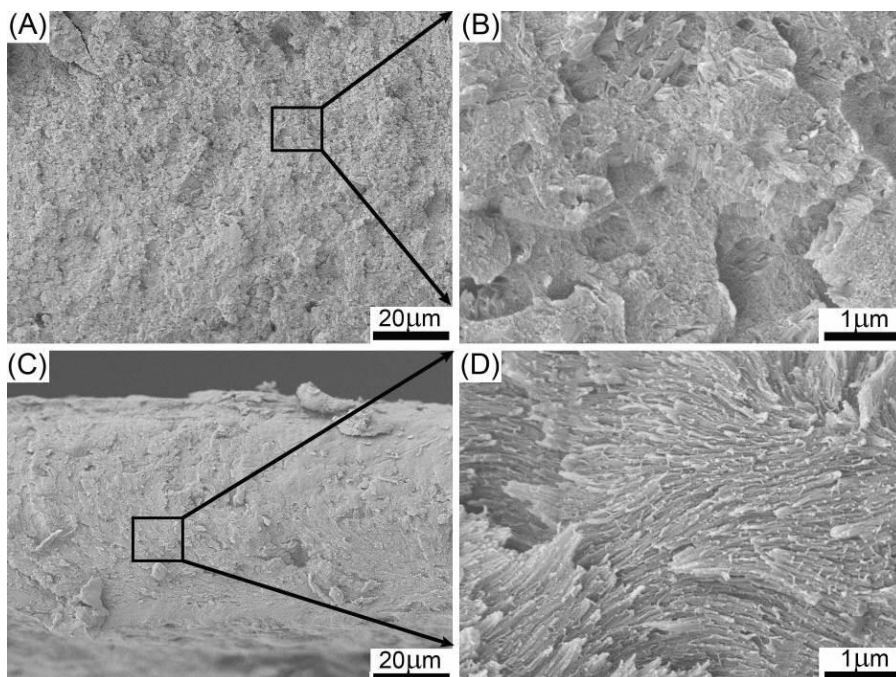
Figure 2.5S. SEM images of 3-IM/7-HBA–5K film fracture surface along the stretching axis. **A-** 3-IM/7-HBA–5K SR1, 1,000 X, **B-** 3-IM/7-HBA–5K SR1, 20,000 X, **C-** 3-IM/7-HBA–5K SR4, 1,000 X, and **D-** 3-IM/7-HBA–5K SR4, 20,000 X.

Scheme 4.1S describes the polymerization mechanism of poly HBA/HNA. The nucleophilic addition of the carboxylic acid to the carbonyl group of the acetate, leading to the formation of a tetrahedral intermediate T1 which can form a mixed anhydride by elimination of HBA. The reaction of the HBA hydroxyl group with the benzoyl group of the mixed anhydride takes place to give another tetrahedral intermediate T2. The growing chain (low molecular weight product, *e.g.* dimer, trimer, etc.) is formed by elimination of acetic acid from the tetrahedral intermediate T2. Although all of these reactions are reversible, the removal of acetic acid can be used as the driving force towards the formation of high molecular weight polymer.[24]

HBA/HNA polymerization
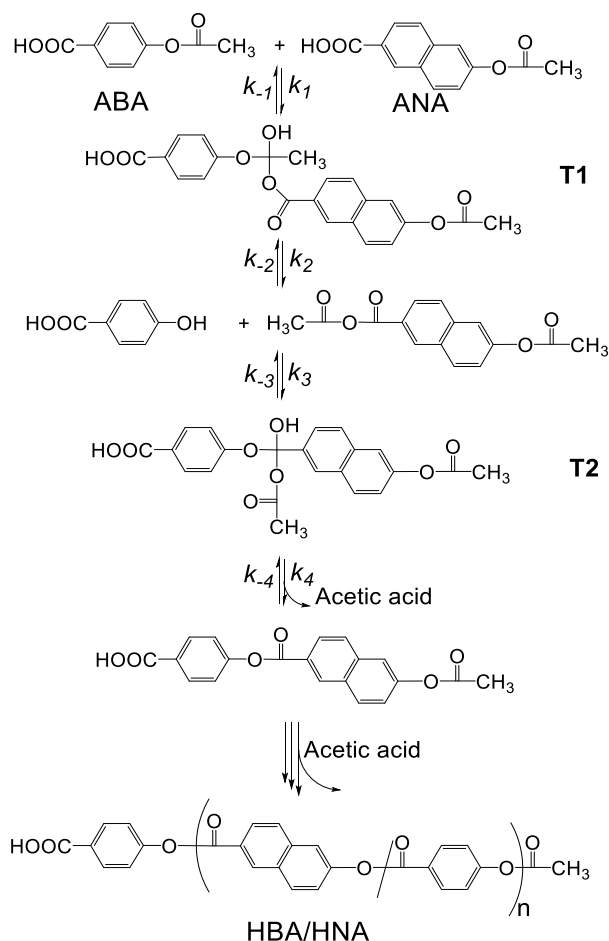
Scheme 4.1S. Melt polycondensation mechanism towards polyHBA/HNA (Vectra-A™). When IM (AIM) is present during the polymerization, this monomer will slowly incorporate into the backbone at the initial stage of the polymerization. Towards the end of the polymerization (T> 300 °C) the rate of incorporation increases and an ABA-triblock copolymer will be obtained.

The orientational order parameter of tensile specimens was calculated by fitting the intensity profiles (Figure 4.1S) as function of the Azimuthal angle (χ) using Maier-Saupe type function eqn. 4.1S.

$$I = I_0 + Ae^{\alpha \cos^2(\chi-\chi_0)} \qquad (4.1S)$$

where I_0 is the free base line, A is the amplitude of scattering intensity, χ_0 is the position of the peak maximum and alpha (α) determines the width of the peak. The value of the alpha (α) parameter was used to calculate the average value of the orientational order $<P_2>$ using eqn. 4.2S.

$$<\overline{P}_2> = \frac{\int_{-1}^{1} P_2(\cos\phi) e^{\alpha \cos^2\phi} \, d\cos\phi}{\int_{-1}^{1} e^{\alpha \cos^2\phi} \, d\cos\phi} \qquad (4.2S)$$
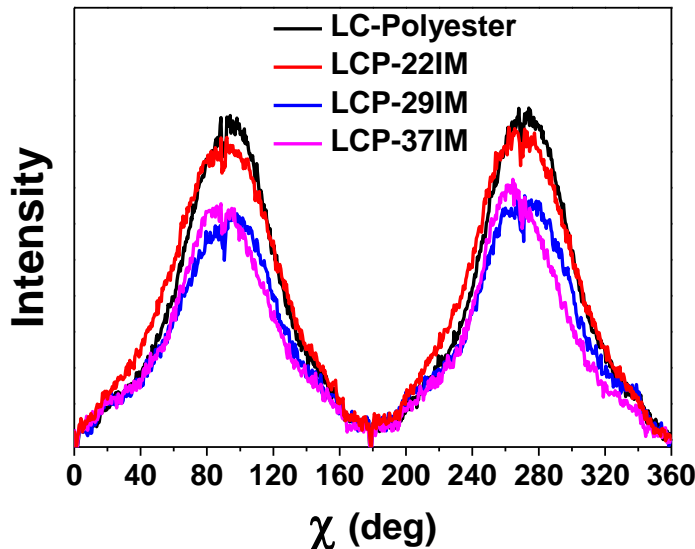
Figure 4.1S Scattering intensity as function of the Azimuthal angle (χ).

Acknowledgements

The completion of this thesis and the work done in the last four and half years would not have been possible without the supervision, help and support of many individuals involved directly or indirectly. I would like to take the opportunity to thank all who have contributed to this work.

First of all I would like to thank my promoter Prof. Theo Dingemans for his wisdom, support, excellent research guidance and commitment to the highest standards. I owe him gratitude for taking the time to discuss ideas and results no matter the time of day and for forcing me to learn to write succinctly. Another special thanks to him for impressive words that "We are not aiming to a marginal improvement. We are doing revolution instead of evolution", which inspired me to keep going in the past years and will be valuable throughout my life.

I owe gratitude to Prof. Stephen Picken (TNW, TU Delft) for his assistance in understanding complex ideas related to polymer physics and for sharing his extensive knowledge on XRD and liquid crystal polymers. Another person that greatly contributed to this research is Prof. Sergei Sheiko (University of North Carolina at Chapel Hill). I am very grateful for all the contributions he made to our study on shape memory polymers.

I owe special thanks to Prof. Sybrand van de Zwaag, for his guidance, critical comments and support during my PhD research. I also thank Prof. Cor E. Koning (TU/e) and Dr. Johan Bijleveld for valuable discussions on the kinetics of melt polycondensation. I thank Ben Norder and Frans Oostrum for performing the XRD and SEM experiments. Without their help, measuring and analysing data would have been much harder. I warmly appreciate the help from Liangyong Chu and Dr. Klaas Besseling (TNW, TU Delft) for AFM experiment and discussion. I would like to thank Lijing for her day to day operations in the lab. I also thank Berthil and

Johan for helping with the machines in the laboratory and Aerospace hangar.

I feel so lucky to be a member of our research group NovAM and there are so many lovely people around me. I enjoyed the time when I worked together with Mazhar, Martino, Srikanth, Jimmy and Hongli, not only in science but also in everyday life. I warmly appreciate the help from Shanta in taking care of all the administrative work, which we mostly don't even know about. I thank Maruti and Jianwei, who are very nice officemates and make a pleasant office environment. It's a great pleasure to spend four and half years with all other group members, whom I want to thank here: Jie, Michiel, Zeljka, Wouter V., Nora, Renee, Erik, Jason, Wei, Xiaojun, Qi, Santiago, Ranjita, Jesus, Mina, Nan, Arijana, Wouter P., Antonio, Marianella, Pim, Nijesh, Daniella, Hamideh, Jibran, Hussein, Hao, Paul.

I thank all my friends from Delft fellowship for their companion. The time we enjoyed together will benefit me for all my rest of life. I also thank Dr. William Clayton for improving my English. I enjoyed the chattering time with William and his wisdom of life, also the journey we had in Germany by the way. I would also like to thank Prof. Guozheng Liang, Prof. Aijuan Gu and Dr. Li Yuan for their encouragement and advice to my study and life.

I am grateful to my family and friends in China, their support made it possible for me to focus on my research. 感谢远在万里之外的父母、家人和朋友们对我始终如一的坚定支持与无言奉献！Last but not least, I would like to thank my beloved wife, Ping, for her endless love, understanding, patience and everything she has done and will do for me. 感谢一路有你陪伴…

Delft, February 2016

Curriculum vitae

Qingbao Guan

Born on November 8, 1986

in Shandong, China

Sept. 2004 – June 2008

Bachelor of Science in Polymer Science and Engineering, Department of Materials Science, Shandong Institute of Light Industry, Jinan, China

Sept. 2008 – June 2011

Master of Science in Materials Science, Department of Materials Science and Engineering, Soochow University, Suzhou, China

Sept. 2011 – Present

PhD candidate in the Novel Aerospace Materials group, Faculty of Aerospace Engineering, Delft University of Technology, Delft, The Netherlands

List of publications and presentations

2016

Q. Guan, B. Norder, L. Chu, K. Besseling, S. J. Picken, T. J. Dingemans. ABA-triblock copolymers via a simple one-step melt condensation method. *Macromolecules*, to be submitted.

Q. Guan, S. Sheiko, S. J. Picken, T. J. Dingemans. High-temperature Shape Memory Behavior of linear and crosslinked Liquid Crystal Poly(esterimide)s. *Macromolecules*, to be submitted.

Q. Guan, S. J. Picken, B. Norder, T. J. Dingemans. All-aromatic Semi-crystalline and Amorphous Poly(esterimide)s: Thermal and Mechanical properties. *Macromol. Mater. Eng.*, to be submitted.

2015

Q Guan, S. J. Picken, B. Norder, T. J. Dingemans. Synthesis and properties of all-aromatic liquid crystalline poly(esterimide)s. Oral presentation, European Polymer Congress, 2015, Dresden, Germany.

Q. Guan, T. J. Dingemans. All-aromatic liquid crystalline poly(esterimide)s: Synthesis, morphology and thermo-mechanical properties. Poster presentation, Dutch Polymer Days, 2015, Lunteren, The Netherlands.

2014

Q. Guan, S. J. Picken, B. Norder, T. J. Dingemans. All-Aromatic high Tg molecular composites. Oral presentation, 9th Asian-Australasian Conference on Composite Materials, 2014, Suzhou, China.

Q. Guan, S. J. Picken, B. Norder, T. J. Dingemans. Poly(P-oxybenzoate) reinforced poly esterimide molecular composites. Poster presentation, 9th Asian-Australasian Conference on Composite Materials, 2014, Suzhou, China.

Q. Guan, T. J. Dingemans. Synthesis and properties of all-aromatic liquid crystal poly(esterimide)s. Poster presentation, Dutch Polymer Days, 2014, Lunteren, The Netherlands.

2013

Q. Guan, T. J. Dingemans. All-aromatic high Tg molecular composites. Oral presentation, 12th SAMPE Benelux Students Meeting, 2013, Almere, The Netherlands.

Q. Guan, T. J. Dingemans. Molecular composites based on polyHBA and poly(ester imide)s. Poster presentation, Dutch Polymer Institute (DPI) Annual Meeting, 2013, Arnhem, The Netherlands.

Q. Guan, T. J. Dingemans. Synthesis and properties of reactive all-aromatic liquid crystal poly (esteramide)s. Poster presentation, Dutch Polymer Days, 2013, Lunteren, The Netherlands.

2012

P. Liu, A. Gu, G. Liang, **Q. Guan**, L. Yuan. Preparation and properties of novel high performance UV-curable epoxy acrylate/hyperbranched polysiloxane coatings. *Prog. Org. Coat.*, 2012, *74*, 142–150.

Q. Guan, T. J. Dingemans. Synthesis and characterization of reactive all-aromatic liquid crystalline polyesteramides. Oral presentation, 11th SAMPE Benelux Students Meeting, 2012, Namur, Belgium.

2011

P. Liu, **Q. Guan**, A. Gu, G. Liang, L. Yuan, J. Chang. Interface and its effect on the interlaminate shear strength of novel glass fiber/hyperbranched polysiloxane modified maleimide-triazine resin composites. *Appl. Surf. Sci.*, 2011, *258*, 572–579.

Q. Guan, A. Gu, G. Liang, C. Zhou, L. Yuan. Preparation and properties of new high performance maleimide-triazine resins for resin transfer molding. *Polym. Adv. Tech.*, 2011, *22*, 1572–1580.

Q. Guan, A. Gu, G. Liang, L. Yuan, F Liao, Y Gong. Curing kinetics and mechanism of novel high performance hyperbranched polysiloxane/ bismaleimide/cyanate ester resins for resin transfer molding. *J. Appl. Polym. Sci.*, 2011, *121*, 304–312.